Distribution Agreement

In presenting this thesis or dissertation as a partial fulfillment of the requirements for an advanced degree from Emory University, I hereby grant to Emory University and its agents the non-exclusive license to archive, make accessible, and display my thesis or dissertation in whole or in part in all forms of media, now or hereafter known, including display on the world wide web. I understand that I may select some access restrictions as part of the online submission of this thesis or dissertation. I retain all ownership rights to the copyright of the thesis or dissertation. I also retain the right to use in future works (such as articles or books) all or part of this thesis or dissertation.

Signature:

_____ _____

Amanda H. Caster Date

Cargo-dependent Recruitment of AP-1 and GGA Adaptors to the Golgi, the TGN, and Recycling Endosomes

By

Amanda H. Caster
Doctor of Philosophy

Graduate Division of Biological and Biomedical Sciences
Neuroscience

_____
Richard A. Kahn, Ph.D.
Advisor

_____
Ranjita Betarbet, Ph.D.
Committee Member

_____
Victor Faundez, M.D., Ph.D.
Committee Member

_____
James J. Lah, M.D., Ph.D.
Committee Member

_____
Allan I. Levey, M.D., Ph.D.
Committee Member

_____
Elizabeth S. Sztul, Ph.D.
Committee Member

Accepted:

_____
Lisa A. Tedesco, Ph.D.
Dean of the James T. Laney School of Graduate Studies

_____
Date

Cargo-dependent Recruitment of AP-1 and GGA Adaptors to the Golgi, the TGN, and Recycling Endosomes

By

Amanda H. Caster
B.S., Antioch University, 2005

Advisor: Richard A. Kahn, Ph.D.

An abstract of
A dissertation submitted to the Faculty of the
James T. Laney School of Graduate Studies of Emory University
in partial fulfillment of the requirements for the degree of
Doctor of Philosophy
in Graduate Division of Biological and Biomedical Science, Neuroscience
2013

Abstract

Cargo-dependent Recruitment of AP-1 and GGA Adaptors to the Golgi, the TGN, and Recycling Endosomes

By

Amanda H. Caster
B.S., Antioch University, 2005

Membrane traffic requires the specific concentration of protein cargos into nascent carriers. Critical components of this selectivity are the protein adaptors that bind to short, linear motifs in the cytoplasmic tails of transmembrane protein cargos and sequester them into nascent carriers. My work examined the specificity and initial sites of recruitment of Arf-dependent adaptors (AP-1, GGAs, and Mint3) in response to the Golgi or endosomal localization of specific cargo proteins. Rigorous localization or co-localization data require quantitative image analyses that can vary widely between fields and laboratories. I developed a novel method for quantifying changes in signal intensity of one protein within any three-dimensional structure, defined by the presence of a different marker. I used the quantification of adaptor recruitment to cargos at the Golgi as examples of this method, though it can be directly applied to any site in the cell. I found that cargo promotes the recruitment of specific adaptors, suggesting that it is part of an upstream signaling event. I further discovered that AP-1 and GGAs are recruited to M6PR at recycling endosomes and not at the Golgi, as suggested by steady state staining profiles. I further demonstrated strict specificity for recruitment of the Mint3 adaptor by APP at the Golgi and identify $LAMP1^{+}$ structures as the proximal destination of APP after leaving the Golgi. These results are discussed with respect to the generation of novel models for cargo-dependent regulation of membrane traffic.

Cargo-dependent Recruitment of AP-1 and GGA Adaptors to the Golgi, the TGN, and Recycling Endosomes

By
Amanda H. Caster
B.S., Antioch University, 2005

Advisor: Richard A. Kahn, Ph.D.

A dissertation submitted to the Faculty of the
James T. Laney School of Graduate Studies of Emory University
in partial fulfillment of the requirements for the degree of
Doctor of Philosophy
in Graduate Division of Biological and Biomedical Science, Neuroscience
2013

Table of Contents

Figure Index

CHAPTER 1

INTRODUCTION AND BACKGROUND[1]

[1] Reproduced and modified with permission from Caster, A. H., and Kahn, R. A. (2010) Roles for ADP-RIbosylation Factors in Membrane Traffic. in *Handbook of Cell Signaling* (Bradshaw, R. A., and Dennis, E. A. eds.), Elsevier. pp 1803-1812*Caster, A. H. and R. A. Kahn (2010). Roles for ADP-RIbosylation Factors in Membrane Traffic. Handbook of Cell Signaling. R. A. Bradshaw and E. A. Dennis, Elsevier: 1803-1812..*

1.1. The ARF Family of Regulatory GTPases

ADP-ribosylation factors (ARFs)[2] are essential and ubiquitous regulators of membrane traffic and are both structurally and functionally very highly conserved across eukaryotes. Biochemical studies of ARFs have revealed them to be regulatory GTPases that act as allosteric activators of several enzymes, including the ADP-ribosyltransferase activity of some bacterial toxins (cholera and E. coli heat labile toxins), and mammalian lipid modifying enzymes, and mediators of protein complex assembly, particularly in the biogenesis of carriers of membrane traffic (several relevant reviews can be found in "ARF Family GTPases" (Kahn 2003) or Randazzo, et al. (Randazzo, Nie et al. 2000)). ARFs were initially identified and named as the co-factor required for *in vitro* cholera toxin- and *E. coli* heat labile toxin-catalyzed ADP-ribosylation of the regulatory subunit of adenylyl cyclase, $G_s\alpha$ (Moss and Vaughan 1977, Enomoto and Gill 1980, Kahn and Gilman 1984) and later confirmed to be obligate host factors for the cellular actions of the human pathogens encoding those toxins (Zhu and Kahn 2001). These biochemical activities were originally used to classify ARFs, as distinct from the structurally highly related proteins that lack these activities, termed ARF-like (ARL) proteins (Kahn, Kern et al. 1991, Tamkun, Kahn et al. 1991, Lee, Haun et al. 1992). Genomic sequencing and phylogenetic analyses have allowed for the complete description of the ARF family that includes ARFs, ARLs, and SAR GTPases and predict that ARF family members are among the earliest GTPases, arising first in prokaryotes (Li, Kelly et al. 2004, Dong, Wen et al. 2007). We provide a summary of ARF background and then focus on the roles of ARFs in membrane traffic; specifically, in the recruitment of protein adaptors to membranes and pairing with cytoplasmic tails of transmembrane protein "cargo" to coordinate the concentration and sorting of cargos to their appropriate destinations.

---

[2] Abbreviations used herein are: AP, adaptin; ARF, ADP ribosylation factor; BFA, Brefeldin A; COP, coatomer; GGA, Golgi localized gamma ear containing adaptin homology; APP, amyloid precursor protein; BFA, Brefeldin A; ER, endoplasmic reticulum; LAMP, lysosomal associated membrane protein; M6PR, mannose 6-phosphate receptor; Mint, Munc interacting protein; PM plasma membrane.

1.1.A. ARF Evolution

The human ARF family is made up of five ARFs, 22 ARLs, and two SARs (Logsdon 2003, Li, Kelly et al. 2004, Kahn, Cherfils et al. 2006). The five ARFs share > 60% sequence identity, while the ARLs have 40-60% sequence identity to any ARF or ARL. This is in contrast to the <30% identity to members of other GTPase families: e.g. RAS, RHO, RAN, or RAB. The functions of ARFs are highly conserved across species as demonstrated by the fact that ARF from *Giardia lamblia* or any of the five human ARFs can complement the lethal deletion of the two ARF genes in *S. cerevisiae* (Kahn, Kern et al. 1991, Lee, Moss et al. 1992). In contrast, the cellular functions of most ARLs appear to be distinct from those of the ARFs; including the regulation of mitochondrial function (Sharer, Shern et al. 2002), microtubule dynamics (Hill, Li et al. 2003, Cunningham and Kahn 2008), ciliogenesis (Fan, Esmail et al. 2004, Caspary, Larkins et al. 2007), and cytokinesis (Zhou, Cunningham et al. 2006). However, a few ARLs, most notably ARL1 and ARFRP1, regulate aspects of membrane traffic that are similar to the actions of ARFs (Panic, Whyte et al. 2003, Setty, Shin et al. 2003). Probably the most complete model we have for any member of the ARF family is for SAR1 regulating protein export from the endoplasmic reticulum (Nishikawa and Nakano 1991, Kuge, Dascher et al. 1994). SAR1 regulates the export of proteins from the endoplasmic reticulum that transit the secretory pathway (Barlowe, Orci et al. 1994, Rowe, Aridor et al. 1996, Lee, Miller et al. 2004). In an analogous fashion, ARF1-5 mediate the traffic of post-ER membrane traffic throughout the endomembrane system, including most secretory and endocytic traffic.

Because ARF1-6 are so highly conserved (e.g., ARF1, ARF2, and ARF3 are each ~96% identical) there are only a few reagents that can distinguish between them. As a result, we have only partial information as to isoform specificity and the extent of functional redundancies. Isoform specific antibodies and Northern blotting confirm that each gene/protein is expressed in every cell or tissue examined (Cavenagh, Whitney et al. 1996). Short interfering RNAs (siRNAs)

have been used to deplete cultured cells of each ARF alone or in pairs (Volpicelli-Daley, Li et al. 2005). These data support the conclusion that ARF1-5 have highly overlapping roles at the Golgi, at endosomes, and likely at the plasma membrane (PM), impacting both organelle morphologies and functions. In contrast, ARF6 has long been known to more stably associate with the PM and endosomes and regulates aspects of both endocytosis, actin organization, and G protein coupled receptor recycling (Hunzicker-Dunn, Gurevich et al. 2002, Donaldson 2003, Claing 2004). In later sections of this introduction, I will emphasize the function of ARFs as recruiters of protein adaptors at the Golgi and thus that information is not relevant to ARF6. Thus, I will focus only on ARF1-5 and direct the reader to recent reviews of ARLs (Burd, Strochlic et al. 2004, Munro 2005), SARs (Pasqualato, Renault et al. 2002, Lee, Miller et al. 2004, Memon 2004), or ARF6 (Hunzicker-Dunn, Gurevich et al. 2002, Donaldson 2003, Claing 2004). Like all members of the RAS superfamily, ARFs interconvert between alternate conformations and bind to different sets of protein partners depending upon whether GTP or GDP is bound, with the GTP-bound conformation typically referred to as the activated state (see Fig. 1.1).

1.1.B. ARFs as Regulators of Critical Cellular Functions

ARFs are unique in that GTP-binding requires a hydrophobic environment and thus activation is accompanied by translocation from cytosol onto a membrane surface (Antonny, Beraud-Dufour et al. 1997). ARFs are co-translationally modified by the addition of the 14-carbon fatty acid, myristate, at the N-terminal glycine (Kahn, Goddard et al. 1988) and this modification is important to both GTP-dependent membrane binding and nucleotide exchange properties of the protein (Regazzi, Ullrich et al. 1991, Antonny, Beraud-Dufour et al. 1997). Cycling between GTP and GDP bound states is regulated by the binding of ARF to guanine nucleotide exchange factors (ARF GEFs) (Cherfils and Chardin 1999, Donaldson and Jackson 2000, Jackson and Casanova 2000) and ARF GTPase activating proteins (ARF GAPs) (Randazzo, Nie et al. 2000, Vetter and Wittinghofer 2001, Cassel 2003). ARF-GEF mediated exchange of

GTP for GDP results in a conformational change in ARF that exposes the amphipathic N-terminal α-helix and associated myristate, leading to a stable association of the activated ARF with the membrane. Once at the membrane, ARF-GTP binds directly to a large number of effectors that can be classed into four different groups: (1) lipid modifying enzymes, (2) protein adaptors that drive membrane traffic, (3) proteins of unknown function, or (4) ARF GAPs (Fig.1.1).

ARF activation is terminated as a result of interaction with an ARF GAP, which promotes the hydrolysis of the bound GTP and return to the "basal" or GDP-bound state, with consequent decreased affinity for effectors. ARF GAPs are a family of 31 human genes encoding proteins containing an ARF GAP domain, almost all of which have been documented to exhibit ARF GAP activity (Kahn, Bruford et al. 2008). This family may not represent the entirety of ARF GAPs because recent work has determined that ARL2 GAPs can also function as ARF GAPs, despite the lack of an ARF GAP domain (Bowzard, Cheng et al. 2007). ARF GAP domain-containing proteins can be quite small, e.g., ARFGAP1-3 are only slightly larger than the ~180 residue ARF GAP domain, or very large, e.g., ARAP1-3 are ~1500 residues in length and contain several different domains. Emerging views of the functions of ARF GAPs suggest both proofreading roles in cargo selection and carrier biogenesis (smaller ARF GAPs) and scaffolding roles in signal transduction (multi-domain ARF GAPs) (Kahn, Bruford et al. 2008). These emerging views are somewhat at odds with the common view of ARF GAPs as simply terminators of the activated state of ARFs, as they suggest effector functions for the ARF GAPs in biological functions downstream of ARFs. The conclusion that ARF GAPs can act as effectors was first proposed and supported by earlier genetic studies in yeast (Zhang, Bowzard et al. 2003).

The role of ARFs in regulation of lipid modifying enzymes, and as initiators of protein complex assembly at the site of carrier biogenesis, though the recruitment of specific protein adaptors likely work together to achieve the specificity, spatial and temporal resolution required for the regulation membrane traffic. However, we still lack holistic models of ARF actions on membranes and so these are presented in separate sections. The other class of ARF effectors

include mitotic kinesin-like protein 1 (MKLP1(Boman, Kuai et al. 1999) , Arfaptins 1 and 2 (Shin and Exton 2001), and Arfophilin(Shin, Ross et al. 1999). These effectors have been implicated in aspects of membrane traffic but there is currently no model that integrates their roles with those of the more prominent effectors, described below.

1.1.C. ARFs as Regulators of Lipid Modifying Enzymes

A number of observations support the conclusion that the actions of ARFs in cells and as regulators of membrane traffic are intimately involved with localized changes in phospholipids, particularly phosphatidylinositides. These observations include both changes in nucleotide binding properties of ARFs and ARF GAPs in response to direct binding of lipids as well as ARFs acting as allosteric regulators of lipid modifying enzymes (Randazzo, Nie et al. 2000). Phosphatidylinositol 4, 5-bisphosphate ($PI(4,5)P_2$) can stimulate the release of GDP and stabilize the nucleotide-free ARF *in vitro* (Terui, Kahn et al. 1994). Both $PI(4,5)P_2$ and phosphatidic acid (PA) can alter the activity of some ARF GAPs (Randazzo and Kahn 1994, Kam, Miura et al. 2000) and thus have the potential to act as allosteric regulators of ARF functions. However, because the lipids that bind ARFs are present in cells at only low levels, are rapidly metabolized, and their actions are expected to be highly localized, we lack convincing evidence that these effects are relevant in cells.

Activated ARFs are allosteric activators of phospholipase D1 (PLD1) (Brown, Gutowski et al. 1993, Cockcroft, Thomas et al. 1994), which converts phosphatidylcholine to PA and choline. Because PA lacks a head group it is ideally suited for localization to the site of high membrane curvature, such as a nascent bud. The potential for ARF activated PLD1 being an important mediator of ARF effects on membrane traffic was first demonstrated by Ktistakis, et al (Ktistakis, Brown et al. 1995, Ktistakis, Brown et al. 1996). It is very likely that both PLD1 activation and adaptor recruitment (see below) play critical roles in the actions of ARFs at the

Golgi, but the relative contributions of these different mechanisms of action remain incompletely understood.

ARFs also have been shown capable of the recruitment and activation of the PI kinases, PI 4-kinase and PI(4P) 5-kinase, that can act sequentially to generate PI(4,5)P_2 (Martin, Brown et al. 1996, Godi, Pertile et al. 1999, Honda, Nogami et al. 1999). It is likely that activated ARFs generate high local concentrations of phosphoinositides, including PI(4,5)P_2, on specific membranes and that products of those lipid kinases play important roles in recruitment of specific proteins to that site and in membrane traffic. For example, ARF activation at the Golgi leads to the generation of PI(4,5)P_2 and recruitment of a specific isoform of the membrane skeletal protein spectrin (Godi, Santone et al. 1998). Locally generated lipids can be even more intimately tied to ARF actions as in the case of the FAPPs, which are required for export of some cargos from the Golgi and do so through direct binding to both ARF and PI(4)P (Godi 2004). Such data highlight the close interplay and overlap in ARF functionalities between localized changes in lipids that are required for protein recruitment and membrane resculpting at the site of carrier biogenesis and the actions of the proteins themselves to sort cargo and coat carriers for transport. Because such localized changes in lipids are hard to manipulate experimentally or to document in cells, more work has been spent on defining the roles of the protein coats that include four different types of ARF-dependent adaptors.

1.2. ARF-dependent Adaptors at the Golgi

The most prominent group of ARF effectors are also the ones that have contributed the most to current models of the molecular actions of ARF as regulators of membrane traffic, termed the ARF-dependent adaptors. We define such adaptors as proteins which (1) bind the activated form of ARFs, (2) are soluble proteins that get recruited to membranes as a result of direct binding to ARFs, (3) are rapidly released from membranes in response to Brefeldin A, and (4) bind directly to the cytoplasmic tails of transmembrane protein “cargos”, typically through

binding to defined sorting motifs. The currently established ARF-dependent adaptors include COPI, adaptins (AP-1, AP-3, and AP-4), the Golgi-associated, γ-ear homologous, ARF-binding (GGA) proteins, and the munc18-interacting proteins (Mint1-3; aka X11α-γ). Other effectors, e.g., FAPP1-2, may later join this list. The presence of an activated ARF on a membrane is predicted to be a nucleating event in the biogenesis of a carrier that will be directed to transport cargo and fuse to a specific destination membrane. The (i) sorting of specific cargo into the nascent bud, (ii) recruitment of protein adaptors that will subsequently recruit the appropriate accessory proteins required for routing, transport, uncoating, and (iii) maturation of the bud into a mature carrier are initiated by the pairing of the activated ARF with an ARF-dependent adaptor and its cargo. Roles for ARFs in later stages of carrier-mediated transport have been proposed but lack convincing experimental support.

1.2.A. COPI

The first of the carriers of membrane traffic to be purified and protein content characterized were the clathrin-coated vesicles (CCVs) (Pearse 1976, Keen, Willingham et al. 1979, Pearse and Robinson 1984, Robinson and Pearse 1986). CCVs originate from two different sites and the composition of the protein coat differs with the origin; those originating at the Golgi contain the tetrameric AP-1 adaptor and those from the PM contain the homologous AP-2 tetramer (Chang, Mallet et al. 1993, Touz, Kulakova et al. 2004). Because clathrin has the ability to assemble into a semi-rigid caged structure it was viewed as providing both a scaffold for the assembly of vesicles and a protein coat that stabilizes the mature vesicle during transport to the site of fusion. Thus, it was surprising when the first non-clathrin coated vesicles were purified and the coating proteins found to be comprised of the heptameric complex termed coatomer or COPI (Waters, Serafini et al. 1991). COPI coated vesicles were purified from the incubation of partially purified Golgi membranes with the non-hydrolyzable GTP analog, GTPγS, and the required GTP-binding component was found to be supplied by ARF (Donaldson, Kahn et al.

1991, Serafini, Orci et al. 1991) . The abundance of ARF in the purified vesicles led to models in which it was viewed as a component of the mature coat and hydrolysis of GTP on ARF proposed as a trigger for disassembly of coating just prior to fusion (Tanigawa, Orci et al. 1993). However, two different ARF-dependent carrier preparations have been analyzed for ARF content and found to be essentially devoid of ARF in the mature vesicles (Faundez, Horng et al. 1998, Shrivastava-Ranjan, Faundez et al. 2008). Thus, it is much more likely that the actions of ARFs in membrane traffic occur during budding and carrier biogenesis. The discovery of COPI and presence of ARF in the purified vesicles sparked a wave of discovery that has contributed tremendously to our understanding of ARF biology; including the use of BFA as a specific inhibitor of some ARF GEFs to study ARF functions in intact cells (Donaldson, Finazzi et al. 1992) and discovery of other non-clathrin coated carriers and adaptors[3] (see below).

1.2.B. Adaptins (AP)

Soon after COPI was found to coat Golgi-derived vesicles, many of the same methods were used to demonstrate that adaptin (AP-1) binding to the Golgi was sensitive to BFA and predicted to require ARF activation (Stamnes and Rothman 1993). Adaptin nomenclature has evolved over the years and currently uses AP to denote the heterotetrameric adaptor protein complexes and the term "adaptin" is used to describe the subunits of APs (Robinson 1993, Boehm and Bonifacino 2001). There are five AP complexes, AP-1 through AP-5, and each is composed of four homologous adaptins, two large (90-130 kDa; named α/γ/δ/ε and β1-4 for the subunits in AP-1 to AP-4, respectively), one medium (~50 kDa; named μ1-4, respectively), and one small (~20 kDa; named σ1-4) subunit (Boehm and Bonifacino 2001, Styers 2003). More recently AP-1 was found to have diverged into two different adaptins, termed AP-1A and AP-1B, differing in the

[3] Purified COPI-coated vesicles contain an electron dense coat, as seen by electron microscopy, that is ascribed to the presence of COPI and justifies the terminology as a coat protein. With the discovery of other mature carriers of membrane traffic that contain neither clathrin nor COPI and likelihood that COPI and its functional homologs act as adaptors in the construction of large protein complexes the term "adaptor" has largely replaced "coat protein". Note that 'adaptor' is the generic term and the adaptins (APs) are one subset of adaptors.

μ subunit(s) (Nakatsu, Kadohira et al. 1999, Ohno, Tomemori et al. 1999), and important in polarized sorting. μ1A and μ1B are 80% identical and each function in basolateral sorting of cargo from the TGN (Nakatsu, Kadohira et al. 1999, Eskelinen, Meyer et al. 2002), but μ1B is expressed only in polarized epithelial cells (Eskelinen, Meyer et al. 2002). AP-2 functions in clathrin-dependent endocytosis at the PM, and is therefore excluded from our studies. We limit our discussion to AP-1, AP-3, and AP-4 recognizing that AP-1 is a generic term for both the ubiquitous AP-1A and the polarized epithelial cell-specific AP-1B. For a detailed review of AP-5, see (Hirst, Barlow et al. 2011).

The gamma subunit of AP-1 was originally cloned and sequenced from mouse and bovine brain libraries (Robinson 1990), and thought to function much as the previously described β subunit of AP-2 that localizes to the PM, binding to both cargo and clathrin. Since the original description, AP-1 has been implicated in the sorting of cargo both in the anterograde pathway out of the Golgi (Boehm and Bonifacino 2001, Doray, Ghosh et al. 2002), as well as in retrieval to the Golgi from endosomes (Thomas 2002), depending upon the cargo (Aridor and Traub 2002).

AP-3 functions in traffic between endosomes, lysosomes, synaptic vesicles and, like AP-1, is recruited to membranes through direct binding to ARFs, though is thought to be clathrin independent(Faundez, Horng et al. 1998). The isolation and characterization of the protein composition of mature AP-3 coated carriers has provided a wealth of information that will be important in future studies of carrier biogenesis, transport, and fusion (Salazar, Craige et al. 2005). Interestingly, purified AP-3 vesicles contain a specific isoform of PI 4-kinase, PI4K IIα (Salazar, Craige et al. 2005). In contrast, a related adaptin, AP-2, functions in endocytosis at the PM. Like the FAPPs, the interactions of at least some of the APs with membranes is sensitive to the localized lipid composition, including binding to phosphatidylinositides, thus ARFs may act both as direct docking sites for APs and indirectly via the generation of high local concentrations of PIs.

While AP-1, 2, and 3 were identified using *in vitro* assays, AP4 and AP-5 were identified based on sequence homology, and are less well characterized (Hirst, Barlow et al. 2011, Hirst, Irving et al. 2013). Both AP-4 and AP-5 localize to late Golgi and endosomes, and function in clathrin-independent sorting (Hirst, Irving et al. 2013). AP-4 has been reported to affect the overall distribution of the amyloid precursor protein (APP, discussed in detail below) via interaction with the YKFFE sorting motif (Burgos, Mardones et al. 2010, Choy, Cheng et al. 2012), and distinct from the canonical adaptin binding motif YXXPhi. The interaction was discovered using a yeast 2-hybrid screen in addition to knockdown studies evaluating the subsequent changes in APP localization (Burgos, Mardones et al. 2010). While AP-4 dependent changes in APP localization were identified, it remains unclear whether this interaction is occurring at the Golgi or in post-Golgi endosomes (Choy, Cheng et al. 2012) (Caster Kahn submitted). AP-5 is less well studied, with no currently identified cargos, though depletion of AP-5 results in changes in endosomal structures, increased retromer staining, and flattened clathrin lattices (Hirst, Barlow et al. 2011).

The APs were originally viewed as serving an adaptor role by coupling direct binding to the cytoplasmic tails of transmembrane protein cargo to direct binding to clathrin. This led to the model that cargo sorting and concentration into a nascent bud involves the binding of a sorting motif within the cytoplasmic tail, e.g., NPXY in the LDL receptor, to a cargo-binding domain in the AP. The most intensively studied cargo for AP-1 at the Golgi is the cation independent mannose 6-phosphate receptor (M6PR, discussed later) that binds lumenal mannose 6-phosphate-containing lysosomal proteases for transport from the Golgi to the lysosome. Subsequent studies indicate that the cytoplasmic tail of M6PR contains more than one sorting motif and binds directly to two different ARF-dependent adaptors; AP-1, using a tyrosine based motif (Johnson, Chan et al. 1990, Storch and Braulke 2001), and the GGAs, using the acidic dileucine motif (Doray, Bruns et al. 2002, Hirst, Seaman et al. 2007). It is unclear at this point if these different adaptors work together or represent alternative sorting routes for the M6PR but the former is

more likely as both AP-1 and GGAs are thought to support traffic from the late Golgi/TGN to endosomes (Doray, Bruns et al. 2002, Doray, Ghosh et al. 2002). With as many as five different ARFs capable of binding the Golgi and multiple ARF-dependent adaptors recruited to the same membranes we lack viable models of the sources of specificity in this essential cellular process.

1.2.C. Golgi localized, gamma ear containing adaptin homology (GGA) proteins

Two experimental approaches have expanded the list of ARF-dependent adaptors and contributed powerful new tools to discovery of ARF mechanisms of action in membrane traffic: homology searches of adaptin subunits (Dell'Angelica, Puertollano et al. 2000, Hirst, Lui et al. 2000) and screening for ARF binding partners (Boman, Zhang et al. 2000) that identified the GGA family of three proteins that share both structural and functional homology to the APs. Because the GGAs are monomers their discovery has greatly facilitated biochemical and cell biological studies of adaptor protein functionalities as earlier adaptors were oligomeric.

As the name reveals GGAs localize to the Golgi, share sequence homology to γ-adaptin at their C-termini, and are recruited to the Golgi by binding to activated ARFs. As predicted by these characteristics they are also BFA sensitive and rapidly dissociated from the Golgi upon exposure of cells to drug. GGAs are comprised of four functional domains: the N-terminal VHS (VPS, HRS, and STAM homologous) domain, an ARF binding domain termed GAT (GGA and TM homology), a hinge region that includes motifs for binding to clathrin and the VHS domain, and a C-terminal domain with homology to γ-adaptin, termed GAE (see Fig. 1.2A).

The VHS domain is ~ 140 residues long and is binds sorting signals in the cytosolic tails of cargo, including sortilin and both the cation-dependent and cation-independent M6PRs. GGAs bind to acidic dileucine motifs with the sequence DXXLL, and do so most avidly when the motif is present at the very C-terminus of the cargo (Bonifacino 2004). The GAT domain binds activated ARFs, required for the recruitment to the TGN (Puertollano, Aguilar et al. 2001, Boman, Salo et al. 2002), and also Rabaptin-5 (Mattera, Arighi et al. 2003). The hinge region

ranges from 80-286 residues in length among the three human GGAs. This region is largely unstructured and, in GGA1 and GGA3, contains a DXXLL-like motif, which can fold back and interact with the VHS domain to serve an auto-inhibitory function (Doray, Bruns et al. 2002). The hinge region also contains clathrin-box motifs which, in APs, interact with clathrin heavy-chain (Dell'Angelica, Klumperman et al. 1998) and also binds to AP-1 (Knuehl, Chen et al. 2006). The GAE domain is structurally related to the subunit of AP-2 and binds a number of proteins including Rabaptin-5 (Hirst, Lui et al. 2000, Mattera, Arighi et al. 2003), and clathrin interacting protein localized in the TGN (CLINT) ((Mills, Praefcke et al. 2003). Thus, by its multi-domain nature, the GGAs serve essential roles in both cargo selection and assembly of a large protein complex needed for carrier transport.

The binding of a specific adaptor to a cargo tail is currently viewed as the key determinant of the route of export from the Golgi. This is perhaps best illustrated by studies of engineered proteins containing the lumenal domain of cluster of differentiation 8 (CD8) fused to the cytoplasmic tail of the M6PR (CD8-M6PR) or a mutant that lacks the GGA binding motif (CD8-M6PR-ΔC (Hirst, Seaman et al. 2007). The CD8-M6PR construct localizes to the Golgi and its expression increases the binding of GGAs at that site, while the mutant does not. This demonstrates that the cellular distribution of cargo hinges on the adaptor with which it preferentially associates. Because cargos can contain more than one sorting motif, its traffic entails sorting at multiple steps, and the adaptors are found at more than one site, there is still confusion as to sources of specificity in the regulation of cargo sorting at the Golgi, and elsewhere.

Another important, but underdeveloped concept in the regulation of membrane traffic is protein phosphorylation. Both the cytoplasmic tails of cargos and the adaptors themselves are substrates for protein kinases and the phosphoproteins have been found to display different conformations and activities related to traffic; e.g., GGA1 and GGA3 are multiply phosphorylated and as a consequence have altered conformation or effects on traffic (Ghosh and

Kornfeld 2003, McKay and Kahn 2004), and phosphorylation of a serine in the acidic dileucine motif of the cation independent-M6PR regulates recognition of the signal by GGAs at the TGN (Kato, Misra et al. 2002). Similarly, the amyloid precursor protein contains an NPXY motif that can be tyrosine phosphorylated. The ARF-dependent Mint adaptors bind this motif with increased affinity when phosphorylated (Borg, Ooi et al. 1996), all potentially regulating traffic events.

1.2.D. Munc Interacting (Mint) Proteins

Mints were independently discovered using different methods and thus possess multiple aliases. The human gene names APBA1-3 are acronyms for amyloid-β precursor protein binding family A but the proteins are more commonly referred to as Mint1-3 (based upon the observation that Mint1 and 2 bind to Munc18 (Okamoto and Sudhof 1997, Okamoto and Sudhof 1998)), or X11α/β/γ, or X11, X11-like1 and X11-like2. Functional studies of a Mint family member were first performed in *C. elegans* where the ortholog LIN-10 was shown to be required for vulva development via its role in localization of the EGF receptor ortholog (LET-23) at the basolateral surface (Simske, Kaech et al. 1996). LIN-10 is found in a stable heterotrimer in both worms and mammals, comprised of LIN-10/Mint1, LIN-2/Cask, and LIN-7/Velas (Kaech, Whitfield et al. 1998). These studies demonstrated roles for Mint orthologs in membrane traffic and later studies have revealed differences among the three human paralogs.

All three human Mints share conserved phosphotyrosine binding (PTB) and dual, C-terminal PDZ (PSD-95, Drosophila disks-large, ZO-1) domains, that together yield a shared ~80% sequence identity and ability to bind multiple partners (Fig. 1.2B). Only Mint1 has an N-terminal Cask interaction domain (CID; Fig. 1.2B) that is required for assembly of the Mint/Cask/Velas trimer, revealing differences in functionalities. Mint2 and Mint3 share a domain (MID) that binds the transmembrane protein Munc18, which acts in synaptic transmission at the cell surface. This role at the synapse and specific expression of Mint1 and Mint2 in neurons has

led to the erroneous assumption that Mint3 in not expressed in brain. In fact, Mint3 is ubiquitously expressed, including in the brain, and is involved in transport of the amyloid precursor protein (APP), a critical protein in Alzheimer's disease (AD) pathogenesis (Shrivastava-Ranjan, Faundez et al. 2008), particularly at the Golgi.

The PTB is functionally homologous to the VHS domain in GGAs in that it binds to a sorting motif (NPXY) in the cytoplasmic tail of cargos that include APP (Borg, Ooi et al. 1996, Zhang, Lee et al. 1997). The PTB domains of Mints bind the NPXY motif in a phosphorylation-independent fashion (Borg, Ooi et al. 1996, Zhang, Lee et al. 1997), and mediate sorting to the basolateral membrane in polarized cells. APP and Mint3 were found to co-localize at the Golgi in an inter-dependent fashion (McLoughlin, Irving et al. 1999, Hill, Li et al. 2003) and both are present in purified vesicles that are predicted to originate at the Golgi (Shrivastava-Ranjan, Faundez et al. 2008). When Mint3 was depleted by siRNA, APP export from the Golgi was altered and displayed kinetics in traffic to the cell surface (Shrivastava-Ranjan, Faundez et al. 2008).

The two PDZ domains at the C-termini of Mints appear to play distinctive roles. PDZ2, along with the C-terminal portion of the PTB domain, is required for binding ARF and is thus functionally homologous to the GAT domain of GGAs. Other proteins that have been found to bind PDZ domains including KIF17 (Setou, Nakagawa et al. 2000), presenilin-1 (Lau, McLoughlin et al. 2000), and copper chaperone for SOD1 (McLoughlin, Standen et al. 2001) and are shown in Fig. 1.2B. These interactions have been less completely characterized. The PDZ domains are also predicted to bind internal sequences in an auto-inhibitory fashion, again analogous to the hinge domain of GGAs binding to the VHS domain.

1.3. Cargo Proteins

1.3.A. Amyloid Precursor Protein (APP)

Structure and Sorting Information

The amyloid precursor protein (APP) is a single-pass, type I transmembrane protein of unknown function and is expressed in many different tissues, as isoforms of different lengths. The 750 and 770 residue isoforms are predominantly expressed in non-neuronal tissue, while the 695 residue form is predominantly expressed in brain. I will focus exclusively on the 695 residue isoform, as it is most relevant to human disease (discussed below). APP has a 640 residue lumenal/extracellular domain, a short, ~8 residue transmembrane domain, and a cytoplasmic tail that is 47 aa in length. APP is proteolytically processed by secretases that traffic throughout the cell to result in the generation of non-pathogenic, or pathogenic fragments. APP at the PM is cleaved by alpha secretases, then internalized for cleavage by gamma secretases to generate non-pathogenic fragments of APP. Alternatively, APP can be cleaved by β- and γ-secretases present at endomembrane structures to result in the generation of pathogenic fragments of APP, termed Aβ and the primary component of plaques, the pathological hallmark of Alzheimer's disease. These processing events are location specific, as the secretases that are responsible for the cleavage of APP have distinct traffic patterns and steady state distributions throughout the endomembrane system. The order in which APP is exposed to different secretases determines the order of cleavage events, dictating whether or not APP proteolysis generates Aβ or non-pathogenic fragments. Because secretases reside in different endomembrane structures, the traffic of APP through the cell and subsequent exposure to specific secretases at various endomembrane compartments is critical to the proteolytic processing, and ultimately pathogenesis of AD.

Traffic of APP

The traffic of APP is directly responsible for its processing into toxic or non-toxic fragments. APP is synthesized in the rough ER and travels to the Golgi where it is glycosylated into its mature form(Tomita, Kirino et al. 1998, Rajendran and Annaert 2012). Glycosylated APP leaves the Golgi, where it is sequestered into carriers by the recruitment of the cytosolic, ARF-dependent adaptor Mint3 (discussed in detail below). APP leaves the Golgi and travels to the PM through unknown compartments to the PM where APP can be endocytosed and targeted to endosomes for subsequent traffic back to the PM (Thinakaran and Koo 2008).

It is unclear where Aβ is generated in the cell. Due to the distribution of the secretases responsible for its processing, Aβ fragments are potentially generated in the Golgi, ER or in endosomes (Kim, Lah et al. 2000, Cupers, Bentahir et al. 2001, Siman and Velji 2003, Kim, Kleizen et al. 2007). Most of the discrepancies in the proposed site of Aβ generation most like stem from different methodologies. For example, the use of the Swedish mutation [K670N/M671L] of APP is more readily cleaved at the TGN compared to wild-type APP (Citron, Oltersdorf et al. 1992). Similarly, studies performed in non-neuronal and neuroblastoma cell lines indicate that Aβ is generated at the Golgi, TGN and endosomes (Small and Gandy 2006), while those performed in polarized Madin Darby canine kidney (MDCK) cells suggest apical sorting sites are more relevant to beta secretase cleavage (Koo, Sisodia et al. 1990). Clearly, differences in model systems contribute largely to discrepancies in the site of Aβ generation and further work required to definitely determine the compartment(s) in which Aβ generation takes place. Understanding how APP moves from one compartment to another is potentially critical to understanding the pathogenesis of Alzheimer's disease.

1.3.B. Furin

Structure and Sorting of Furin

Furin is a single-pass, type I transmembrane protein, 794 aa in length, and synthesized in the endoplasmic reticulum with a pro-region, also termed prodomain, that is a leader peptide sequence that is later cleaved, a large lumenal domain, and a short cytoplasmic tail that is 56 residues in length. The prodomain is 83 residues long, and folds back on the lumenal domain to serve as a regulatory chaperone, and is necessary for the traffic of furin from the ER to the Golgi (Teuchert, Schafer et al. 1999). While furin is in the ER, it undergoes an autocatalytic event, cleaving the prodomain at R107, the C-terminal end of the canonical, minimal furin cleavage sequence RXXK, though RXXXKR/RR can also be cleaved (Thomas 2002). Though cleaved, the prodomain remains associated with furin until the complex reaches the late Golgi where the prodomain is again cleaved by furin at R75, within the sequence ^{70}RGVTKR^{75}. This second cleavage causes the prodomain to be released from furin, and unmasks the catalytic site (consisting of Asp, His, and Ser residues) as well as pH and calcium sensing domains. The cytoplasmic tail of furin contains at four sorting motifs that contribute to furin localization, ^{756}LI^{757}, ^{759}YKGL^{762}, F^{790}, and the acidic cluster ^{768}EECPSDSEEDE^{780} (discussed later).

Once at the Golgi, furin functions as an endoprotease, cleaving substrates that traffic both the endocytic and exocytic pathways (Molloy, Thomas et al. 1994, Teuchert, Schafer et al. 1999, Thomas 2002) including receptors, grown factors, viral envelope proteins, and cell adhesion molecules (Gotoh, Ohnishi et al. 1992). Furin can also exit the Golgi and travels to the PM, where it is endocytosed for subsequent rounds of traffic. Though furin is thought to function predominantly in the Golgi, it is catalytically competent while at the PM (Schafer, Stroh et al. 1995) and in endosomal/lysosomal compartments (Molloy, Thomas et al. 1994, Thomas 2002).

Motifs and Adaptors Critical to the Traffic of Furin

There are at least four known sorting motifs within the cytoplasmic tail of furin: the membrane proximal LI, YKGL, the acidic cluster (^{768}EECPSDSEEDE^{780}), and F790 (refer to Fig. 1.3). These sorting motifs can work in concert, or competitively to mediate adaptor recruitment to affect sorting at various organelles. The LI, YKGL, and F790 motifs are internalization signals, and the acidic cluster (^{768}EECPSDSEEDE^{780}) is a Golgi retention signal. These motifs interact with various adaptors to promote the accurate sorting of furin at various steps in the secretory pathway.

The YKGL motif (that conforms to the canonical adaptin binding motif) mediates AP-2 binding to furin at the PM for endocytosis, as well as the binding of both mu1 and gamma1 subunits of AP-1 (Teuchert, Schafer et al. 1999) at the Golgi, in a casein kinase 2 phosphorylation-dependent manner (Teuchert, Schafer et al. 1999). The YKGL motif seems to be less important for furin localization to the Golgi, as deletion of this motif results in both full-length and chimeric forms of furin localizing to the Golgi (Schafer, Stroh et al. 1995). Phosphorylation of residues within the cytoplasmic tail also contributes to the regulation of adaptor binding, as AP-1 binding is enhanced by the phosphorylation of serine residues immediately before the YKGL sequence.

The acidic cluster is critical for the Golgi localization of furin. It mediates binding to both AP-1 (Teuchert, Schafer et al. 1999) and Mint3 (Han, Wang et al. 2008), and is necessary for the basolateral sorting of furin in polarized MDCK cells (Simmen, Nobile et al. 1999). Deletion of the acidic cluster, or depletion of Mint3 in non-polarized cells results in an increase of furin at the PM (Schafer, Stroh et al. 1995) or endosomal structures (Han, Wang et al. 2008), consistent with this motif being critical to the retention of furin at the Golgi.

The complicated traffic of furin is achieved through sorting signals contained within the cytoplasmic tail (Schafer, Stroh et al. 1995). Studies by multiple groups have examined the

sorting of furin, in different cell models using various experimental approaches. The emerging picture of furin traffic suggests that, though there are multiple sorting signals contained in the cytoplasmic tail, these sorting signals have relevance only at specific endomembrane structures. The regulation of signal priority at various endomembranes is of great interest, and understanding the location at which a given motif is relevant to cargo traffic is critical to understanding basic trafficking events with potential sites of intervention.

1.3.C. Mannose 6 Phosphate Receptor (M6PR)

Structure and Sorting of M6PR

The mannose 6 phosphate receptors (M6PR) are single-pass transmembrane proteins that shuttle soluble lysosomal hydrolases from the Golgi to endosomes (Medigeshi and Schu 2003). There are two forms of M6PR in mammalian cells, the 300kDa cation independent (CI-M6PR), and the 46kDa cation dependent (CD-M6PR), often expressed simultaneously in multiple cells types, with functional redundancies (Nadimpalli and Amancha 2010). CD-M6PR associates with hydrolases in the late Golgi, and traffics to endosomes where the hydrolase is released and the receptor travels back to the Golgi, or to the PM to internalize extracellular ligands. CI-M6PR follows a similar traffic route, with less escape to the PM. The work presented here uses CI-M6PR.

CI-M6PR is 277 amino acids long, with an N-terminal lumenal domain of 123 amino acids, and unstructured C-terminal cytoplasmic tail 154 amino acids long. Contained with the cytoplasmic tail are sorting motifs that bind adaptors to facilitate sorting. The YKYSKV motif that contains a canonical adaptin binding motif, and a C-terminal dileucine motif (LLHV), a canonical GGA binding motif, both of which are important for the efficient delivery of lysosomal hydrolases to lysosomes (Johnson, Chan et al. 1990).

Adaptors that bind M6PR

M6PR binds directly or indirectly to at least four different adaptors to influence its bidirectional sorting and traffic between the Golgi and endosomes, including GGAs, AP-1, tail interacting protein of 47 kDa (TIP47), and phosphofurin acidic cluster sorting protein (PACS). M6PR traffic from the Golgi is a clathrin-dependent process (Dahms, Lobel et al. 1989, Lobel, Fujimoto et al. 1989, Canfield, Johnson et al. 1991, Jadot, Canfield et al. 1992) and as such, led to the implication of AP-1 and GGAs (both containing clathrin binding regions) as critical to M6PR traffic from the Golgi. GGAs and AP-1 (discussed earlier) were first described as cooperative components of the M6PR traffic machinery functioning at the Golgi, as both were present there in scanning electron micrographs (Doray, Ghosh et al. 2002). Based on their presence at the Golgi, and the fact that they both contain clathrin binding domains, it was proposed that GGAs and AP-1 cooperated to sort M6PR from the Golgi to endosomes, as the expression of a mutated form of GGA1 that lacked the hinge and GAE regions resulted in mis-localization of M6PR (Puertollano, Aguilar et al. 2001). However, follow-up studies indicate that GGAs and AP-1 were present at the Golgi even in the absence of M6PR (Meyer, Zizioli et al. 2000), suggesting that their recruitment was independent from the presence of M6PR. Similarly, data obtained from a knockout mouse in which the mu subunit of AP-1 was deleted showed no defect in the ability of M6PR to leave the Golgi and travel to endosomes, suggesting that M6PR traffic out of the Golgi is not dependent on AP-1 (Meyer, Zizioli et al. 2000).

TIP47 is a soluble, ARF-independent adaptor protein that interacts specifically with both CD-M6PR and CI-M6PR cytoplasmic tails to facilitate traffic of M6PR from endosomes back to the Golgi (Diaz and Pfeffer 1998). There are two PACS isoforms in mammalian cells (PACS1, and 2) that bind to the acidic cluster in the cytoplasmic tail of CI-M6PR, in a phosphorylation dependent manner (Scott, Gu et al. 2003). PACS proteins compete with GGAs for binding to the

CI-M6PR (Scott, Fei et al. 2006), and depletion of PACS2 affects CI-M6PR retrieval from endosomes to the Golgi (Scott, Fei et al. 2006). Though these proteins are clearly important to the regulated sorting of CI-M6PR, they are BFA insensitive, and therefore considered to be ARF-independent.

1.4. Guanine Nucleotide Exchange Factors (GEF)

Three large ARF guanine nucleotide exchange factors (GEF)[4] function at the Golgi and endosomes to promote the exchange of GDP for GTP bound to ARFs; Brefeldin A inhibited (BIG) 1 and 2, and Golgi associated, BFA-resistant, guanine nucleotide exchange factor (GBF1, (Jones, Moss et al. 2005)). BIG2 was the first large ARF GEF to be purified from bovine brain in a complex of ~670 kDa, components of which showed nucleotide exchange activity. Digests of denatured components of the 670kDa complex identified Sec7 sequence (previously identified in yeast, for review see (Bui, Golinelli-Cohen et al. 2009)), ultimately leading to the cloning of BIG1 and BIG2, both of which are BFA sensitive (Togawa, Morinaga et al. 1999, Jones, Moss et al. 2005). In contrast, GBF1 was originally identified using a Brefeldin A resistance screen, looking for mutant CHO cells that were capable of growth in the presence of BFA. All three proteins contain a Sec7 domain that is responsible for ARF activation.

BIG1 and BIG2 function in the secretory pathway to regulate the activation of ARFs with preference for specific ARFs in *in vitro* studies. Both BIG proteins preferentially activate ARF1 and ARF3. Though the proteins are very similar, they show distinct cellular distributions. BIG1 localizes to endosomes and overlaps with GBF1 (Mansour, Skaug et al. 1999), and translocates to the nucleus after serum starvation (Padilla, Pacheco-Rodriguez et al. 2004), while BIG2 localizes more distinctly to endosomes and overlaps with AP-1 and TfR, but not GBF1 (Shin, Morinaga et

[4] Guanine nucleotide exchange factors (GEF) are also termed guanine nucleotide exchange proteins (GEP) and both abbreviations are found in the literature. We use GEF throughout, for simplicity.

al. 2004), suggesting that the large ARF GEFs play distinct roles in the regulation of membrane traffic, at specific locations.

GBF1 localizes predominantly to the Golgi, and is specifically active for ARF5, but not ARF1 and ARF3 at physiological Mg concentrations (Claude, Zhao et al. 1999). Though it functions as an ARF GEF, GBF1 localization is largely insensitive to BFA treatment, suggesting its recruitment is ARF-independent. Instead, the Arf-like 1 protein (Arl1)(Christis and Munro 2012) regulates its localization to the early Golgi. Models for GEF localization and subsequent ARF activation include Arl1 recruiting GBF1 to early Golgi where it acts preferentially on ARF5, to in turn recruit BIG1 and BIG2 to late Golgi and endosomes (Lowery, Szul et al. 2013).

1.5. Key Concepts in Image Analysis

Much of the work on membrane traffic has relied on imaging, and specifically the quantitative analysis of fluorescence based imaging, to determine the subcellular distribution of proteins. In most cases, a protein of interest and a protein with a known distribution (e.g. an organelle marker) are fluorescently labeled and imaged on two separate channels. These two images are then overlaid, and the amount of overlap gives some indication of the location of the protein of interest relative to the marker, allowing for inferences about (i) where it resides, (ii) likely trafficking routes, (iii) and possible interacting partners. Historically, this kind of information has been quantified using Pearson's correlation coefficient (PCC), a statistical measure used to calculate the relationship between two parameters. In the case of image analysis, those parameters are red (R) and green (G) fluorescence. The values obtained can range from -1 to 1, indicating an inverse or perfect correlation, respectively. They are a reflection of how well the intensity on one channel correlates with that on the other, and are calculated using the equation below:

$$r = \frac{(R_i - R_\mu) \bullet (G_i - G_\mu)}{\sqrt{\sum (R_i - R_\mu)^2} \bullet \sqrt{\sum (G_i - G_\mu)^2}}$$

A value of '0' would indicate no correlation.

The Pearson's coefficient has been extensively cited as being sensitive to intensity, the common criticism being that, given two fluorophores of unequal intensity, Pearson's fails to detect 'colocalization' (Barlow, Macleod, et al. 2010). This assumption stems from the fact that the numerator is the sum of weighted intensities, or a large value on one channel results in a weighted contribution of the other (see Eq. 1). As a result, a number of other equations were derived from the PCC to describe how well two channels overlap; the most commonly used being the Mander's overlap coefficient (MOC). The MOC simply rearranges the PCC to interrogate each pixel within an image, and asks 'for every pixel with red signal, is there also green signal?' This approach requires that images be pre-processed to exclude any background signal, coming from cytosolic staining or from the electronics within the system.

The real shortcoming of the PCC and MOC in image analysis is the need to threshold images prior to their analysis. The process of thresholding requires manually interacting with the image to (typically arbitrarily) determine what constitutes as noise vs. signal. When performing quantitative analysis on images collected from a large numbers of cells, it is time consuming and difficult to uniformly apply thresholding techniques. Additionally, performing statistical analysis on mean correlational scores yields a value with unclear meaning for the physical world of cells.

1.6. Central Hypothesis

With the discovery of several ARF-dependent adaptors and lack of conserved role for clathrin, a newer three-component model for cargo selection and budding has emerged that involves the recruitment of adaptors to a membrane containing activated ARF, and coordination of the localized adaptor to its cognate cargo. This is a central tenet of models of cargo

selection/concentration and carrier biogenesis today yet the details of the roles played by ARFs are incomplete. Carrier biogenesis is likely a stochastic process that is initiated by increasing cargo concentration and current models of molecular membrane traffic are likely hampered by the very limited number of cargos that have been studied in any detail. What is the signal to activate an ARF GEF? Is there specificity for the different ARF isoforms at different membranes? Do ARF GEFs or ARF GAPs participate directly in carrier biogenesis via direct interactions with components other than ARFs? Do different ARF-dependent adaptors work in concert for a single cargo, antagonistically, or independently at one membrane site? Do ARFs work as homo- or hetero-dimers?

It is clear that ARF-dependent adaptors play dual roles in cargo sorting and recruitment of accessory proteins that are important to maturation and traffic of the mature carriers of membrane traffic. Each family of monomeric or multimeric adaptors contains multiple domains that are used to coordinate these functions. While functionally analogous mechanisms are beginning to emerge amongst the different adaptors, we still lack many important details that should come in the near future. These details are predicted to give researchers unprecedented control over membrane traffic, and tools to design the means to alter traffic in ways that will be beneficial in a clinical setting.

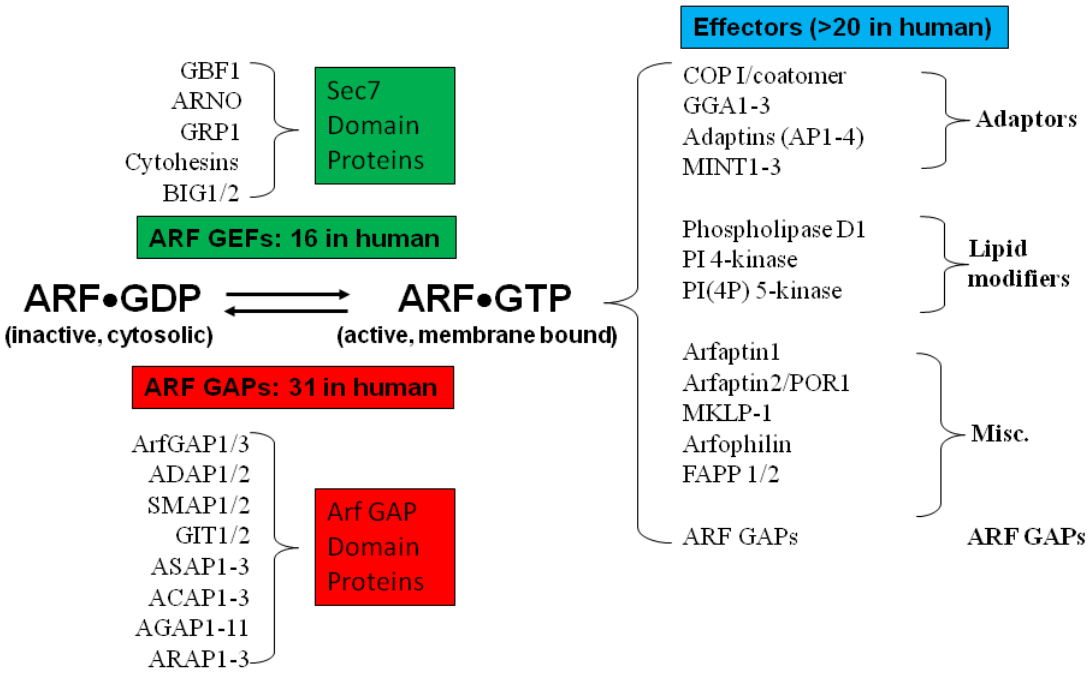

Figure 1.1 *ARFs interact with many regulatory proteins, including families of ARF GEFs and ARF GAPs, and a large variety of effectors.* The ARF GEFs mediate the release of GDP and binding of GTP to form the activated, membrane bound ARF. ARF GAPs promote the hydrolysis of the bound GTP and return the ARF to its basal state and release from the membrane. Activated, GTP-bound ARFs bind four groups of effectors that mediate the actions of ARFs in cells, including the ARF-dependent adaptors, lipid modifying enzymes, miscellaneous partners, and ARF GAPs. See the text for details.

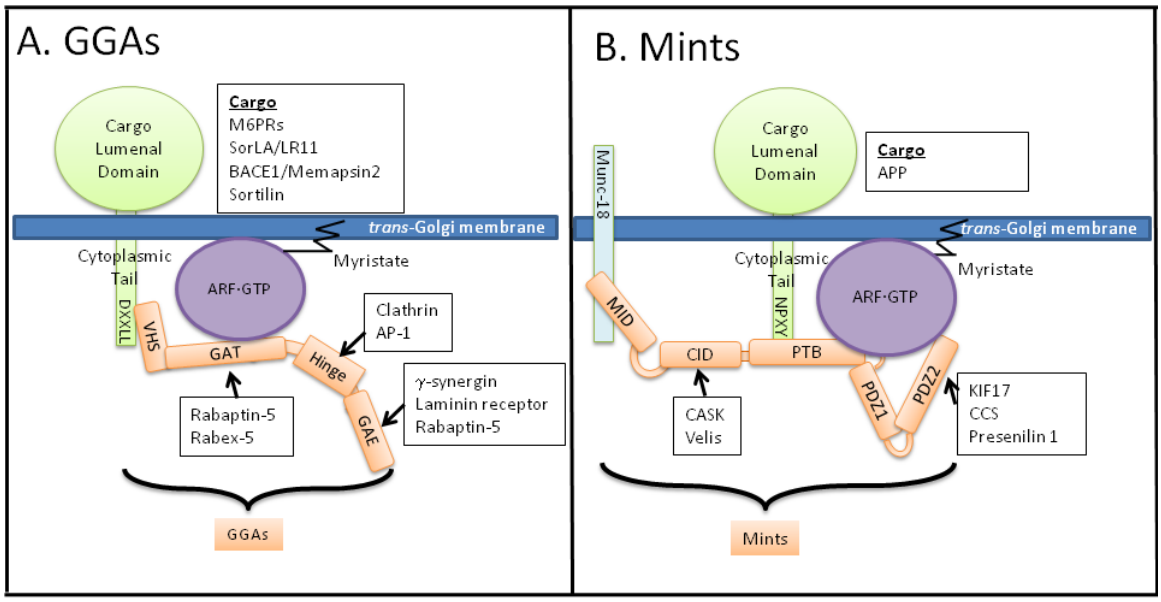

Figure 1.2: *Schematic representation of the role of ARFs in coordinating the recruitment of multi-domain, monomeric adaptors with transmembrane cargoes to initiate their sorting and inclusion into carriers of membrane traffic.* (**A**) The four domains of GGAs are shown along with their binding partners. The VHS domain binds the DXXLL motif in cargo, the GAT domain binds ARFs and other partners, the Hinge domain binds clathrin and AP-1, and the GAE domain binds accessory proteins with ill-defined functions. All three GGAs share the same domains and closely related functions. (**B**) Mints perform homologous roles to GGAs, with up to five domains. The PTB and PDZ domains bind cargo and ARFs, along with other proteins, and are present in all three Mints. Only Mint1 contains the CASK interacting domain (CID) and is capable of incorporation into the trimeric Mint1/CASK/Velis complex. Mint1 and Mint2 share the conserved Munc18-interacting domain (MID) that mediates binding to the ortholog of SEC1/SLY1 family of transmembrane proteins, in this case active in synaptic transmission.

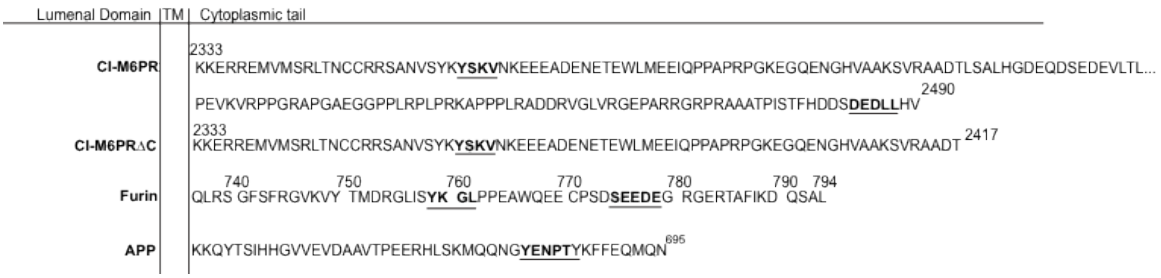

Figure 1.3. *Schematic of sorting signals in the cytoplasmic tails of cargos.* Relevant motifs are underlined, and in bold font. The Ci-M6PR contains a tyrosine based motif, as well as an acidic dileucine motif. The CI-M6PRΔC cargo contains only a tyrosine-based motif, as the acidic dileucine motif has been truncated. Furin contains a tyrosine motif, as well as an acidic cluster, and APP contains the canonical Mint3 binding motif YENPTY.

Antonny, B., S. Beraud-Dufour, P. Chardin and M. Chabre (1997). "N-terminal hydrophobic residues of the G-protein ADP-ribosylation factor-1 insert into membrane phospholipids upon GDP to GTP exchange." Biochemistry **36**(15): 4675-4684.
Aridor, M. and L. M. Traub (2002). "Cargo selection in vesicular transport: the making and breaking of a coat." Traffic **3**(8): 537-546.
Barlowe, C., L. Orci, T. Yeung, M. Hosobuchi, S. Hamamoto, N. Salama, M. F. Rexach, M. Ravazzola, M. Amherdt and R. Schekman (1994). "COPII: a membrane coat formed by Sec proteins that drive vesicle budding from the endoplasmic reticulum." Cell **77**(6): 895-907.
Boehm, M. and J. S. Bonifacino (2001). "Adaptins: the final recount." Mol Biol Cell **12**(10): 2907-2920.
Boman, A. L., J. Kuai, X. Zhu, J. Chen, R. Kuriyama and R. A. Kahn (1999). "Arf proteins bind to mitotic kinesin-like protein 1 (MKLP1) in a GTP-dependent fashion." Cell Motil Cytoskeleton **44**(2): 119-132.
Boman, A. L., P. D. Salo, M. J. Hauglund, N. L. Strand, S. J. Rensink and O. Zhdankina (2002). "ADP-ribosylation factor (ARF) interaction is not sufficient for yeast GGA protein function or localization." Mol Biol Cell **13**(9): 3078-3095.
Boman, A. L., C. Zhang, X. Zhu and R. A. Kahn (2000). "A family of ADP-ribosylation factor effectors that can alter membrane transport through the trans-Golgi." Mol Biol Cell **11**(4): 1241-1255.
Bonifacino, J. S. (2004). "The GGA proteins: adaptors on the move." Nat Rev Mol Cell Biol **5**(1): 23-32.
Borg, J. P., J. Ooi, E. Levy and B. Margolis (1996). "The phosphotyrosine interaction domains of X11 and FE65 bind to distinct sites on the YENPTY motif of amyloid precursor protein." Mol Cell Biol **16**(11): 6229-6241.
Bowzard, J. B., D. Cheng, J. Peng and R. A. Kahn (2007). "ELMOD2 is an Arl2 GTPase-activating protein that also acts on Arfs." J Biol Chem **282**(24): 17568-17580.
Brown, H. A., S. Gutowski, C. R. Moomaw, C. Slaughter and P. C. Sternweis (1993). "ADP-ribosylation factor, a small GTP-dependent regulatory protein, stimulates phospholipase D activity." Cell **75**(6): 1137-1144.
Bui, Q. T., M. P. Golinelli-Cohen and C. L. Jackson (2009). "Large Arf1 guanine nucleotide exchange factors: evolution, domain structure, and roles in membrane trafficking and human disease." Mol Genet Genomics **282**(4): 329-350.
Burd, C. G., T. I. Strochlic and S. R. Gangi Setty (2004). "Arf-like GTPases: not so Arf-like after all." Trends Cell Biol **14**(12): 687-694.
Burgos, P. V., G. A. Mardones, A. L. Rojas, L. L. daSilva, Y. Prabhu, J. H. Hurley and J. S. Bonifacino (2010). "Sorting of the Alzheimer's disease amyloid precursor protein mediated by the AP-4 complex." Dev Cell **18**(3): 425-436.
Canfield, W. M., K. F. Johnson, R. D. Ye, W. Gregory and S. Kornfeld (1991). "Localization of the signal for rapid internalization of the bovine cation-independent mannose 6-phosphate/insulin-like growth factor-II receptor to amino acids 24-29 of the cytoplasmic tail." J Biol Chem **266**(9): 5682-5688.
Caspary, T., C. E. Larkins and K. V. Anderson (2007). "The graded response to Sonic Hedgehog depends on cilia architecture." Dev Cell **12**(5): 767-778.
Cassel, D. (2003). Arf GTPase-Activating Protein-1, Kluwer Academic Publishers.

Caster, A. H. and R. A. Kahn (2010). Roles for ADP-RIbosylation Factors in Membrane Traffic. Handbook of Cell Signaling. R. A. Bradshaw and E. A. Dennis, Elsevier**:** 1803-1812.
Cavenagh, M. M., J. A. Whitney, K. Carroll, C. Zhang, A. L. Boman, A. G. Rosenwald, I. Mellman and R. A. Kahn (1996). "Intracellular distribution of Arf proteins in mammalian cells. Arf6 is uniquely localized to the plasma membrane." J Biol Chem **271**(36): 21767-21774.
Chang, M. P., W. G. Mallet, K. E. Mostov and F. M. Brodsky (1993). "Adaptor self-aggregation, adaptor-receptor recognition and binding of alpha-adaptin subunits to the plasma membrane contribute to recruitment of adaptor (AP2) components of clathrin-coated pits." Embo J **12**(5): 2169-2180.
Cherfils, J. and P. Chardin (1999). "GEFs: structural basis for their activation of small GTP-binding proteins." Trends Biochem Sci **24**(8): 306-311.
Choy, R. W., Z. Cheng and R. Schekman (2012). "Amyloid precursor protein (APP) traffics from the cell surface via endosomes for amyloid beta (Abeta) production in the trans-Golgi network." Proc Natl Acad Sci U S A **109**(30): E2077-2082.
Christis, C. and S. Munro (2012). "The small G protein Arl1 directs the trans-Golgi-specific targeting of the Arf1 exchange factors BIG1 and BIG2." J Cell Biol **196**(3): 327-335.
Citron, M., T. Oltersdorf, C. Haass, L. McConlogue, A. Y. Hung, P. Seubert, C. Vigo-Pelfrey, I. Lieberburg and D. J. Selkoe (1992). "Mutation of the beta-amyloid precursor protein in familial Alzheimer's disease increases beta-protein production." Nature **360**(6405): 672-674.
Claing, A. (2004). "Regulation of G protein-coupled receptor endocytosis by ARF6 GTP-binding proteins." Biochem Cell Biol **82**(6): 610-617.
Claude, A., B. P. Zhao, C. E. Kuziemsky, S. Dahan, S. J. Berger, J. P. Yan, A. D. Armold, E. M. Sullivan and P. Melancon (1999). "GBF1: A novel Golgi-associated BFA-resistant guanine nucleotide exchange factor that displays specificity for ADP-ribosylation factor 5." J Cell Biol **146**(1): 71-84.
Cockcroft, S., G. M. Thomas, A. Fensome, B. Geny, E. Cunningham, I. Gout, I. Hiles, N. F. Totty, O. Truong and J. J. Hsuan (1994). "Phospholipase D: a downstream effector of ARF in granulocytes." Science **263**(5146): 523-526.
Cunningham, L. A. and R. A. Kahn (2008). "Cofactor D functions as a centrosomal protein and is required for the recruitment of the gamma-tubulin ring complex at centrosomes and organization of the mitotic spindle." J Biol Chem **283**(11): 7155-7165.
Cupers, P., M. Bentahir, K. Craessaerts, I. Orlans, H. Vanderstichele, P. Saftig, B. De Strooper and W. Annaert (2001). "The discrepancy between presenilin subcellular localization and gamma-secretase processing of amyloid precursor protein." J Cell Biol **154**(4): 731-740.
Dahms, N. M., P. Lobel and S. Kornfeld (1989). "Mannose 6-phosphate receptors and lysosomal enzyme targeting." J Biol Chem **264**(21): 12115-12118.
Dell'Angelica, E. C., J. Klumperman, W. Stoorvogel and J. S. Bonifacino (1998). "Association of the AP-3 adaptor complex with clathrin." Science **280**(5362): 431-434.
Dell'Angelica, E. C., R. Puertollano, C. Mullins, R. C. Aguilar, J. D. Vargas, L. M. Hartnell and J. S. Bonifacino (2000). "GGAs: a family of ADP ribosylation factor-

binding proteins related to adaptors and associated with the Golgi complex." J Cell Biol **149**(1): 81-94.
Diaz, E. and S. R. Pfeffer (1998). "TIP47: a cargo selection device for mannose 6-phosphate receptor trafficking." Cell **93**(3): 433-443.
Donaldson, J. G. (2003). "Multiple roles for Arf6: sorting, structuring, and signaling at the plasma membrane." J Biol Chem **278**(43): 41573-41576.
Donaldson, J. G., D. Finazzi and R. D. Klausner (1992). "Brefeldin A inhibits Golgi membrane-catalysed exchange of guanine nucleotide onto ARF protein." Nature **360**(6402): 350-352.
Donaldson, J. G. and C. L. Jackson (2000). "Regulators and effectors of the ARF GTPases." Curr Opin Cell Biol **12**(4): 475-482.
Donaldson, J. G., R. A. Kahn, J. Lippincott-Schwartz and R. D. Klausner (1991). "Binding of ARF and beta-COP to Golgi membranes: possible regulation by a trimeric G protein." Science **254**(5035): 1197-1199.
Dong, J. H., J. F. Wen and H. F. Tian (2007). "Homologs of eukaryotic Ras superfamily proteins in prokaryotes and their novel phylogenetic correlation with their eukaryotic analogs." Gene **396**(1): 116-124.
Doray, B., K. Bruns, P. Ghosh and S. Kornfeld (2002). "Interaction of the cation-dependent mannose 6-phosphate receptor with GGA proteins." J Biol Chem **277**(21): 18477-18482.
Doray, B., K. Bruns, P. Ghosh and S. A. Kornfeld (2002). "Autoinhibition of the ligand-binding site of GGA1/3 VHS domains by an internal acidic cluster-dileucine motif." Proc Natl Acad Sci U S A **99**(12): 8072-8077.
Doray, B., P. Ghosh, J. Griffith, H. J. Geuze and S. Kornfeld (2002). "Cooperation of GGAs and AP-1 in packaging MPRs at the trans-Golgi network." Science **297**(5587): 1700-1703.
Enomoto, K. and D. M. Gill (1980). "Cholera toxin activation of adenylate cyclase. Roles of nucleoside triphosphates and a macromolecular factor in the ADP ribosylation of the GTP-dependent regulatory component." J Biol Chem **255**(4): 1252-1258.
Eskelinen, E. L., C. Meyer, H. Ohno, K. von Figura and P. Schu (2002). "The polarized epithelia-specific mu 1B-adaptin complements mu 1A-deficiency in fibroblasts." EMBO Rep **3**(5): 471-477.
Fan, Y., M. A. Esmail, S. J. Ansley, O. E. Blacque, K. Boroevich, A. J. Ross, S. J. Moore, J. L. Badano, H. May-Simera, D. S. Compton, J. S. Green, R. A. Lewis, M. M. van Haelst, P. S. Parfrey, D. L. Baillie, P. L. Beales, N. Katsanis, W. S. Davidson and M. R. Leroux (2004). "Mutations in a member of the Ras superfamily of small GTP-binding proteins causes Bardet-Biedl syndrome." Nat Genet **36**(9): 989-993.
Faundez, V., J. T. Horng and R. B. Kelly (1998). "A function for the AP3 coat complex in synaptic vesicle formation from endosomes." Cell **93**(3): 423-432.
Ghosh, P. and S. Kornfeld (2003). "Phosphorylation-induced conformational changes regulate GGAs 1 and 3 function at the trans-Golgi network." J Biol Chem **278**(16): 14543-14549.
Godi, A., Di Campli, A., Konstantakopoulos, A., Di Tullio, G., Alessi, DR., Kular, GS., Daniele, T., Marra, P., Lucocq, JM., De Matteis, A. (2004). "FAPPs control Golgi-to-cell-surface membrane traffic by binding to ARF and PtdIns(4)P." Nat Cell Biol **6**: 393-404.

Godi, A., P. Pertile, R. Meyers, P. Marra, G. Di Tullio, C. Iurisci, A. Luini, D. Corda and M. A. De Matteis (1999). "ARF mediates recruitment of PtdIns-4-OH kinase-beta and stimulates synthesis of PtdIns(4,5)P2 on the Golgi complex." Nat Cell Biol **1**(5): 280-287.
Godi, A., I. Santone, P. Pertile, P. Devarajan, P. R. Stabach, J. S. Morrow, G. Di Tullio, R. Polishchuk, T. C. Petrucci, A. Luini and M. A. De Matteis (1998). "ADP ribosylation factor regulates spectrin binding to the Golgi complex." Proc Natl Acad Sci U S A **95**(15): 8607-8612.
Gotoh, B., Y. Ohnishi, N. M. Inocencio, E. Esaki, K. Nakayama, P. J. Barr, G. Thomas and Y. Nagai (1992). "Mammalian subtilisin-related proteinases in cleavage activation of the paramyxovirus fusion glycoprotein: superiority of furin/PACE to PC2 or PC1/PC3." J Virol **66**(11): 6391-6397.
Han, J., Y. Wang, S. Wang and C. Chi (2008). "Interaction of Mint3 with Furin regulates the localization of Furin in the trans-Golgi network." Journal of Cell Science **121**(Pt 13): 2217-2223.
Hill, K., Y. Li, M. Bennett, M. McKay, X. Zhu, J. Shern, E. Torre, J. J. Lah, A. I. Levey and R. A. Kahn (2003). "Munc18 interacting proteins: ADP-ribosylation factor-dependent coat proteins that regulate the traffic of beta-Alzheimer's precursor protein." J Biol Chem **278**(38): 36032-36040.
Hirst, J., L. D. Barlow, G. C. Francisco, D. A. Sahlender, M. N. Seaman, J. B. Dacks and M. S. Robinson (2011). "The fifth adaptor protein complex." PLoS Biol **9**(10): e1001170.
Hirst, J., C. Irving and G. H. Borner (2013). "Adaptor protein complexes AP-4 and AP-5: new players in endosomal trafficking and progressive spastic paraplegia." Traffic **14**(2): 153-164.
Hirst, J., W. W. Lui, N. A. Bright, N. Totty, M. N. Seaman and M. S. Robinson (2000). "A family of proteins with gamma-adaptin and VHS domains that facilitate trafficking between the trans-Golgi network and the vacuole/lysosome." J Cell Biol **149**(1): 67-80.
Hirst, J., M. N. Seaman, S. I. Buschow and M. S. Robinson (2007). "The role of cargo proteins in GGA recruitment." Traffic **8**(5): 594-604.
Honda, A., M. Nogami, T. Yokozeki, M. Yamazaki, H. Nakamura, H. Watanabe, K. Kawamoto, K. Nakayama, A. J. Morris, M. A. Frohman and Y. Kanaho (1999). "Phosphatidylinositol 4-phosphate 5-kinase alpha is a downstream effector of the small G protein ARF6 in membrane ruffle formation." Cell **99**(5): 521-532.
Hunzicker-Dunn, M., V. V. Gurevich, J. E. Casanova and S. Mukherjee (2002). "ARF6: a newly appreciated player in G protein-coupled receptor desensitization." FEBS Lett **521**(1-3): 3-8.
Jackson, C. L. and J. E. Casanova (2000). "Turning on ARF: the Sec7 family of guanine-nucleotide-exchange factors." Trends Cell Biol **10**(2): 60-67.
Jadot, M., W. M. Canfield, W. Gregory and S. Kornfeld (1992). "Characterization of the signal for rapid internalization of the bovine mannose 6-phosphate/insulin-like growth factor-II receptor." J Biol Chem **267**(16): 11069-11077.
Johnson, K. F., W. Chan and S. Kornfeld (1990). "Cation-dependent mannose 6-phosphate receptor contains two internalization signals in its cytoplasmic domain." Proc Natl Acad Sci U S A **87**(24): 10010-10014.

Jones, H. D., J. Moss and M. Vaughan (2005). "BIG1 and BIG2, brefeldin A-inhibited guanine nucleotide-exchange factors for ADP-ribosylation factors." Methods Enzymol **404**: 174-184.
Kaech, S. M., C. W. Whitfield and S. K. Kim (1998). "The LIN-2/LIN-7/LIN-10 complex mediates basolateral membrane localization of the C. elegans EGF receptor LET-23 in vulval epithelial cells." Cell **94**(6): 761-771.
Kahn, R. A., Ed. (2003). ARF Family GTPases. Proteins and Cell Regulation, Kluwer Academic Publishers.
Kahn, R. A., E. Bruford, H. Inoue, J. M. Logsdon, Jr., Z. Nie, R. T. Premont, P. A. Randazzo, M. Satake, A. B. Theibert, M. L. Zapp and D. Cassel (2008). "Consensus nomenclature for the human ArfGAP domain-containing proteins." J Cell Biol **182**(6): 1039-1044.
Kahn, R. A., J. Cherfils, M. Elias, R. C. Lovering, S. Munro and A. Schurmann (2006). "Nomenclature for the human Arf family of GTP-binding proteins: ARF, ARL, and SAR proteins." J Cell Biol **172**(5): 645-650.
Kahn, R. A. and A. G. Gilman (1984). "Purification of a protein cofactor required for ADP-ribosylation of the stimulatory regulatory component of adenylate cyclase by cholera toxin." J Biol Chem **259**(10): 6228-6234.
Kahn, R. A., C. Goddard and M. Newkirk (1988). "Chemical and immunological characterization of the 21-kDa ADP-ribosylation factor of adenylate cyclase." J Biol Chem **263**(17): 8282-8287.
Kahn, R. A., F. G. Kern, J. Clark, E. P. Gelmann and C. Rulka (1991). "Human ADP-ribosylation factors. A functionally conserved family of GTP-binding proteins." J Biol Chem **266**(4): 2606-2614.
Kam, J. L., K. Miura, T. R. Jackson, J. Gruschus, P. Roller, S. Stauffer, J. Clark, R. Aneja and P. A. Randazzo (2000). "Phosphoinositide-dependent activation of the ADP-ribosylation factor GTPase-activating protein ASAP1. Evidence for the pleckstrin homology domain functioning as an allosteric site." J Biol Chem **275**(13): 9653-9663.
Kato, Y., S. Misra, R. Puertollano, J. H. Hurley and J. S. Bonifacino (2002). "Phosphoregulation of sorting signal-VHS domain interactions by a direct electrostatic mechanism." Nat Struct Biol **9**(7): 532-536.
Keen, J. H., M. C. Willingham and I. H. Pastan (1979). "Clathrin-coated vesicles: isolation, dissociation and factor-dependent reassociation of clathrin baskets." Cell **16**(2): 303-312.
Kim, J., B. Kleizen, R. Choy, G. Thinakaran, S. S. Sisodia and R. W. Schekman (2007). "Biogenesis of gamma-secretase early in the secretory pathway." J Cell Biol **179**(5): 951-963.
Kim, S. H., J. J. Lah, G. Thinakaran, A. Levey and S. S. Sisodia (2000). "Subcellular localization of presenilins: association with a unique membrane pool in cultured cells." Neurobiol Dis **7**(2): 99-117.
Knuehl, C., C. Y. Chen, V. Manalo, P. K. Hwang, N. Ota and F. M. Brodsky (2006). "Novel binding sites on clathrin and adaptors regulate distinct aspects of coat assembly." Traffic **7**(12): 1688-1700.
Koo, E. H., S. S. Sisodia, D. R. Archer, L. J. Martin, A. Weidemann, K. Beyreuther, P. Fischer, C. L. Masters and D. L. Price (1990). "Precursor of amyloid protein in Alzheimer

disease undergoes fast anterograde axonal transport." Proc Natl Acad Sci U S A **87**(4): 1561-1565.
Ktistakis, N. T., H. A. Brown, P. C. Sternweis and M. G. Roth (1995). "Phospholipase D is present on Golgi-enriched membranes and its activation by ADP ribosylation factor is sensitive to brefeldin A." Proc Natl Acad Sci U S A **92**(11): 4952-4956.
Ktistakis, N. T., H. A. Brown, M. G. Waters, P. C. Sternweis and M. G. Roth (1996). "Evidence that phospholipase D mediates ADP ribosylation factor-dependent formation of Golgi coated vesicles." J Cell Biol **134**(2): 295-306.
Kuge, O., C. Dascher, L. Orci, T. Rowe, M. Amherdt, H. Plutner, M. Ravazzola, G. Tanigawa, J. E. Rothman and W. E. Balch (1994). "Sar1 promotes vesicle budding from the endoplasmic reticulum but not Golgi compartments." J Cell Biol **125**(1): 51-65.
Lau, K. F., D. M. McLoughlin, C. Standen and C. C. Miller (2000). "X11 alpha and x11 beta interact with presenilin-1 via their PDZ domains." Mol Cell Neurosci **16**(5): 557-565.
Lee, C. M., R. S. Haun, S. C. Tsai, J. Moss and M. Vaughan (1992). "Characterization of the human gene encoding ADP-ribosylation factor 1, a guanine nucleotide-binding activator of cholera toxin." J Biol Chem **267**(13): 9028-9034.
Lee, F. J., J. Moss and M. Vaughan (1992). "Human and Giardia ADP-ribosylation factors (ARFs) complement ARF function in Saccharomyces cerevisiae." J Biol Chem **267**(34): 24441-24445.
Lee, M. C., E. A. Miller, J. Goldberg, L. Orci and R. Schekman (2004). "Bi-directional protein transport between the ER and Golgi." Annu Rev Cell Dev Biol **20**: 87-123.
Li, Y., W. G. Kelly, J. M. Logsdon, Jr., A. M. Schurko, B. D. Harfe, K. L. Hill-Harfe and R. A. Kahn (2004). "Functional genomic analysis of the ADP-ribosylation factor family of GTPases: phylogeny among diverse eukaryotes and function in C. elegans." Faseb J **18**(15): 1834-1850.
Lobel, P., K. Fujimoto, R. D. Ye, G. Griffiths and S. Kornfeld (1989). "Mutations in the cytoplasmic domain of the 275 kDa mannose 6-phosphate receptor differentially alter lysosomal enzyme sorting and endocytosis." Cell **57**(5): 787-796.
Logsdon, J. M. a. K., R.A (2003). ARF Family GTPases, Kluwer Academic Publishers.
Lowery, J., T. Szul, M. Styers, Z. Holloway, V. Oorschot, J. Klumperman and E. Sztul (2013). "The Sec7 guanine nucleotide exchange factor GBF1 regulates membrane recruitment of BIG1 and BIG2 guanine nucleotide exchange factors to the trans-Golgi network (TGN)." J Biol Chem **288**(16): 11532-11545.
Mansour, S. J., J. Skaug, X. H. Zhao, J. Giordano, S. W. Scherer and P. Melancon (1999). "p200 ARF-GEP1: a Golgi-localized guanine nucleotide exchange protein whose Sec7 domain is targeted by the drug brefeldin A." Proc Natl Acad Sci U S A **96**(14): 7968-7973.
Martin, A., F. D. Brown, M. N. Hodgkin, A. J. Bradwell, S. J. Cook, M. Hart and M. J. Wakelam (1996). "Activation of phospholipase D and phosphatidylinositol 4-phosphate 5-kinase in HL60 membranes is mediated by endogenous Arf but not Rho." J Biol Chem **271**(29): 17397-17403.
Mattera, R., C. N. Arighi, R. Lodge, M. Zerial and J. S. Bonifacino (2003). "Divalent interaction of the GGAs with the Rabaptin-5-Rabex-5 complex." Embo J **22**(1): 78-88.
McKay, M. M. and R. A. Kahn (2004). "Multiple phosphorylation events regulate the subcellular localization of GGA1." Traffic **5**(2): 102-116.

McLoughlin, D. M., N. G. Irving, J. Brownlees, J. P. Brion, K. Leroy and C. C. Miller (1999). "Mint2/X11-like colocalizes with the Alzheimer's disease amyloid precursor protein and is associated with neuritic plaques in Alzheimer's disease." Eur J Neurosci **11**(6): 1988-1994.
McLoughlin, D. M., C. L. Standen, K. F. Lau, S. Ackerley, T. P. Bartnikas, J. D. Gitlin and C. C. Miller (2001). "The neuronal adaptor protein X11alpha interacts with the copper chaperone for SOD1 and regulates SOD1 activity." J Biol Chem **276**(12): 9303-9307.
Medigeshi, G. R. and P. Schu (2003). "Characterization of the in vitro retrograde transport of MPR46." Traffic **4**(11): 802-811.
Memon, A. R. (2004). "The role of ADP-ribosylation factor and SAR1 in vesicular trafficking in plants." Biochim Biophys Acta **1664**(1): 9-30.
Meyer, C., D. Zizioli, S. Lausmann, E. L. Eskelinen, J. Hamann, P. Saftig, K. von Figura and P. Schu (2000). mu1A-adaptin-deficient mice: lethality, loss of AP-1 binding and rerouting of mannose 6-phosphate receptors. EMBO J. **19:** 2193-2203.
Mills, I. G., G. J. Praefcke, Y. Vallis, B. J. Peter, L. E. Olesen, J. L. Gallop, P. J. Butler, P. R. Evans and H. T. McMahon (2003). "EpsinR: an AP1/clathrin interacting protein involved in vesicle trafficking." J Cell Biol **160**(2): 213-222.
Molloy, S. S., L. Thomas, J. K. VanSlyke, P. E. Stenberg and G. Thomas (1994). "Intracellular trafficking and activation of the furin proprotein convertase: localization to the TGN and recycling from the cell surface." EMBO J **13**(1): 18-33.
Moss, J. and M. Vaughan (1977). "Choleragen activation of solubilized adenylate cyclase: requirement for GTP and protein activator for demonstration of enzymatic activity." Proc Natl Acad Sci U S A **74**(10): 4396-4400.
Munro, S. (2005). "The Arf-like GTPase Arl1 and its role in membrane traffic." Biochem Soc Trans **33**(Pt 4): 601-605.
Nadimpalli, S. K. and P. K. Amancha (2010). "Evolution of mannose 6-phosphate receptors (MPR300 and 46): lysosomal enzyme sorting proteins." Curr Protein Pept Sci **11**(1): 68-90.
Nakatsu, F., T. Kadohira, D. J. Gilbert, N. A. Jenkins, H. Kakuta, N. G. Copeland, T. Saito and H. Ohno (1999). "Genomic structure and chromosome mapping of the genes encoding clathrin-associated adaptor medium chains mu1A (Ap1m1) and mu1B (Ap1m2)." Cytogenet Cell Genet **87**(1-2): 53-58.
Nishikawa, S. and A. Nakano (1991). "The GTP-binding Sar1 protein is localized to the early compartment of the yeast secretory pathway." Biochim Biophys Acta **1093**(2-3): 135-143.
Ohno, H., T. Tomemori, F. Nakatsu, Y. Okazaki, R. C. Aguilar, H. Foelsch, I. Mellman, T. Saito, T. Shirasawa and J. S. Bonifacino (1999). "Mu1B, a novel adaptor medium chain expressed in polarized epithelial cells." FEBS Lett **449**(2-3): 215-220.
Okamoto, M. and T. C. Sudhof (1997). "Mints, Munc18-interacting proteins in synaptic vesicle exocytosis." J Biol Chem **272**(50): 31459-31464.
Okamoto, M. and T. C. Sudhof (1998). "Mint 3: a ubiquitous mint isoform that does not bind to munc18-1 or -2." Eur J Cell Biol **77**(3): 161-165.
Padilla, P. I., G. Pacheco-Rodriguez, J. Moss and M. Vaughan (2004). "Nuclear localization and molecular partners of BIG1, a brefeldin A-inhibited guanine nucleotide-

exchange protein for ADP-ribosylation factors." Proc Natl Acad Sci U S A **101**(9): 2752-2757.
Panic, B., J. R. Whyte and S. Munro (2003). "The ARF-like GTPases Arl1p and Arl3p act in a pathway that interacts with vesicle-tethering factors at the Golgi apparatus." Curr Biol **13**(5): 405-410.
Pasqualato, S., L. Renault and J. Cherfils (2002). "Arf, Arl, Arp and Sar proteins: a family of GTP-binding proteins with a structural device for 'front-back' communication." EMBO Rep **3**(11): 1035-1041.
Pearse, B. M. (1976). "Clathrin: a unique protein associated with intracellular transfer of membrane by coated vesicles." Proc Natl Acad Sci U S A **73**(4): 1255-1259.
Pearse, B. M. and M. S. Robinson (1984). "Purification and properties of 100-kDa proteins from coated vesicles and their reconstitution with clathrin." Embo J **3**(9): 1951-1957.
Puertollano, R., R. C. Aguilar, I. Gorshkova, R. J. Crouch and J. S. Bonifacino (2001). "Sorting of mannose 6-phosphate receptors mediated by the GGAs." Science **292**(5522): 1712-1716.
Rajendran, L. and W. Annaert (2012). "Membrane trafficking pathways in Alzheimer's disease." Traffic **13**(6): 759-770.
Randazzo, P. A. and R. A. Kahn (1994). "GTP hydrolysis by ADP-ribosylation factor is dependent on both an ADP-ribosylation factor GTPase-activating protein and acid phospholipids." J Biol Chem **269**(14): 10758-10763.
Randazzo, P. A., Z. Nie, K. Miura and V. W. Hsu (2000). "Molecular aspects of the cellular activities of ADP-ribosylation factors." Sci STKE **2000**(59): RE1.
Regazzi, R., S. Ullrich, R. A. Kahn and C. B. Wollheim (1991). "Redistribution of ADP-ribosylation factor during stimulation of permeabilized cells with GTP analogues." Biochem J **275 (Pt 3)**: 639-644.
Robinson, M. S. (1990). "Cloning and expression of gamma-adaptin, a component of clathrin-coated vesicles associated with the Golgi apparatus." J Cell Biol **111**(6 Pt 1): 2319-2326.
Robinson, M. S. (1993). "Assembly and targeting of adaptin chimeras in transfected cells." J Cell Biol **123**(1): 67-77.
Robinson, M. S. and B. M. Pearse (1986). "Immunofluorescent localization of 100K coated vesicle proteins." J Cell Biol **102**(1): 48-54.
Rowe, T., M. Aridor, J. M. McCaffery, H. Plutner, C. Nuoffer and W. E. Balch (1996). "COPII vesicles derived from mammalian endoplasmic reticulum microsomes recruit COPI." J Cell Biol **135**(4): 895-911.
Salazar, G., B. Craige, B. H. Wainer, J. Guo, P. De Camilli and V. Faundez (2005). "Phosphatidylinositol-4-kinase type II alpha is a component of adaptor protein-3-derived vesicles." Mol Biol Cell **16**(8): 3692-3704.
Schafer, W., A. Stroh, S. Berghofer, J. Seiler, M. Vey, M. L. Kruse, H. F. Kern, H. D. Klenk and W. Garten (1995). "Two independent targeting signals in the cytoplasmic domain determine trans-Golgi network localization and endosomal trafficking of the proprotein convertase furin." EMBO J **14**(11): 2424-2435.
Scott, G. K., H. Fei, L. Thomas, G. R. Medigeshi and G. Thomas (2006). "A PACS-1, GGA3 and CK2 complex regulates CI-MPR trafficking." EMBO J **25**(19): 4423-4435.

Scott, G. K., F. Gu, C. M. Crump, L. Thomas, L. Wan, Y. Xiang and G. Thomas (2003). "The phosphorylation state of an autoregulatory domain controls PACS-1-directed protein traffic." EMBO J **22**(23): 6234-6244.
Serafini, T., L. Orci, M. Amherdt, M. Brunner, R. A. Kahn and J. E. Rothman (1991). "ADP-ribosylation factor is a subunit of the coat of Golgi-derived COP-coated vesicles: a novel role for a GTP-binding protein." Cell **67**(2): 239-253.
Setou, M., T. Nakagawa, D. H. Seog and N. Hirokawa (2000). "Kinesin superfamily motor protein KIF17 and mLin-10 in NMDA receptor-containing vesicle transport." Science **288**(5472): 1796-1802.
Setty, S. R., M. E. Shin, A. Yoshino, M. S. Marks and C. G. Burd (2003). "Golgi recruitment of GRIP domain proteins by Arf-like GTPase 1 is regulated by Arf-like GTPase 3." Curr Biol **13**(5): 401-404.
Sharer, J. D., J. F. Shern, H. Van Valkenburgh, D. C. Wallace and R. A. Kahn (2002). "ARL2 and BART enter mitochondria and bind the adenine nucleotide transporter." Mol Biol Cell **13**(1): 71-83.
Shin, H. W., N. Morinaga, M. Noda and K. Nakayama (2004). "BIG2, a guanine nucleotide exchange factor for ADP-ribosylation factors: its localization to recycling endosomes and implication in the endosome integrity." Mol Biol Cell **15**(12): 5283-5294.
Shin, O. H. and J. H. Exton (2001). "Differential binding of arfaptin 2/POR1 to ADP-ribosylation factors and Rac1." Biochem Biophys Res Commun **285**(5): 1267-1273.
Shin, O. H., A. H. Ross, I. Mihai and J. H. Exton (1999). "Identification of arfophilin, a target protein for GTP-bound class II ADP-ribosylation factors." J Biol Chem **274**(51): 36609-36615.
Shrivastava-Ranjan, P., V. Faundez, G. Fang, H. Rees, J. J. Lah, A. I. Levey and R. A. Kahn (2008). "Mint3/X11{gamma} Is an ADP-Ribosylation Factor-dependent Adaptor that Regulates the Traffic of the Alzheimer's Precursor Protein from the Trans-Golgi Network." Mol Biol Cell **19**(1): 51-64.
Siman, R. and J. Velji (2003). "Localization of presenilin-nicastrin complexes and gamma-secretase activity to the trans-Golgi network." J Neurochem **84**(5): 1143-1153.
Simmen, T., M. Nobile, J. S. Bonifacino and W. Hunziker (1999). "Basolateral sorting of furin in MDCK cells requires a phenylalanine-isoleucine motif together with an acidic amino acid cluster." Mol Cell Biol **19**(4): 3136-3144.
Simske, J. S., S. M. Kaech, S. A. Harp and S. K. Kim (1996). "LET-23 receptor localization by the cell junction protein LIN-7 during C. elegans vulval induction." Cell **85**(2): 195-204.
Small, S. A. and S. Gandy (2006). "Sorting through the cell biology of Alzheimer's disease: intracellular pathways to pathogenesis." Neuron **52**(1): 15-31.
Stamnes, M. A. and J. E. Rothman (1993). "The binding of AP-1 clathrin adaptor particles to Golgi membranes requires ADP-ribosylation factor, a small GTP-binding protein." Cell **73**(5): 999-1005.
Storch, S. and T. Braulke (2001). "Multiple C-terminal motifs of the 46-kDa mannose 6-phosphate receptor tail contribute to efficient binding of medium chains of AP-2 and AP-3." J Biol Chem **276**(6): 4298-4303.
Styers, M. L., Faundez, V. (2003). Heterotetrameric Coat Protein-ARF Interactions. ARF Family GTPases. R. A. Kahn. Dordrecht/Boston/London, Kluwer Academic Publishers**:** 259-281.

Tamkun, J. W., R. A. Kahn, M. Kissinger, B. J. Brizuela, C. Rulka, M. P. Scott and J. A. Kennison (1991). "The arflike gene encodes an essential GTP-binding protein in Drosophila." Proc Natl Acad Sci U S A **88**(8): 3120-3124.
Tanigawa, G., L. Orci, M. Amherdt, M. Ravazzola, J. B. Helms and J. E. Rothman (1993). "Hydrolysis of bound GTP by ARF protein triggers uncoating of Golgi-derived COP-coated vesicles." J Cell Biol **123**(6 Pt 1): 1365-1371.
Terui, T., R. A. Kahn and P. A. Randazzo (1994). "Effects of acid phospholipids on nucleotide exchange properties of ADP-ribosylation factor 1. Evidence for specific interaction with phosphatidylinositol 4,5-bisphosphate." J Biol Chem **269**(45): 28130-28135.
Teuchert, M., W. Schafer, S. Berghofer, B. Hoflack, H. D. Klenk and W. Garten (1999). "Sorting of furin at the trans-Golgi network. Interaction of the cytoplasmic tail sorting signals with AP-1 Golgi-specific assembly proteins." J Biol Chem **274**(12): 8199-8207.
Thinakaran, G. and E. H. Koo (2008). "Amyloid precursor protein trafficking, processing, and function." J Biol Chem **283**(44): 29615-29619.
Thomas, G. (2002). "Furin at the cutting edge: from protein traffic to embryogenesis and disease." Nat Rev Mol Cell Biol **3**(10): 753-766.
Togawa, A., N. Morinaga, M. Ogasawara, J. Moss and M. Vaughan (1999). "Purification and cloning of a brefeldin A-inhibited guanine nucleotide-exchange protein for ADP-ribosylation factors." J Biol Chem **274**(18): 12308-12315.
Tomita, S., Y. Kirino and T. Suzuki (1998). "Cleavage of Alzheimer's amyloid precursor protein (APP) by secretases occurs after O-glycosylation of APP in the protein secretory pathway. Identification of intracellular compartments in which APP cleavage occurs without using toxic agents that interfere with protein metabolism." J Biol Chem **273**(11): 6277-6284.
Touz, M. C., L. Kulakova and T. E. Nash (2004). "Adaptor protein complex 1 mediates the transport of lysosomal proteins from a Golgi-like organelle to peripheral vacuoles in the primitive eukaryote Giardia lamblia." Mol Biol Cell **15**(7): 3053-3060.
Vetter, I. R. and A. Wittinghofer (2001). "The guanine nucleotide-binding switch in three dimensions." Science **294**(5545): 1299-1304.
Volpicelli-Daley, L. A., Y. Li, C. J. Zhang and R. A. Kahn (2005). "Isoform-selective effects of the depletion of ADP-ribosylation factors 1-5 on membrane traffic." Mol Biol Cell **16**(10): 4495-4508.
Waters, M. G., T. Serafini and J. E. Rothman (1991). "'Coatomer': a cytosolic protein complex containing subunits of non-clathrin-coated Golgi transport vesicles." Nature **349**(6306): 248-251.
Zhang, C. J., J. B. Bowzard, A. Anido and R. A. Kahn (2003). "Four ARF GAPs in Saccharomyces cerevisiae have both overlapping and distinct functions." Yeast **20**(4): 315-330.
Zhang, Z., C. H. Lee, V. Mandiyan, J. P. Borg, B. Margolis, J. Schlessinger and J. Kuriyan (1997). "Sequence-specific recognition of the internalization motif of the Alzheimer's amyloid precursor protein by the X11 PTB domain." Embo J **16**(20): 6141-6150.
Zhou, C., L. Cunningham, A. I. Marcus, Y. Li and R. A. Kahn (2006). "Arl2 and Arl3 regulate different microtubule-dependent processes." Mol Biol Cell **17**(5): 2476-2487.

Zhu, X. and R. A. Kahn (2001). "The Escherichia coli heat labile toxin binds to Golgi membranes and alters Golgi and cell morphologies using ADP-ribosylation factor-dependent processes." J Biol Chem **276**(27): 25014-25021.

CHAPTER 2

COMPUTATIONAL METHOD FOR CALCULATING FLUORESCENCE INTENSITIES WITHIN THREE-DIMENSIONAL STRUCTURES IN CELLS[5]

[5] Reproduced and modified with permission from Caster, A. H., and Kahn, R. A. (2012) Computational method for calculating fluorescence intensities within three-dimensional structures in cells, *Cellular Logistics*, 2:4, 176-188.

2.1. Summary

The use of fluorescence microscopy is central to cell biology in general, and essential to many fields (e.g., membrane traffic) that rely upon it to identify cellular locations of molecules under study and the extent to which they co-localize with others. Rigorous localization or co-localization data require quantitative image analyses that can vary widely between fields and laboratories. While most published data use two-dimensional images, there is an increasing appreciation for the advantages of collecting three-dimensional datasets. These include the ability to evaluate the entire cell and avoidance of focal plane bias. This is particularly important when imaging and quantifying changes in organelles with irregular borders and which vary in appearance between cells in a population, e.g., the Golgi. We describe a method developed for quantifying changes in signal intensity of one protein within any three-dimensional structure, defined by the presence of a different marker. We use as examples of this method the quantification of adaptor recruitment to transmembrane protein cargos at the Golgi though it can be directly applied to any site in the cell. Together, these advantages facilitate rigorous statistical testing of differences between conditions, despite variations in organelle structure, and we believe that this method of quantification of fluorescence data can be productively applied to a wide array of experimental questions.

2.2. Introduction

The use of fluorescence microscopy has grown increasingly common throughout the biological sciences with continuous improvements in sensitivity, resolution, and applications. Fluorescence-based microscopy is routinely used to answer questions about where in a cell a given protein can be found, which organelle(s) it transits through, which other proteins are found in the same locations or in the same traffic pattern. These questions are increasingly important to cell signaling research, in which soluble proteins may be recruited to membrane surfaces, often in a highly regulated and transient fashion. In such cases the percentage of one protein co-localizing

with another can change dramatically and rapidly. Co-localization, or the quantification of the amount of overlap between two fluorophores, within two dimensional dual-colored images has been an important and powerful tool in determining a protein's location and its potential for acting at specific sites or with specific binding partners. Localization of a protein to discrete structures (e.g., centrosomes, nuclear pores, ER exit sites) can provide striking evidence of co-localization with markers of those structures (γ-tubulin, lamin B, Sec13, respectively) that often do not require statistical analyses. In contrast, other structures (e.g., the Golgi, endosomes) are irregular in morphology, vary in their three dimensional structures across individual cells within a population, and contain within them multiple overlapping domains that require more sophisticated statistical analyses. This variability in organelle morphology and within the sampled population also introduces a much greater potential for focal plane bias that can unintentionally skew the later analyses or images used to portray results. These concerns are ameliorated by the collection of data from the entire cell and multiple cells within the population but require specific statistical analyses to draw conclusions regarding differences between conditions in the experimental design. How the imaging data are collected and processed is obviously critical to those analyses.

All images contain both in focus and out of focus light, potentially confounding quantitative analysis. Confocal microscopy, in which the use of a laser light source and pinhole apertures filter unwanted light from the sample (for reviews see refs. 1,2) can greatly reduce the amount of out of focus light in an image. But confocal microscopy requires a relatively strong signal, can suffer from rapid photobleaching of the sample, and can require multiple passes (averaging) over the sample to obtain the image.(Shaw 2006) Alternatively, widefield microscopy illuminates the entire sample simultaneously (with a lower energy light source) and the image is acquired using a charged coupled device (CCD) camera, allowing for less photobleaching and much more rapid data acquisition.(Biggs 2010) However, the resultant image contains light originating from throughout the entire sample, i.e. out of focus light is present in each slice of the

stack. Algorithms have been developed to deconvolve the image, to remove out of focus light and reassign it to its point of origin (for review see ref. 3). This process can be applied to two dimensional images, or stacks of images collected on either confocal or widefield systems.(McNally, Karpova et al. 1999) For detailed reviews of deconvolution see refs. 3, 5, 6.

Once images are acquired and deconvolved, most methods of quantification require the images to be thresholded, or processed to discard noise, which includes low intensity, background signal, or signal contributed by the electronics within the system itself (often referred to as Poisson noise).(Pawley 2006) Thresholding effectively removes noise by disregarding pixels with intensities that fall below a specified value, often determined by visually inspecting the intensity profile or a histogram of intensities within the image. Thresholding can affect the outcome of the analysis by inadvertently removing low intensity signal that should have been included. While the method of thresholding should always be carefully considered it is particularly important when the source of the signal under study is present in both diffuse, soluble (cytoplasmic) and particulate, membrane-associated forms, such as proteins (adaptors, kinases, lipid modifiers, etc) whose binding to membranes is transient and regulated. Images of this nature often benefit from statistical analysis of a collection of images because of the potential for thresholding-induced bias, the irregular, three dimensional structure being observed, the large area over which the protein of interest may be recruited and the reversible nature of the interactions.

Co-localization, or quantification of the amount that two fluorophores correlate or overlap, is commonly used to evaluate location when one is a previously characterized marker of an organelle/structure. There are several ways to statistically analyze co-localization; including, but not limited to, Pearson's correlation coefficient (PCC) and Mander's overlap coefficient (MOC). These measures are commonly applied to confocal images, and work very well with fluorophores of comparable, strong pixel intensities. However, co-localization methods require thresholding and well-defined regions of interest (ROI), the more tightly defined the ROI the better the analysis. Additionally, the output of a co-localization analysis yields a single,

correlative value for each image that contains far less information than is available from using other methods. Further statistical analyses of multiple images and their corresponding co-localization scores produce a mean correlative score from which one can conclude the extent of overlap. In contrast, other methods make use of the information available in three dimensional datasets and allow users to extract more spatial information, including numbers of objects, relationships among objects (clustered vs. dispersed, etc), and regional differences within objects based upon intensity.(Hammond 2000, Woodcroft 2009)

We wanted to be able to generate irregularly shaped three dimensional ROIs that are defined by the presence of a marker of a specific cellular compartment and evaluate pixel intensities within those volumes, or isosurfaces. Isosurfaces are computational, three dimensional representations of a structure within an image stack and can be generated using a number of methods that are designed to detect boundaries between regions of signal and non-signal. Such methods include watershed segmentation, gradient detection, or iterative selection.

Watershed segmentation uses a theory first described 100 years ago(Cayley 1859) and imagines water falling onto or flooding from the bottom of a topological representation of pixel intensities within an image to determine where water would pool on the topology map. It then defines objects by drawing borders around areas from which the theoretical water was shed.(Gauch 1999) The user can set the amount of theoretical water allowed to fall in the system, and determine the amount of 'land' identified as 'object' in the image. Gradient detection calculates intensity differences between two pixels and uses that information to identify objects. Contiguous pixels with small intensity differences that are above a certain user-defined threshold define an object. Software packages e.g., Imaris (Bitplane Scientific Software) use watershed and gradient detection as methods of identifying objects. Some methods use combinations of these approaches to automatically identify and count objects, such as the freely available ImageJ plug-in "WatershedCounting3D'.(Gniadek and Warren 2007) WatershedCounting3D is very good at detecting areas of local contrast over a wide range of pixel intensities and when dealing with

strong signal that is clearly distinct from background. However, this approach employs thresholding, and images that contain diffuse, cytosolic staining can result in the identification of objects in areas that are distinctly background or cytosolic staining.

Finally, iterative pixel selection, or the Calvard method(Ridler 1978), and its variations, evaluates an image a number of times (Imaris software default is four times), each time scoring pixels as "object" or "non-object". It calculates two populations of pixel intensities, maximizing the statistical differences between them and defines pixels within the higher population to be those containing signal that corresponds to an object, and the lower population to comprise noise. It then generates a map, or mask, of pixels that were identified as object and applies it to the original image. The process is then repeated on pixels that fall into the region defined by the mask. Each iteration results in a more refined object, each time optimizing the statistical difference between the two populations to result in the largest possible difference between foreground (object) and background (non-object). This approach is advantageous because it (a) retains all information in the dataset, i.e., does not throw out data below any limit, (b) does not require thresholding prior to object identification and therefore evaluates all pixel intensities within the raw image, (c) is dynamic in that it can be applied equivalently to images that vary in their intensity profiles (may be dimmer or brighter than other images in a data set, or have more background, etc.), and (d) can be applied automatically to all images included in an analysis. In a comparison of multiple methods of object identification, iterative selection was the only approach that was determined to be a suitable replacement for manual inspection.(Yang 2001)

We present a method specifically designed for the quantification of three dimensional datasets that identifies volumetric structures and evaluates signal intensity information within those structures using three dimensional (3D) **i**mage-based **i**sosurface generation and **i**ntensity analysis (3D3I). We believe this method provides a useful addition to imaging data analyses with the specific advantages of (a) automatic object identification that can be applied easily to many images of comparable or disparate intensity profiles (i.e. applicable to strong localized signal or

diffuse cytosolic staining), (b) eliminating the need for thresholding, (c) generating real values rather than correlative ones, (d) allowing for the statistical detection of outliers based on the characteristics of the image and (e) being particularly well suited for analyses of protein recruitment to membranes but can be applied to other changes in protein distribution in cells.

2.3. Results

Procedure for 3D3I image analysis

Z-stacks of wide field images using a 60X objective were collected for two channels from the entire volume of the cell using a step size of 0.2 μm, as described under Materials and Methods. Exposure times of 200 ms were used for each channel. This method can accommodate the use of either confocal or wide field imaging systems, however we chose to use wide field to minimize problems resulting from photobleaching. The acquired stack of images was then deconvolved to remove out of focus light. The deconvolved stacks were imported into Imaris. The channel used to identify a cellular structure (e.g. Golgi marker) was automatically segmented using the iterative selection method as implemented with Imaris software, and an isosurface, or computational volume that represents the intensities within the channel used to generate it, was generated. Intensity values for both channels within the isosurface were then exported to Excel. This output includes a list of each isosurface identified in the image, their volumes, and intensities of signal in each. Figure 1 highlights the workflow for quantification of isosurfaces from cells.

Problems arising from the collection and analysis of three dimensional datasets

The ability to collect images at different z-positions throughout the volume of the cell allows the generation of three dimensional reconstructions that provide much more information than that present in a single two dimensional image but raises an important issue that is worthy of

specific elaboration. The analysis of one image from a single plane of focus can result in unintentionally biased results, termed focal plane selection bias. Collecting and using data from an entire cell volume should effectively eliminate such bias. This is apparent when two spatially separated images collected from the same cell are evaluated for co-localization. Co-localization methods can evaluate how well two channels correlate in their intensities (e.g. bright pixels on one channel coincide with bright pixels on the other), or how well two channels overlap (e.g. where there is signal on one channel there is signal on another).

The classical measure of co-localization is the Pearson's Correlation Coefficient (PCC) and is the origin for most co-localization measures used today.(Adler 2010, Barlow 2010) A PCC value of -1 would be interpreted as inverse correlation (where pixels in one channel are brighter than the mean, pixels in the other channel are likely to be dimmer than the mean pixel intensity) while a PCC value of 0 would indicates no correlation (there is no relationship between the two channels), and a PCC value of +1 indicates perfect correlation (where pixels in one channel are brighter than the mean, pixels in the other channel are also brighter than the mean). While the PCC indicates how well or how poorly two channels vary with one another, some questions are better answered with information about the degree to which two channels overlap, rather than how well their intensities co-vary. To obtain an equation that monitors overlap of pixels, the PCC is modified to evaluate absolute pixel intensity rather than deviation from the mean intensity, and results in the Mander's Overlap Coefficient (MOC).(Manders 1993, Barlow 2010) Because the MOC evaluates absolute intensities rather than the co-variance of two channels it eliminates the possibility of a negative correlation. The MOC can be further rearranged to give two scores, one for each channel, rather than one score for an entire image. These coefficients are referred to as M1 and M2 and indicate how much 'red signal is also green', or vice versa.

To illustrate these issues, PCC and MOC measures were calculated for two slices isolated from a single stack of deconvolved wide field images to evaluate the degree of co-localization in two spatially distinct regions of the same cell. Stacks of images were collected from fixed HeLaM

cells expressing a protein containing the lumenal and transmembrane domains of CD8 fused to the cytoplasmic tail of furin (CD8-furin), which (like furin itself) localizes predominantly to the Golgi.(Teuchert, Berghofer et al. 1999, Thomas 2002) Fixed cells were labeled with antibodies directed against TGN46, a marker of the trans-Golgi network (TGN) compartment (Fig. 2A, red), and to CD8, to detect the cargo (Fig. 2A, green). Stacks were deconvolved with Huygens SVI software, the two channels were merged and a montage was generated (Fig.2A). The 6th and the 16th images were arbitrarily selected, extracted from the stack and evaluated for co-localization using the "Co-localization Threshold" plug-in (http://pacific.mpi-cbg.de/wiki/index.php/Colocalization_Threshold) from FiJi (Fig. 2B). This plug-in calculates the PCC as well as the MOC and thresholded M1, M2 (tM1, tM2) scores for each channel. The PCC and tM1/M2 measures were calculated for the two slices and are shown in Fig. 2B, along with a scattergram of overlapping intensities where the colder/darker pixels represent less frequent occurrences of a given pixel intensity, while warmer/yellow colors indicate a higher frequency of occurrence. The amount of co-localization, as determined by either PCC or tM, differs quite a bit between the two, spatially distinct slices. This variation results from different focal planes will certainly add to the variation between samples, e.g., when averaging a correlative score among different cells from a single population, and can even alter conclusions drawn from the dataset. Allowing the user to select by visual inspection one image from the z-stack for comparison to other cells increases the potential for introducing unintentional bias. The use of three dimensional datasets avoids focal plane bias by using data from throughout the cell but require optimized methods for analysis.

Image segmentation using WatershedCounting3D and 3D3I

We compared objects identified using 3D3I analysis to those identified using a similar method, watershed segmentation.(Gniadek and Warren 2007) Using the same stack of images shown in Fig. 2 in which cells expressing CD8-furin were fixed and stained for TGN46, a marker

of the trans-Golgi network and CD8, we compared the regions identified as objects/structures using watershed segmentation to those identified using 3D3I. The images used have a linear range of pixel intensities as shown for the TGN46 marker in Fig. 3A (CD8 staining intensities not shown), with no easily identifiable, discrete populations of pixel intensities, making them difficult to threshold manually. The merged CD8 and TGN46 stacks were mapped onto a three dimensional intensity plot to represent intensities of the two channels (Fig. 3B). Note the gray, textured regions of low intensity, illustrating variations in background signal, and corresponding to low-intensity pixels seen in the histogram shown in Figure 3A. WatershedCounting3D segmentation was applied to the TGN46 channel and a mask of the segmented regions was generated(Gniadek and Warren 2007) (Fig. 3C). We believe that (perhaps because there is a linear range of pixel intensities) the Watershed method identifies a large number of discrete isosurfaces; far more than would be expected for the biological structures that contain TGN46. This conclusion was further supported by the observation that the staining seen in the upper right quadrant of the images shown in Fig. 3 is coming from the nucleus, which is expected to lack TGN46. The mask was then falsely colored blue, and applied to the three dimensional intensity plot (Fig. 3D). Comparing Fig. 3B to 3D, (Fig. 3D is the addition of Fig. 3B and 3C) it is clear that while the WatershedCounting3D algorithm is excellent at detecting areas of local contrast over a wide range of pixel intensities, its ability to detect areas of local contrast resulted in the identification of objects containing very low-intensity pixels (Fig. 3D, arrows). These low-intensity objects can be removed by thresholding the image prior to analysis. However, to do so we must manually assign a cutoff intensity that may or may not be applicable over large numbers of image stacks. In comparison, we generated an isosurface based on TGN46 signal using the iterative selection method implemented in Imaris (Fig. 3E, green) and compared it with the TGN46 channel (Fig. 3E, red). It is evident by simple inspection that the isosurfaces generated using the iterative selection method (Fig. 3E, green) faithfully capture the overwhelming majority of the staining seen in the primary data (Fig. 3E, red).

A comparison of the isosurface in Fig. 3E to the blue regions identified in Fig. 3D revealed that far fewer objects (discrete isosurfaces) were identified using the Imaris isosurface generation approach than in watershed segmentation. Due to file format incompatibility we were unable to project the Imaris isosurface onto the ImageJ three dimensional intensity space. Given our current understanding of the TGN compartment we believe that many of the low peaks seen in Fig. 3D (e.g., arrows) do not faithfully identify the TGN. Because the iterative selection method maximizes the statistical difference between signal and non-signal pixels, and effectively utilizes the dynamic range of pixel intensities within an image, the overall intensity of a signal is less of an issue in identifying isosurfaces. In addition, in our hands each image evaluated using WatshedCounting3D required continuous adjustments to the settings to filter out the objects identified in regions of low signal intensity. We also noted that two dimensional confocal images resulted in better segmentation using the WatershedCounting3D method but the use of three dimensional data sets, and the individual settings necessary to analyze each image, make this method prohibitive to the analysis of large numbers of images. For studies that will use statistical analyses comparing different conditions or datasets, a method is required that involves as little image processing as possible, and yet is robust enough to be applicable over a wide range of signal profiles. In summary, a direct comparison of 3D3I to watershed counting reveals that fewer objects are identified in regions of low contrast (refer to Fig. 3A) using 3D3I and, at least in the case of this marker of the TGN, give us higher confidence that we are quantifying the biologically relevant compartment under study. Further testing and comparisons should be performed to determine if this holds up over a wider array of organelle markers; though we have used this method for quantification of transferrin receptor containing vesicles (recycling endosomes), early endosomes, and lysosomes, with similar results to those obtained for Golgi proteins.

Development of the 3D3I method for quantifying recruitment of adaptors to irregular, three-dimensional structures, such as the Golgi and endosomes

Because the Golgi and endosomes are irregularly shaped structures that can appear quite different between cells and in different focal planes of the same cell, we sought a method that is inclusive of all staining in each cell used for quantification. A related issue is that diffuse, cytosolic staining can be difficult to appropriately threshold and depending upon how it is handled, can result in exaggerated or understated co-localization scores (see below). To address these issues, we wanted a method that would allow for the identification of three dimensional objects without discarding cytosolic staining. To this end, we used wide field imaging with deconvolution followed by analyses using Imaris software, as described under Materials and Methods. Organelle marker staining (e.g., giantin for the Golgi) was used to generate isosurfaces and the staining of the adaptor Mint3 was determined within those isosurfaces. Note that this method allows for the identification of multiple, discrete objects within the same cell and outputs include numbers and volumes of all objects (see Fig. 1). Though many parameters are calculated for each isosurface, we chose to score images as a ratio of total pixel intensity of adaptor per unit volume of isosurface (defined by the marker of the Golgi) from each cell in the units, intensity/μm^3. We chose this metric (intensity/μm^3) because it best addressed the question 'how much Mint3 is on the Golgi?' and allowed us to compare the answers from different cell populations in a statistically rigorous fashion. However, the 3D3I method can be tailored to evaluate other questions that are better described using other metrics. For example, if one is interested in fragmentation 3D3I can address that simply by arranging the values that are exported to best describe the question. The isosurface serves as a tightly defined three dimensional ROI, or volume within which we wish to monitor changes. This method has a number of advantages: (1) all data included are defined by a biologically relevant marker used to define the isosurface (avoiding over-estimates resulting from correlational co-localization methods), (2) we monitor changes throughout the entire volume of the cell and thus avoid sampling or focal plane bias, and (3) we perform statistical analyses on a number of cells, comparing intensity per unit volume in control vs. experimental conditions, as opposed to performing statistical analysis on mean

correlational scores. Importantly, because all data are included, including low intensity signal throughout the cell, we typically observe smaller fold-changes in response to experimental manipulations using 3D3I than those found in more commonly used co-localization methods.

An example of the use of 3D3I to quantify adaptor recruitment is shown in Fig. 4, with comparison to co-localization methods. Wide field images of control HeLaM cells were collected and deconvolved using Huygens' Deconvolution software (SVI Inc.). Deconvolved images were opened in Imaris and analyzed for co-localization using automatic thresholding. A co-localization mask, or a graphical representation of pixels that overlap, was generated (Fig. 4A, 'Co-localization Mask'). Imaris calculated a Pearson's coefficient of 0.5211, as well as thresholded Mander's coefficients of 0.7605 and 0.3871 for giantin and Mint3, respectively (Fig. 4B). These coefficients were calculated for the entire stack though the images shown are maximum intensity projections. We then performed the same type of analysis using ImageJ and compared the results to those obtained using the colocalization calculator in Imaris. The same deconvolved images were opened in ImageJ and converted to 16-bit images, which were used to generate the values in Fig. 4B, and a frequency plot of intensities (Fig. 4C) using the 'Mander's Calculator' plug-in from the MacMaster Biophotonics Facility (http://www.macbiophotonics.ca/imagej). The overall shape of the scattergram indicates a positive correlation between giantin and Mint3 pixels. It is clear that there are more Mint3 pixels that do not have giantin signal in them (see the clustering of warm colors along the y-axis) than giantin pixels devoid of Mint3 intensity as indicated by the absence of a similar lobe of intense pixels along the x-axis. That is, most giantin positive pixels are also positive for Mint3 but not all Mint3 positive pixels are positive for giantin. Such incompleteness in overlap is not surprising, given the complex organization of the Golgi itself and the extensive documentation that markers of this organelle display regions of non-overlap (i.e. giantin stains a portion of the Golgi but not all of it, and Mint3 is present on surfaces of the Golgi as well as endosomes). We interpret this partial overlap as evidence of Mint3 recruitment to the Golgi, including some areas that are giantin positive and some that are not. The Pearson's

coefficient generated using the ImageJ software is similar to that obtained from Imaris. Mander's coefficients obtained from both methods determined that most of the giantin intensity was also positive for Mint3 (compare the Imaris value of 0.7605 to the ImageJ value of 0.979) while there were fewer Mint3 positive pixels that were also positive for giantin (compare the Imaris value of 0.3871 to the ImageJ value of 0.678). The differences between values generated by ImageJ and Imaris most likely arise from the manner in which each software package handles thresholding. Though neither value is more correct than the other, it suggests that thresholding be approached cautiously, and used sparingly. However, both methods generate the same rank order of tM coefficients in that giantin is higher than Mint3 under each treatment. In summary, the manner in which co-localization calculations are implemented within a given software package can influence substantially the quantification of an image.

We wanted a method to generate values containing absolute intensity information about a given channel within a defined three-dimensional region of interest as opposed to an entire image or cell. To do this, the same images used in Fig. 4A were analyzed with the Imaris software package using the iterative selection method to automatically define an isosurface that was representative of all giantin staining (Fig. 4D). From this surface, a heat map of Mint3 intensities was generated to illustrate the point that not all giantin staining has a uniform amount of Mint3 staining. Instead there are regions of the isosurface that have high (white) or low (dark red) levels of Mint3 intensity (Fig. 4E). This level of spatial detail is lost when the image is evaluated using co-localization, or statistical correlation methods. Data describing the isosurface, such as total isosurface volume, and the pixel intensities of Mint3 and giantin contained within that volume are shown (Fig. 4E, right). When expressed as a ratio of sum intensity per isosurface volume, the information can be used to make comparisons across many groups and are suitable for statistical analysis. We then wanted to compare the region of pixels that were determined to co-localize with the region that was defined by the isosurface (Fig. 4F). The isosurface (red) and the co-localization mask (green) were displayed simultaneously in Imaris (merge), and exported as a .tif

file. From the merged image it is clear that there are regions defined by the co-localization mask that do not also contain regions defined by the isosurface. However, all of the isosurface volume contains volumes defined by the co-localization mask.

2.4. 3D3I Applications

3D3I analysis can be used to analyze data from many different types of experiments and is particularly well suited to making comparisons across multiple conditions. To illustrate this point, 3D3I was used to analyze Mint3 recruitment to isosurfaces defined by the presence of the amyloid precursor protein (APP; Fig. 5A). The cytosolic tail of APP interacts with the adaptor protein Mint3 at the Golgi for packaging and export.(Borg, Ooi et al. 1996, Borg, Yang et al. 1998, Shrivastava-Ranjan, Faundez et al. 2008) APP is a transmembrane protein that transits both the secretory and endocytic pathways and is proteolytically processed in the process. This can lead to difficulties in interpretation when using N- or C-terminal directed antibodies or tags on APP as they may become separated as a result of protease activities. For this reason, we compared our results of expressed wild type human APP to those of a recombinant protein consisting of the lumenal and transmembrane domain of CD8 and the cytoplasmic tail of APP (CD8-APP) that is completely comparable to the CD8-furin construct used above. Use of the CD8-APP construct also allows us to monitor traffic of a protein independently of lumenal domain interactions, which have been described previously for APP.(Andersen, Schmidt et al. 2006) We obtained the same results whether full length APP or CD8-APP was expressed so examples of each are presented in Fig. 5. We also used the previously characterized temperature block protocol, in which cells were maintained at 20°C for four hours, during which time protein synthesis and export from the ER continued (albeit at slower rates than if cells are cultured at 37°C) but export from the Golgi/TGN was compromised.(Lodish and Kong 1983, Saraste and Kuismanen 1984, Griffiths, Pfeiffer et al. 1985, Mottet, Tuffereau et al. 1986) HeLaM cells were transfected with a plasmid directing expression of human APP^{695} (Fig. 5A, B, C), or CD8-APP

(Fig. 5D) and the next day were either maintained at 37°C or the temperature block was imposed. Cells were then fixed and stained with the antibodies indicated, as described under Materials and Methods. Stacks of wide field images were collected and deconvolved using Huygens SVI software. Deconvolved images were opened with Imaris and isosurfaces were generated based on APP staining (Fig. 5A, C) or based on giantin staining (Fig. 5B, D). The amount of Mint3 staining within those isosurfaces was compared between conditions.

The increased recruitment of Mint3 to APP isosurfaces in response to imposition of the temperature block is easily seen in the heat map at the bottom of Fig. 5A and quantified in Fig. 5C. We quantified the amount of Mint3 signal within isosurfaces defined by APP staining and compared the results obtained from cells maintained at 37°C and 20°C (Fig. 5C). Sum intensity values were expressed as the ratio of Mint3 per isosurface volume and the data from at least seven cells were averaged and used in statistical analyses. Results demonstrated that the temperature block led to a statistically significant increase ($p<0.01$) in Mint3 within APP isosurfaces.

We predicted that the temperature blockade would lead to an increase in APP at the Golgi due to the decrease in anterograde traffic from the Golgi under this condition and asked whether the Mint3 adaptor was being recruited to that site. Thus, in a parallel set of experiments Mint3 recruitment to the Golgi (defined by giantin staining) was quantified in control cells and compared to those expressing CD8-APP, with or without temperature block (Fig. 5D). It is evident from the bar graph (Fig. 5D) that imposition of the temperature block alone does not cause an increase in Mint3 at the Golgi. In contrast, expression of CD8-APP does increase Mint3 at the Golgi and this effect is further increased upon imposition of the temperature block.

We evaluated sum intensity within an isosurface in these examples, but many other parameters can be measured using 3D3I; including isosurface volume, number of isosurfaces, number of voxels within an isosurface, mean intensity, and intensity standard deviation. These

parameters are more tangible than the correlative measures generated in co-localization analyses and retain the spatial information present in the original image.

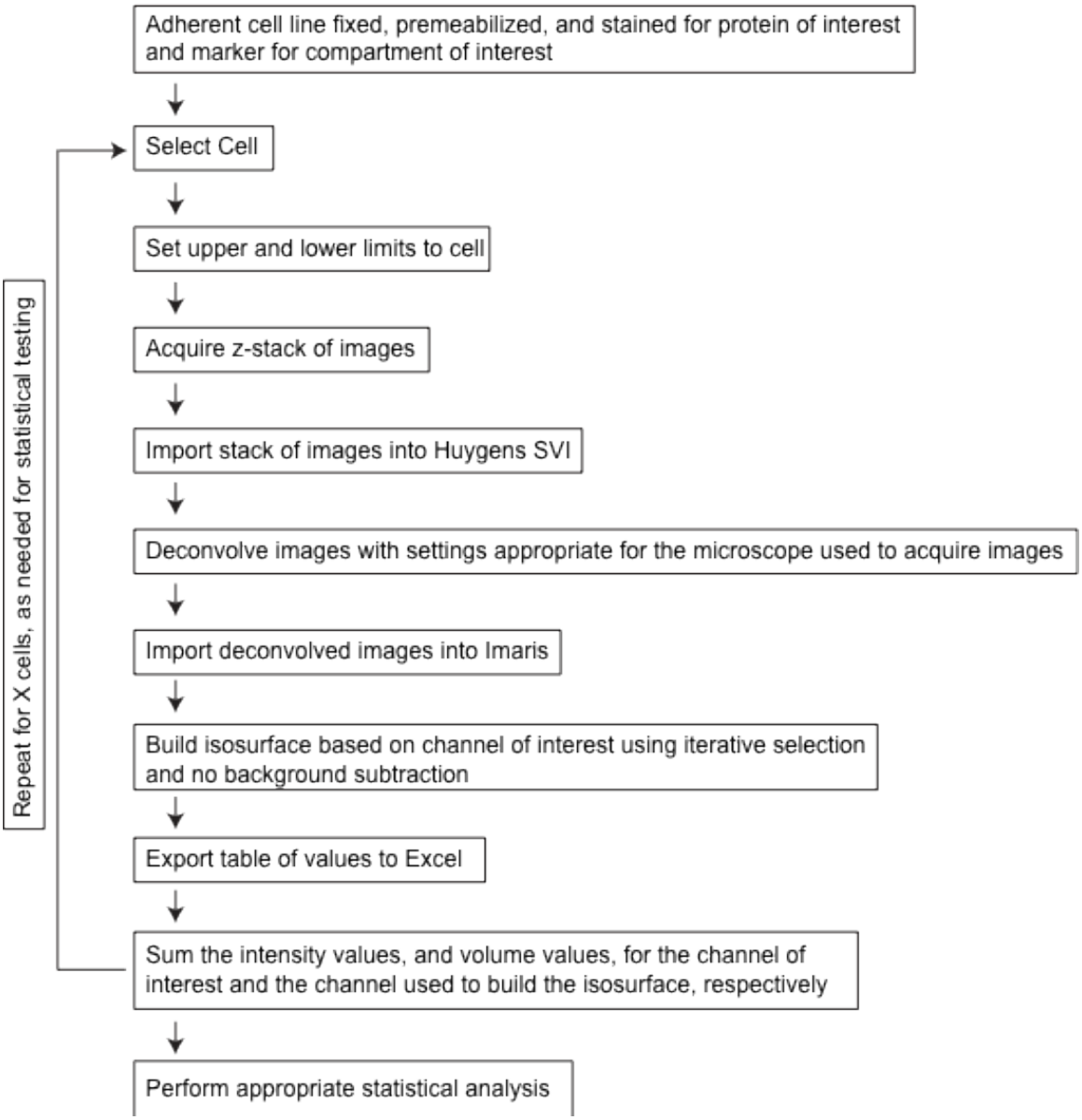

Figure 1. *3D3I Workflow.* Steps in the performance of 3D3I to quantify staining in fixed adherent cells in culture are illustrated. We describe throughout the use of one well defined organelle marker (e.g., giantin, TGN46, etc) to define the isosurface into which the other antigen is compared but any two antigens can be compared in the same way. Wide field images were collected in z-series throughout the volume of the cell to create an image stack. This stack is imported into Huygens SVI software and deconvolved to remove out of focus light. The deconvolved stack is imported into Imaris and an isosurface is built, based upon staining of the

organelle marker. An important aspect of this method is that the isosurface is generated without thresholding the stack in any way. Information about the isosurfaces generated by Imaris are then exported to Excel for use. Each object within the isosurface is assigned an identification number with corresponding volumes, sum channel intensities within each object, maximum intensities per object, intensity mean, intensity minimum, standard deviation of intensity, and surface areas. This list of exported values is not comprehensive but representative. The return loop is intended to show that the process can be repeated on as many cells as required for the statistical tests used.

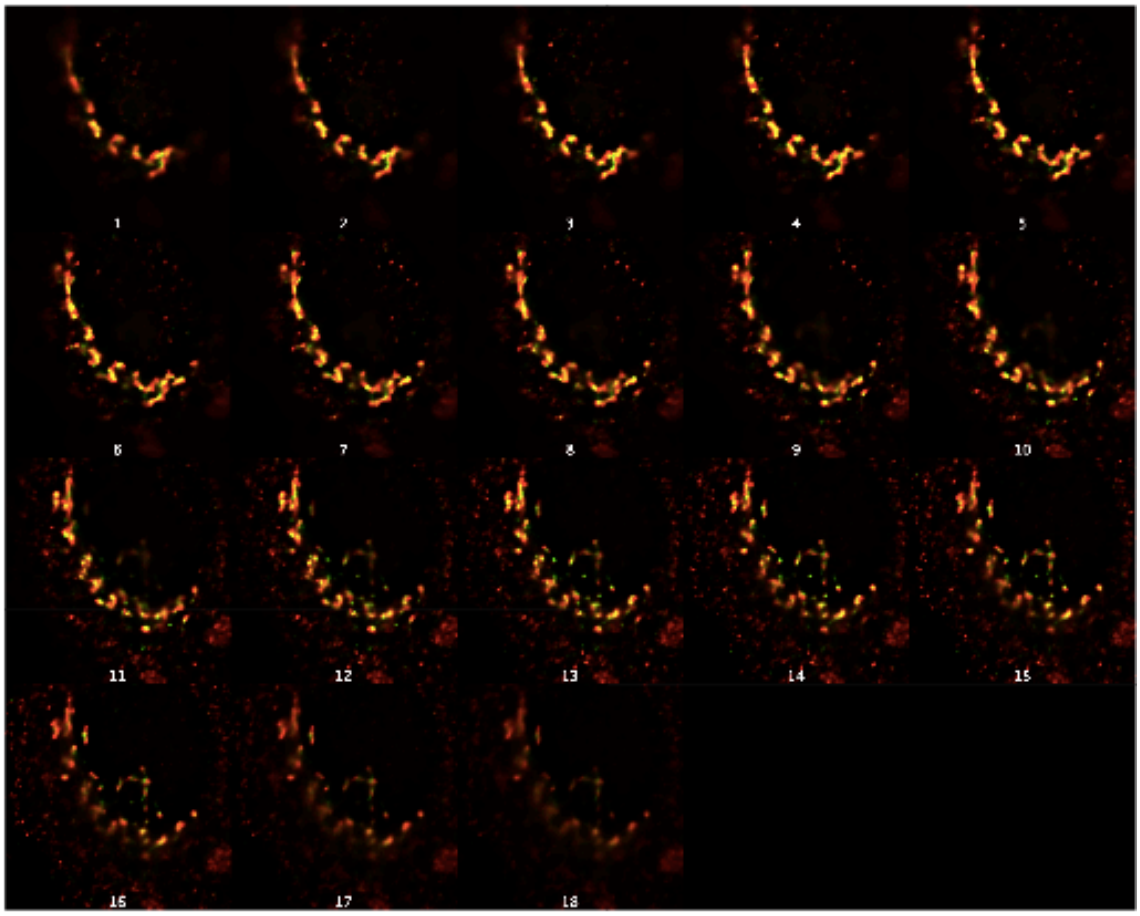

B.

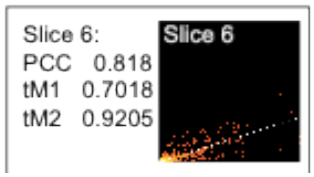

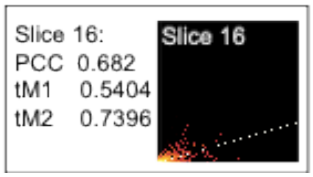

Figure 2. Focal plane bias in use of single images. (**A**) Stacks of images were collected from HeLaM cells expressing CD8-furin and stained for both CD8 and TGN46, as described under Materials and Methods. Z-stacks for each channel were deconvolved, opened in ImageJ, merged, and a montage was created showing 18 images at different depths in the z-plane. (**B**) Choice of focal plane can affect results of quantification of co-localization. The 6th and the 16th slices within the z-stack were arbitrarily selected for co-localization analysis. The two slices were evaluated for PCC, and thresholded Mander's coefficients (tM1, tM2), and intensity histograms generated.

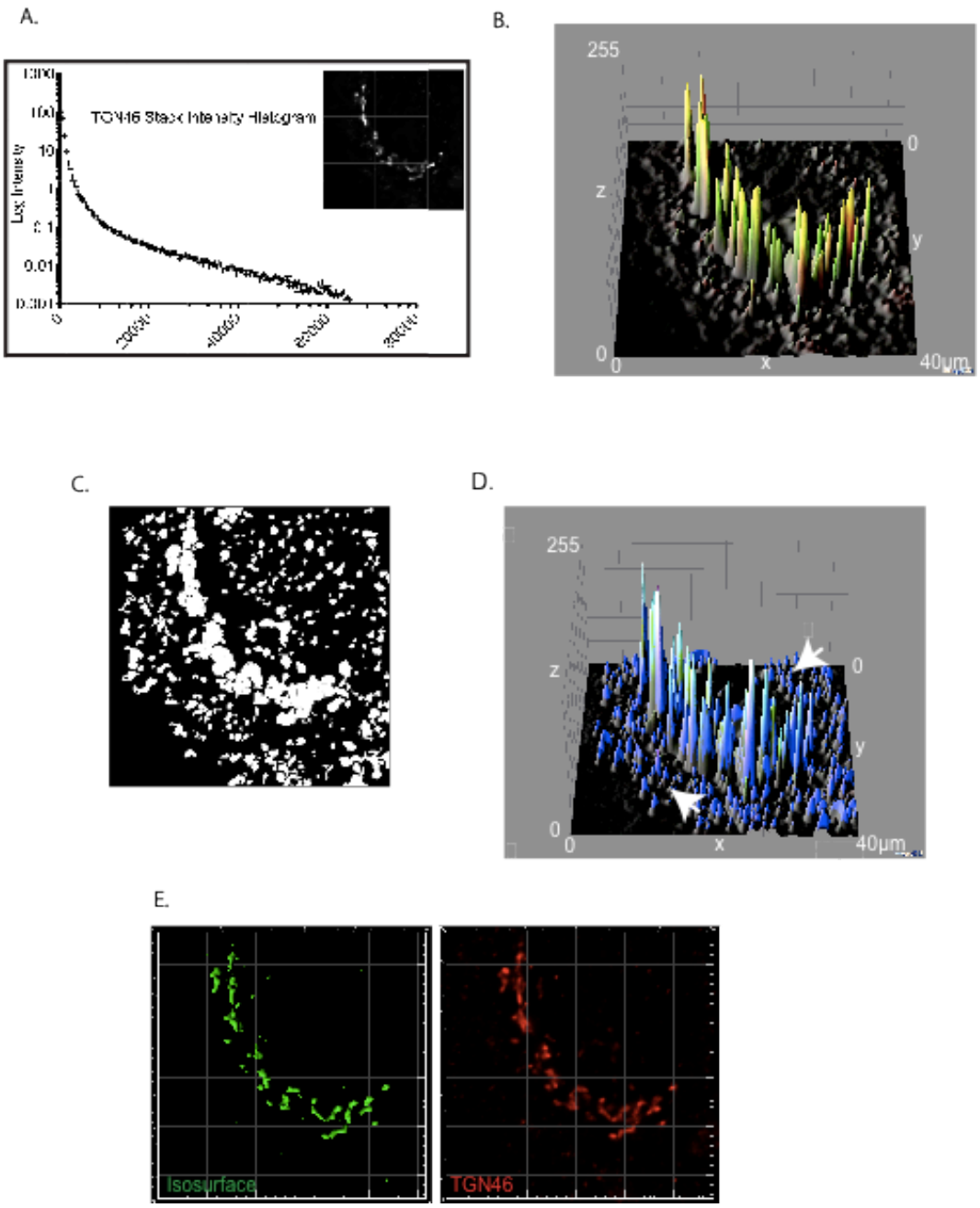

Figure 3. Comparison of image segmentation using WatershedCounting3D and 3D3I. The same HeLaM cell, expressing CD8-furin and stained for CD8 and TGN46, shown in Fig. 2 was used for analyses. (**A**) Histogram of intensities from a z-stack of deconvolved images of TGN46 staining; the maximum intensity projection is shown in the inset. (**B**) The three dimensional surface plot of pixel intensities for TGN46 (red) and CD8 (green) is shown as the merged image.

Height indicates relative intensity. (**C**) WatershedCounting3D was used to identify objects and create a mask based on TGN46 staining. (**D**) The mask shown in (C) was false-colored blue and imported into the three dimensional intensity plot shown in (B). Blue regions indicate areas contained in the segmented mask. Arrows highlight regions of the mask that occur in areas of low intensity. (**E**) We used the same deconvolved z-stack of TGN46 (red) staining to generate an isosurface using Imaris (shown in green) as described under Materials and Methods. Isosurface generation results in fewer objects being identified in the regions of low signal intensity (e.g., compare panel E to C).

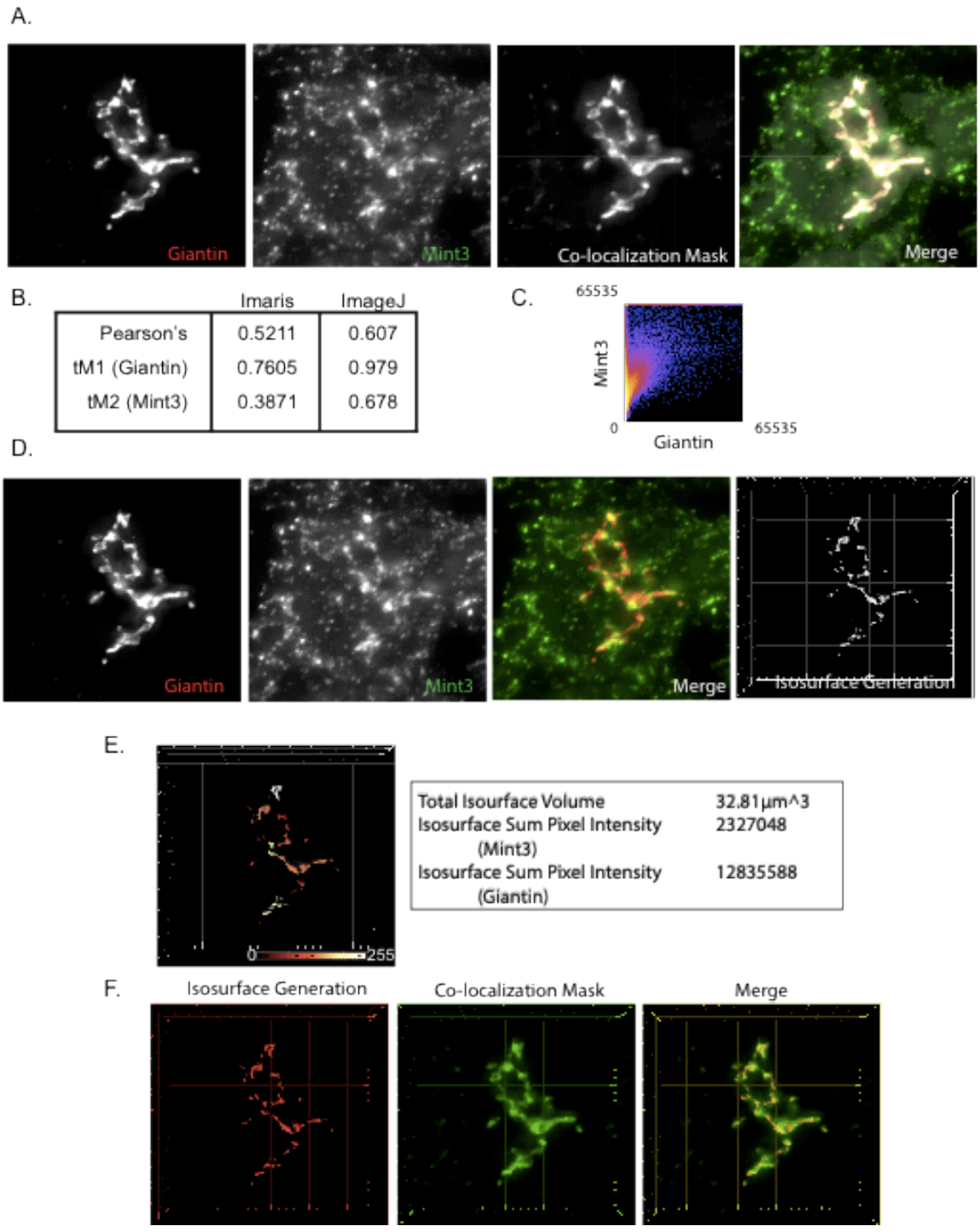

Figure 4. Comparison of 3D3I to other co-localization methods. HeLaM cells were fixed and labeled with antibodies against giantin and Mint3. (**A**) Images were collected using widefield imaging and a step size of 0.2 µm. Stacks were deconvolved using Huygens deconvolution

software (left two panels), and Imaris was used to generate the co-localization mask of the two channels (third panel), as described under Materials and Methods. A merge of the two channels and the colocalization mask are shown (fourth panel). Maximum intensity projections are shown. (**B**) Pearson's, and thresholded Mander's (tM) coefficients were calculated using Imaris and ImageJ, as described under Materials and Methods. (**C**) Imaris was used to generate a scatter plot of pixel intensities using the merged giantin and Mint3 channels shown in A. (**D**) The same deconvolved images shown in A (left two panels) were opened in Imaris and merged (third panel). The giantin channel (red) was used to create the isosurface (right panel). (**E**) The isosurface generated in panel D is color-coded as a heat map of Mint3 intensities contained within each object in the isosurface. Representative values describing the isosurface are shown in the panel to the right of the color-coded isosurface. Note the variations in Mint3 intensity within the giantin isosurface, based on the color-coding shown. (**F**) The co-localization mask shown in A was falsely-colored green, and the isosurface generated in D was falsely-colored red. The two are displayed simultaneously in the merged image. The isosurface is a more tightly defined volume as the two representations overlap, but the co-localization mask highlights regions not identified by the isosurface.

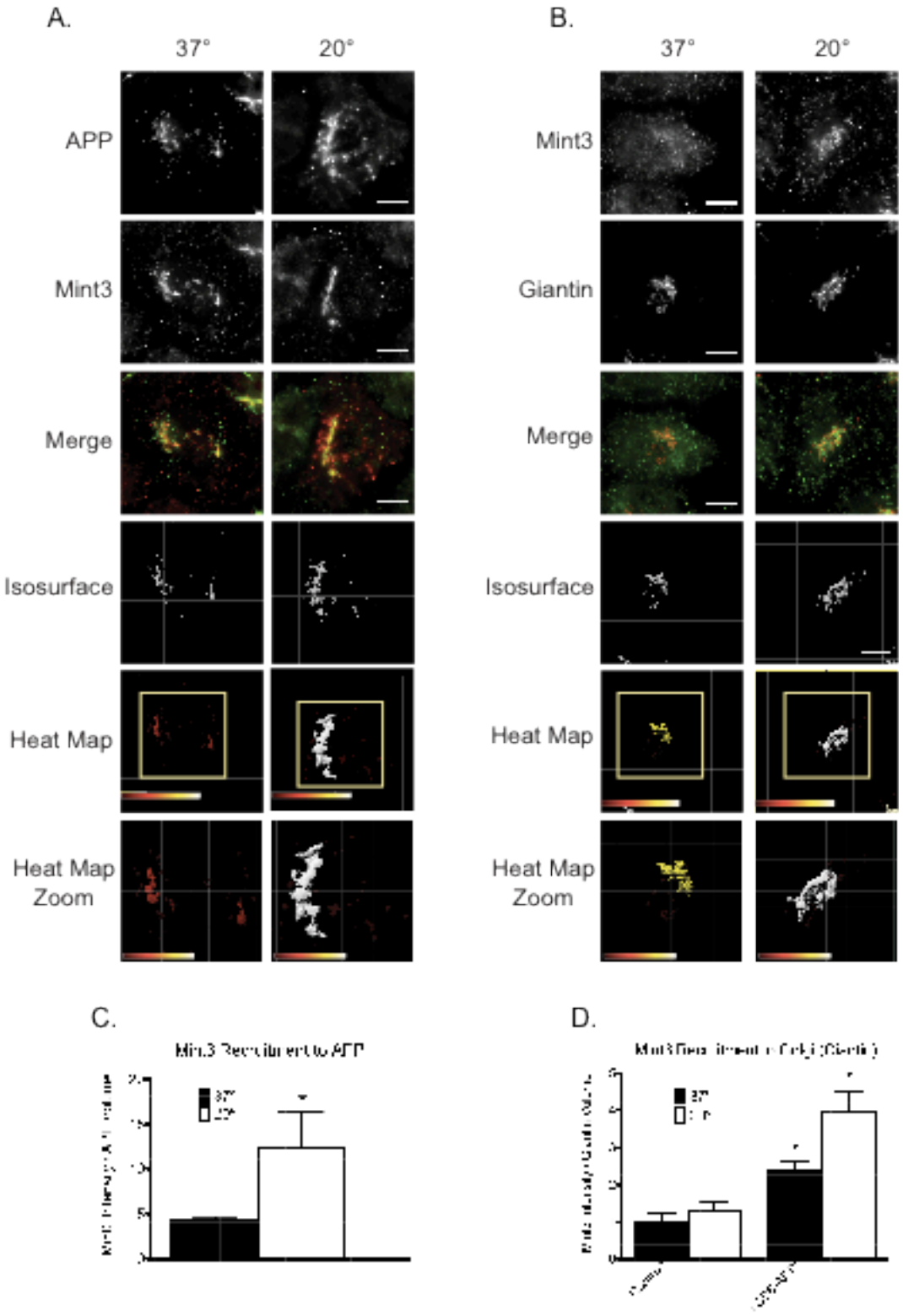

Figure 5. Example of a 3D3I application. Temperature block increases the recruitment of Mint3 to APP at the Golgi. HeLaM cells were transfected with empty plasmid or ones directing

expression of full length human APP (**A**, **B**) or CD8-APP (**D**) and the next day were fixed with or without imposition of the temperature blockade, as described under Materials and Methods. Cells were then stained for (**A**) APP and Mint3 or (**B**) Mint3 and giantin. Maximum intensity projections of widefield images are shown with isosurface generation using APP (**A**) or giantin (**B**) staining. Heat maps indicate the intensity of Mint3 staining within those isosurfaces. (**C**) The amount of Mint3 staining per APP volume was determined under the conditions shown in panel A. (**D**) Control HeLaM cells, or cells expressing CD8-APP were maintained 37°C or temperature blocked prior to fixation, and stained with antibodies directed against Mint3 or CD8. Bars in C and D show the average from $N \geq 7$ cells per condition, representative of at least three independent experiments. Error bars indicate standard error of the mean (SEM). Asterisks indicate a $p<0.01$, each compared to control, steady state staining.

2.5. Discussion

We conclude that the use of three dimensional isosurface generation and of intensities contained within that volume (termed 3D **i**mage-based **i**sosurface generation and **i**ntensity analysis, or 3D3I analysis) generates non-correlative, raw values suitable for statistical analysis of large numbers of cells and confined to marker-defined, physiologically relevant regions or structures. As such we believe this method is a valuable alternative to correlative values when information about a three dimensional structure is of interest. This method is particularly suited to irregularly shaped organelles and ones that can appear so different between cells in the same population, like the Golgi and endosomes, but is flexible enough to be used to address a variety of types of questions that may be relevant to any site or cellular organelle.

2.6. Materials and Methods

Cell Culture

HeLaM cells were maintained at 37°C and 5% CO_2 in 10% fetal bovine serum (GemCell Cat# 100-500) in DMEM medium (GIBCO Cat# 11965). Temperature blockade was performed as previously described (Lodish and Kong 1983, Saraste and Kuismanen 1984, Griffiths, Pfeiffer et al. 1985, Mottet, Tuffereau et al. 1986) and involved aspirating off medium from cells grown on coverslips, replacing it with DMEM containing 20 mM HEPES, pH 7.4 with 10% fetal bovine serum, pre-warmed to 19.5°C, and maintaining cells in a water bath at the same temperature for four hours. Cells were then either fixed and processed immediately or allowed to recover by return to 37°C for the times indicated, as described below.

Plasmids and Transfections

The pIRESneo parent plasmid used to express the lumenal and transmembrane domain of CD8 fused to the cytoplasmic domain of furin, termed CD8-furin, was a generous gift from Dr. Matthew Seaman (University of Cambridge).(Seaman 2004) Expression of full-length human amyloid precursor protein, APP^{695}, was achieved as described in Shrivastava-Ranjan et al.(Shrivastava-Ranjan, Faundez et al. 2008) We also generated a plasmid encoding the CD8 lumenal and transmembrane domains fused to the cytoplasmic tail of APP, consisting of the 46 C-terminal residues (residues 650-695), termed CD8-APP. The APP tail was inserted into pIRESneo-CD8 using NotI and AflII restriction sites.

Cells were plated at ~80% confluence and the next day were rinsed with pre-warmed, serum free Opti-MEM (GIBCO cat# 11058) and then placed in 1.0 mL of pre-warmed Opti-MEM. Fugene transfection reagent (6 μL; Roche cat #11814443001) was added to OptiMEM (93 μL) in a microfuge tube. DNA (1 μg) was then added to the Opti-MEM/Fugene solution, tapped gently to mix, and incubated at room temperature for 20 min. The transfection mixture was then added drop wise to one well of a 6-well plate and placed at 37°C for 5 hours. The transfection was stopped by rinsing cells once with pre-warmed Trypsin-EDTA (GIBCO cat# 25300) and then adding 0.5 ml 0.05% Trypsin-EDTA and incubating at 37°C for ~5 min. Cells were triturated off the plate using 3.5 mL of pre-warmed growth medium and plated onto 6 cm dishes containing Matrigel (BD Biosciences Cat. #356234)-coated coverslips and allowed to attach overnight.

Immunocytochemistry

Cells plated onto coverslips the night before were fixed with 2% paraformaldehyde diluted in phosphate buffered saline (PBS; 137 mM NaCl, 2.7 mM KCl, 10 mM sodium phosphate dibasic, 2 mM potassium phosphate monobasic, pH 7.4) for 20 min at room temperature. Fixative was aspirated off and cells were rinsed four times for 5 min each with PBS.

Non-specific staining was blocked by incubating cells in 200 μL of blocking solution (1% bovine serum albumin (Sigma cat #A3059) and 0.05% saponin (Sigma #S5881) in PBS for 20 min at room temperature. Antibodies against human TGN46 (Serotec cat. # AHP500, 1:1000), APP (Synaptic Systems cat. #127002, 1:500), Mint3 (BD Transduction 611380, 1:200), or giantin (Covance cat. #prb114c, 1:1000) were diluted in blocking solution and applied to the cells overnight (~16 hours) at 4°C. The following morning, cells were washed four times for 5 min each in 0.05% saponin (Sigma #S5881) in PBS (SAP) at room temperature. Secondary antibodies (Alexa 594 and Alexa 488; Invitrogen, cat. # A11016 and A11008, respectively) were diluted 1:500 in blocking solution and applied to the cells for one hour at room temperature, protected from light. Cells were then washed twice in SAP, 5 min each. When indicated, FITC-conjugated anti-human CD8 (Ancell Corp. cat #153-040) was diluted 1:1000 in blocking solution and ~150 μL was added for one hour at room temperature, protected from light. Cover slips were then washed two times 5 min each in SAP. Hoechst dye was diluted 1:5000 in blocking solution and applied to cells for 5 min. Cells were washed twice more in SAP, rinsed once in PBS, 5 min each. Coverslips were mounted onto slides using Mowiol (CalBiochem #475904), prepared as described in Valnes and Brandtzaeg (Valnes and Brandtzaeg 1985).

Wide Field Image Acquisition and Deconvolution

Stacks of images were collected using a Nikon TE300 microscope with a 60x 1.4NA oil immersion objective with a Photometrics Quantix camera. Cells were randomly selected for imaging if they (1) expressed CD8-furin or other cargo at a level that did not (obviously) alter its normal localization, (2) contained no other obvious abnormality (and thus was deemed representative of the population), and (3) was not dividing, as evidenced by Hoechst staining. We study effects of transmembrane cargo on adaptor protein recruitment so it is important to use minimal recombinant protein expression to mimic the endogenous cargos. Thus, a fourth criterion

in our studies was to choose cells with low intensity staining, compared to the general cell population. However, 3D3I is not limited to the analysis of proteins expressed at minimal levels. For example, if one wanted to evaluate organelle fragmentation in response to over-expression of a protein, this could be achieved simply by selecting cells expressing the higher levels of the protein of interest (based on intensity of staining), and compare them to cells expressing low levels or no recombinant protein. In our case we are interested in the percentage of a signal that is found within an isosurface defined by another marker but the output also gives number and volumes of isosurfaces, which may be the more relevant information to addressing different questions.

Once cells are selected, points above and below the cell in the z-plane were defined by driving the microscope to a point just out of focus on both the top and bottom of the cell. Images were recorded as a series of .tif files with dimensions of 1316x1035 pixels and a file-depth of 16 bits. Stacks of images were collected for two channels with a step-size of 0.2 μm. Exposure times of 200 ms were used for both channels. Serial images, composing the stack of images for each channel, were opened in Huygens SVI Deconvolution software, and were deconvolved using settings appropriate for Alexa594 and Alexa488 fluorophores with a total image change threshold of 0.1, block processing on, and a maximum iteration value of 40. Deconvolved images were returned in .ics format. Images were not processed in any other way prior to the performance of the calculations described.

Image Analysis

Images were analyzed using Imaris6.4 software. For comparison, calculations performed using Imaris were repeated using ImageJ software where indicated. It is of note that after version 7.1, the iterative selection method of object identification is no longer the default setting. For ImageJ analysis, deconvolved .ics files were opened and converted to 16-bit files. The Co-localization Threshold plugin (http://pacific.mpi-

cbg.de/wiki/index.php/Colocalization_Threshold) and the Mander's Calculator plugin (http://www.macbiophotonics.ca/downloads.htm) were used to calculate Pearson's, Mander's M1 and M2, and tM1 and tM2 coefficients. For co-localization analysis performed using Imaris, the deconvolved .ics files were opened and the pixel dimensions were assigned to those corresponding to the wide field microscope described above (0.113 x 0.113 x 0.2 μm per voxel). The merged image was analyzed using the "Co-localization" function and the resulting co-localization coefficients were copied into a text file and saved. A mask of co-localizing pixels, and the scattergram of pixel intensities was later exported. For isosurface generation within Imaris, the image was loaded as described above. The 'Generate Isosurface' function within Imaris, in which the user indicates the channel of interest, was launched and used to define the object. We generated isosurfaces using the 'absolute intensity' settings without filtering. The tabular results were then exported to Excel and a 'snapshot' of the scene containing the isosurface was saved. See Fig. 1 for workflow. Statistical analyses were performed by importing the tabular results from Imaris into GraphPad Prism 5.0 and analyzed using the methods indicated.

2.7. Acknowledgements

The authors would like to thank Victor Faundez for critical reading of the manuscript. This research was supported by funding from the National Institutes of General Medical Sciences (R01-GM067226) and in part by the Microscopy Core of the Emory Neuroscience NINDS Core Facilities (P30-NS055077).

Adler, J., Parmryd, I. (2010). "Quantifying Colocalization by Correlation: The Pearson Correlation Coefficient is Superior to the Mander's Overlap Coefficient." Cytometry Part A **77A**: 733-742.
Andersen, O. M., V. Schmidt, R. Spoelgen, J. Gliemann, J. Behlke, D. Galatis, W. J. McKinstry, M. W. Parker, C. L. Masters, B. T. Hyman, R. Cappai and T. E. Willnow (2006). "Molecular dissection of the interaction between amyloid precursor protein and its neuronal trafficking receptor SorLA/LR11." Biochemistry **45**(8): 2618-2628.
Barlow, A., MacLeod, A., Noppen, S., Sanderson, J., Guefin, CJ. (2010). "Colocalization Analysis in Fluorescence Micrographs: Verification of a More Accurate Calculation of Pearsons' Corelation Coefficient." Microscopy and Microanalysis **16**: 710-724.
Biggs, D. S. (2010). "3D deconvolution microscopy." Curr Protoc Cytom **Chapter 12**: Unit 12 19 11-20.
Borg, J. P., J. Ooi, E. Levy and B. Margolis (1996). "The phosphotyrosine interaction domains of X11 and FE65 bind to distinct sites on the YENPTY motif of amyloid precursor protein." Mol Cell Biol **16**(11): 6229-6241.
Borg, J. P., Y. Yang, M. De Taddeo-Borg, B. Margolis and R. S. Turner (1998). "The X11alpha protein slows cellular amyloid precursor protein processing and reduces Abeta40 and Abeta42 secretion." J Biol Chem **273**(24): 14761-14766.
Cayley, A. (1859). "On Contour and Slope Lines." Philosophical Magazine **18**: 264-268.
Gauch, J. M. (1999). "Image segmentation and analysis via multiscale gradient watershed hierarchies." IEEE Trans Image Process **8**(1): 69-79.
Gniadek, T. J. and G. Warren (2007). "WatershedCounting3D: a new method for segmenting and counting punctate structures from confocal image data." Traffic **8**(4): 339-346.
Griffiths, G., S. Pfeiffer, K. Simons and K. Matlin (1985). "Exit of newly synthesized membrane proteins from the trans cisterna of the Golgi complex to the plasma membrane." J Cell Biol **101**(3): 949-964.
Hammond, A., Glick, BS (2000). "Dynamics of transitional endoplsmic reticulum sites in vertebrate cells." Mol Biol Cell **11**: 3013-3030.
Lodish, H. F. and N. Kong (1983). "Reversible block in intracellular transport and budding of mutant vesicular stomatitis virus glycoproteins." Virology **125**(2): 335-348.
Manders, E., Verbeek, FJ., Aten, JA. (1993). "Measurement of co-localization of objects in dual-color confocal images." Joural of Microscopy **169**(3): 375-382.
McNally, J. G., T. Karpova, J. Cooper and J. A. Conchello (1999). "Three-dimensional imaging by deconvolution microscopy." Methods **19**(3): 373-385.
Mottet, G., C. Tuffereau and L. Roux (1986). "Reduced temperature can block different glycoproteins at different steps during transport to the plasma membrane." J Gen Virol **67 (Pt 9)**: 2029-2035.
Pawley, J. B. (2006). Points, Pixels, and Gray Levels: Digitizing Image Data. Handbook of Confocal Microscopy. J. B. Pawley. New York, NY, Springer Science+Business Media**:** 59-79.
Ridler, T., Calvard, S. (1978). "Picture threholding using an iterative selection method." IEEE Trans on Systems, Man, and Cybernetics **SMC-8**(8): 630-632.
Saraste, J. and E. Kuismanen (1984). "Pre- and post-Golgi vacuoles operate in the transport of Semliki Forest virus membrane glycoproteins to the cell surface." Cell **38**(2): 535-549.
Seaman, M. N. (2004). "Cargo-selective endosomal sorting for retrieval to the Golgi requires retromer." J Cell Biol **165**(1): 111-122.
Shaw, P. J. (2006). Comparison of Widefield/Deconvolution and Confocal Microscopy for Three-Dimensional Imaging. Handbook of Confocal Microscopy. J. B. Pawley. New York, NY, Springer Science+Business Media**:** 453-467.
Shrivastava-Ranjan, P., V. Faundez, G. Fang, H. Rees, J. J. Lah, A. I. Levey and R. A. Kahn (2008). "Mint3/X11{gamma} Is an ADP-Ribosylation Factor-dependent Adaptor that Regulates

the Traffic of the Alzheimer's Precursor Protein from the Trans-Golgi Network." Mol Biol Cell **19**(1): 51-64.
Teuchert, M., S. Berghofer, H. D. Klenk and W. Garten (1999). "Recycling of furin from the plasma membrane. Functional importance of the cytoplasmic tail sorting signals and interaction with the AP-2 adaptor medium chain subunit." J Biol Chem **274**(51): 36781-36789.
Thomas, G. (2002). "Furin at the cutting edge: from protein traffic to embryogenesis and disease." Nat Rev Mol Cell Biol **3**(10): 753-766.
Valnes, K. and P. Brandtzaeg (1985). "Retardation of immunofluorescence fading during microscopy." J Histochem Cytochem **33**(8): 755-761.
Woodcroft, B., Hammond, L., Stow, JL., Hamilton, NA. (2009). "Automated organelle-based coloclaizaiton in whole-cell imaging." Cytometry Part A **75A**: 941-950.
Yang, X., Beyenal, H., Harin, G., Lewandowski, Z. (2001). "Evaluation of Biofilm Image Thresholding Methods " Water Research **35**(5): 1149-1158.

CHAPTER 3

A ROLE FOR CARGO IN ARF-DEPENDENT ADAPTOR RECRUITMENT[6]

[6] Reproduced and modified with permission from Caster, A. H., Sztul, E., and Kahn, R. A. (2013) A role for cargo in Arf-dependent adaptor recruitment, *J. Biol. Chem.*, 288(21): 14788-14804.

3.1. Summary

Membrane traffic requires the specific concentration of protein cargos and exclusion of other proteins into nascent carriers. Critical components of this selectivity are the protein adaptors that bind to short, linear motifs in the cytoplasmic tails of transmembrane protein cargos and sequester them into nascent carriers. The recruitment of the adaptors is mediated by activated Arf GTPases and the Arf-adaptor complexes mark sites of carrier formation. However, the nature of the signal(s) that initiate carrier biogenesis remains unknown. We examined the specificity and initial sites of recruitment of Arf-dependent adaptors (AP-1 and GGAs) in response to the Golgi or endosomal localization of specific cargo proteins (furin, mannose-6-phosphate receptor (M6PR) and M6PR lacking a C-terminal domain M6PRΔC). We find that cargo promotes the recruitment of specific adaptors, suggesting that it is part of an upstream signaling event. Cargos do not promote adaptor recruitment to all compartments in which they reside and thus additional factors regulate the cargo's ability to promote Arf activation and adaptor recruitment. We document that within a given compartment different cargos recruit different adaptors suggesting that there is little or no free, activated Arf at the membrane and that Arf activation is spatially and temporally coupled to the cargo and the adaptor. Using temperature block, Brefeldin A, and recovery from each, we found that the cytoplasmic tail of M6PR causes the recruitment of AP-1 and GGAs to recycling endosomes and not at the Golgi, as predicted by steady state staining profiles. These results are discussed with respect to the generation of novel models for cargo-dependent regulation of membrane traffic.

3.2 Introduction

Members of the ADP-ribosylation factor (Arf) family of regulatory GTPases, within the larger Ras superfamily, play fundamental roles in the regulation of membrane traffic at multiple sites in all eukaryotes, including at least the Golgi, endosomes, endoplasmic reticulum (ER), ER-Golgi intermediate compartments, and plasma membrane. Probably the most completely

characterized is Sar1, the most divergent member of the Arf family, and its role in recruitment of the COPII coat to nascent buds emanating from the ER (Nakano and Muramatsu 1989, Kuge, Dascher et al. 1994). A far more complicated picture emerges for the specific roles of the Arfs in the regulation of membrane traffic at the Golgi and endosomes. At these sites multiple Arfs (Arf1-5) have been implicated as regulators with at least some level of redundancy in functions (Volpicelli-Daley, Li et al. 2005). The best known of these functions is the direct recruitment of soluble protein adaptors that also bind directly to linear motifs present in the cytosolic "tails" of transmembrane protein "cargos" (Aridor and Traub 2002, Bonifacino and Lippincott-Schwartz 2003). Perhaps the most vivid demonstration of this is through the use of the drug Brefeldin A (BFA), which prevents Arf activation by direct binding and inhibition of a subset of the Arf guanine nucleotide exchange factors (GEFs) and causes rapid release of Arf-dependent adaptors in live cells. However, Arfs have also been shown to directly bind and/or activate phospholipase D, PI 4-kinase and PI(4)P 5-kinase (Cockcroft, Thomas et al. 1994, Godi, Pertile et al. 1999, Jones, Morris et al. 2000). It is the combination of functional redundancy and multiplicity of effectors that has made dissection of signaling demanding and resulted in delays in advance of molecular models of the mechanisms of Arf actions. Even more importantly, we still lack a fundamental understanding of what spatially regulates Arf activities and thus struggle to understand Arf's role in membrane traffic.

Like all regulatory GTPases, Arfs act in cells as molecular switches, toggling between activated (GTP-bound) and inactivated (GDP-bound) states. These different states are conformational and result in different affinities for binding partners, notably the effector proteins that lead to the generation of the biological response. Inter-conversion between conformational states is controlled by the actions of guanine nucleotide exchange factors (GEFs), which promote the rate-limiting dissociation of GDP and allow GTP to bind and activate the GTPase. Conversely, return to the inactive state is controlled kinetically by the actions of GTPase activating proteins (GAPs), which increase the rate of GTP hydrolysis by the GTPase.

The heterotrimeric G proteins are paradigms for regulatory GTPase signaling and use G protein coupled receptors (GPCRs), which act directly as G protein GEFs, to acutely and locally activate G proteins in response to ligand binding (Luttrell, Daaka et al. 1999). This binding initiates signaling by G proteins, with consequent changes in effector activation and generation of second messengers. Even a cursory review of the history of G protein research reveals that knowledge of the ligand as initiator of signaling and the ability to acutely activate G protein signaling allowed researchers to identify components that are required for signal generation and modulation. In addition, the use of different ligands allowed clear descriptions of the sources of specificity in G protein signaling. Similarly, ligand binding to receptor tyrosine kinases (RTKs) can result in phosphorylation of specific residues in the cytoplasmic tails that act as binding sites for Grb2/SOS, which is a Ras GEF (Luttrell, Daaka et al. 1999). Thus, paradigms for activation of regulatory GTPases are found within these two homologous systems in which ligand binding to transmembrane proteins leads to localized activation of a GEF activity and consequently the activation of a specific and narrow subset of cellular GTPases. In contrast, despite over 25 years of research into Arf biology, we still don't know the initiator of signaling or whether the process is initiated via a "ligand equivalent" or may be constitutive. To begin to address this central question of Arf biology we developed a cell-based model for Arf activation using the best characterized Arf effectors, the Arf-dependent adaptors.

Adaptors are soluble proteins or protein complexes that are recruited to membranes through direct binding to activated Arf and to sorting signals in transmembrane proteins, which we term cargos. The function of adaptor recruitment is the initiation of formation of a coated bud, later maturing into a carrier, that (i) concentrates cargo by binding specific sorting signals, (ii) deforms planar bilayers into tubes and carriers, (iii) and recruits accessory proteins required for carrier maturation, scission, binding to cytoskeletal elements, targeting to and destination membranes, and initiating uncoating and fusion at that site (Rothman and Orci 1992, Rothman and Wieland 1996, Robinson and Bonifacino 2001, Bonifacino and Lippincott-Schwartz 2003,

Lee, Miller et al. 2004). At least eight of these Arf-dependent adaptors have been reported to be recruited to Golgi membranes by activated Arf(s) and each has been described as binding distinctive sorting motifs; the heptameric COPI complex binds KKXX (Cosson and Letourneur 1994, Letourneur, Gaynor et al. 1994) and FF motifs (Fiedler, Veit et al. 1996, Sohn, Orci et al. 1996), GGAs1-3 bind DXXXLL (Jacobsen, Madsen et al. 2002), Mint3 binds the YENPXY motif (Borg, Ooi et al. 1996), and adaptins (AP-1-AP-4) bind the YXXϕ (Owen and Evans 1998) and XXXLL (Aguilar, Ohno et al. 1997) motifs. Each of these Arf-dependent adaptors is soluble and present in cytosol until recruited to the membrane of budding carriers by activated Arfs. Arfs also reside in cytosol and are recruited to membranes through hydrophobic interactions involving the amphipathic N-terminal α-helix and covalently attached N-terminal myristate (Liu, Kahn et al. 2010). The association of Arfs with membranes is tightly linked to their activation, exchange of GDP for GTP, catalyzed by an Arf GEF. Thus, monitoring Arf recruitment to membranes might be one way to assay for their activation in cells. However, we lack antibodies capable of recognizing specific Arfs on membranes. In addition, there have been well-documented concerns over the use of tagged Arfs or fusion proteins (Jian, Cavenagh et al. 2010). Thus, to begin the search for factors that lead to Arf GEF activation in cells, we use Arf-dependent adaptor recruitment as an indirect assay for Arf activation in cells.

Because specific adaptors have been associated in the literature with specific transmembrane cargos and at specific sites in cells, we chose a set of cargos for our cell-based assays that would provide overlapping but also specific differences in adaptor recruitment; specifically, the cation-independent, mannose 6-phosphate receptor (M6PR) and furin. These are previously characterized single pass, type I transmembrane proteins that bind directly to overlapping sets of adaptors via previously defined sorting signals. M6PR binds to AP-1 and GGAs in what has widely been interpreted as a requirement for its anterograde traffic from the Golgi to the endosome (Puertollano, Aguilar et al. 2001, Doray, Bruns et al. 2002). The M6PR has been extensively studied as a model for bi-directional Golgi-endosome traffic (Geuze,

Stoorvogel et al. 1988, Karlsson and Carlsson 1998, Klumperman, Kuliawat et al. 1998, Tikkanen, Obermüller et al. 2000, Arighi, Hartnell et al. 2004). M6PRs act in cells to transport soluble, lumenal, mannose 6-phosphate modified hydrolases from the Golgi to their site of action in lysosomes. The binding site for GGAs on the M6PR C-terminal, cytoplasmic tail is known, allowing members of the Robinson lab to generate a truncation mutant, M6PRΔC, which retains AP-1 binding but has lost the ability to recruit GGAs (Hirst, Seaman et al. 2007). M6PRs are found predominantly on Golgi, endosomal, and plasma membranes with different steady state distributions in different cell types. Furin is a protease that cleaves proteins at RR/KK motifs within the Golgi lumen (for review, see Thomas (Thomas 2002)). It is localized predominantly to the Golgi, but can escape to endosomes, where it may also function prior to retrieval back to the Golgi. Furin contains within its cytoplasmic tail a sorting sequence that binds directly to AP-1 (Teuchert, Schafer et al. 1999). This interaction has been reported to be responsible for the export of furin from the Golgi to endosomes (Teuchert, Schafer et al. 1999). Furin can also bind to Mint3 (Han, Wang et al. 2008). Mint3 binds the cytoplasmic tail of furin at the Golgi, but it acts to retain furin there (Han, Wang et al. 2008).

We originally chose to focus our studies on adaptor recruitment to the Golgi. Focusing on this location allowed us to take advantage of two well-characterized protocols that affect cargo traffic there: low temperature incubation (20°C) serves as a kinetic block of export from the Golgi (Matlin and Simons 1983, Griffiths, Pfeiffer et al. 1985, Saraste, Palade et al. 1986, Ladinsky, Wu et al. 2002), and BFA treatment that causes the rapid and reversible loss of Arf-dependent adaptors from membranes (Lippincott-Schwartz, Yuan et al. 1989, Donaldson, Lippincott-Schwartz et al. 1990, Traub, Ostrom et al. 1993). Our data confirm the specificities of cargo tail-adaptor interactions established previously from *in vitro* binding data and highlight important differences in the sites of adaptor recruitment by different cargos.

3.3. Results

To identify the signal(s) leading to Arf activation we sought to develop cell-based assays for Arf activation that are spatially and temporally restricted, as expected for biologically relevant processes. Because the Arfs and adaptors reside in excess in cytosol, we expect that the transmembrane cargos will be limiting for generation of the cargo-adaptor-Arf complexes. To ensure that the cargo-dependent adaptor recruitment being studied results primarily or exclusively from cytoplasmic surface interactions we performed studies using fusion proteins made up of the lumenal and transmembrane domains of CD8, fused to the cytoplasmic tails of furin or M6PR; termed CD8-furin and CD8-M6PR, respectively. The value of such CD8 fusion proteins has been demonstrated by previous work in the laboratories of Robinson and Seaman (Seaman 2004, Hirst, Seaman et al. 2007, Seaman 2007). We obtained from them the CD8-M6PR plasmid and a C-terminal truncation mutant of CD8-M6PR, termed CD8-M6PRΔC, which retains binding to AP-1 but has lost the GGA binding motif and ability to recruit GGAs ((Hirst, Seaman et al. 2007), and see below). To ensure that the CD8-fusion proteins are indeed representative of the full-length proteins we also performed the same studies using either an N-terminal fusion of GFP-M6PR or N-terminal FLAG tagged furin (FLAG-furin). HeLaM cells were used in most of our studies because they are adherent, flat, and display low levels of perinuclear adaptor staining, facilitating imaging of cargo-dependent adaptor recruitment. The availability of stably transfected HeLaM cells expressing CD8-M6PR or CD8-M6PRΔC also provided a useful control for potential artifacts resulting from the more variable levels of expression seen after transient transfections. Each of the major findings described below were confirmed using these stably transfected cells.

Cargo defines the specificity of Arf-dependent adaptor recruitment

HeLaM cells were transiently transfected with plasmids encoding CD8-furin, CD8-M6PR, or CD8-M6PRΔC and analyzed by indirect immunofluorescence for the effects of cargo

expression on adaptor recruitment. Conditions were chosen to minimize the level of protein expression (see Experimental Procedures); e.g., only those cells displaying minimal but clear evidence of protein expression were chosen for analyses. Immunoblotting of total cell lysates revealed that each of the CD8 fusion proteins was expressed to similar levels (not shown).

Expression of the three cargos resulted in specific profiles of adaptor recruitment. The expression of CD8-furin (Fig. 1A) or FLAG-furin (data not shown) led to the specific recruitment of AP-1 and Mint3 but not GGA1. Expression of CD8-M6PR (Fig. 1A) or GFP-M6PR caused specific increases in the perinuclear staining of AP-1 and GGA1 (Fig. 1C) but not Mint3, while expression of CD8-M6PRΔC led to increases in AP-1 staining but not that of GGA1 or Mint3 (Fig. 1A). We also stained fixed cells for GGA2 and GGA3 and in each case they behaved qualitatively the same as described for GGA1 (data not shown). Transient transfection resulted in cells with varying levels of expression of M6PR or CD8-M6PR within a cell population and we noted by visual inspection a good correlation between the levels of cargo expression and levels of recruitment of AP-1 and GGAs, with no changes to staining of Mint3, even in cells expressing the highest levels of cargo. HeLaM cells stably transfected with CD-M6PR or CD8-M6PRΔC resulted in adaptor recruitment profiles identical to those seen using transient transfections. The data shown in Figure 1A are single cell representatives of the consequences on adaptor recruitment from specific cargo expression. The detailed and rigorous quantification of these responses is described below.

Thus, the cell-based assay for cargo-dependent adaptor recruitment faithfully recapitulates the specificity with which sorting motifs in the cytoplasmic tails of these cargos bind adaptors *in vitro* (Heilker, Manning-Krieg et al. 1996, Honing, Griffith et al. 1996, Takatsu, Katoh et al. 2001). Importantly, in every experiment described herein, we didn't observe a change in the endogenous levels of the adaptors being studied, as determined by immunoblotting of total cell lysates for γ-adaptin (a component of AP-1), GGA1, and MINT3 (Fig. 1B). Thus, we interpret the

increased staining of each adaptor at a membrane surface to result from its recruitment from a cytosolic pool and not from a change in expression levels. Together, these results suggest that cargo levels modulate activation of ARFs and subsequent adaptor recruitment, positioning cargo upstream in the activation pathway. Our data suggest that cargo-mediated activation of ARFs is restricted in the sense that no free ARF is produced to recruit non-relevant adaptor, i.e., although CD8-M6PR activates ARFs, those ARFs only recruit AP-1 and GGA1 but not Mint3. Thus, the activated ARFs function within the context of the cargo responsible for its activation. Unfortunately, technical limitations currently prohibit us from identifying which ARFs are involved in each adaptor recruitment and whether they differ with cargo.

To further confirm that recruitment of Arf-dependent adaptors and their responsiveness to different perturbations are consistent between full-length cargos and their CD8-fusion constructs, we compared results with an N-terminal tagged form of full length M6PR (Fig. 1C). GFP-M6PR expression resulted in increased GGA1 (Fig. 1C) and AP-1 (data not shown) recruitment to the Golgi. As fixation can affect the ability of GFP to fluoresce (REF), we indirectly labeled cells expressing GFP-M6PR by staining them with a primary antibody against GFP, using a secondary antibody conjugated to Alexa 405, allowing us to image GFP-M6PR on a channel distinct from the GFP excitation/emission profile (488nm/519nm, respectively). Cells were chosen for imaging if they showed low levels of GFP expression on both the 405nm and 488nm channels. The GFP-M6PR dependent recruitment of GGA1 (Fig. 1C) or AP-1 (data not shown) to the Golgi were lost in response to 20°C temperature block, as described in detail below. Thus, these properties and others reported below were consistent throughout for both full-length proteins and the CD8-fusions of the paralogous cargo.

Cargos localize differently within the endomembrane system and within the Golgi

The adaptor recruitment shown in Fig. 1A was quite striking and unambiguous. Despite this, and to be able to compare results with different cargos and to determine sites of recruitment for adaptors that potentially act at more than one site, we developed protocols for quantifying adaptor recruitment. Because the Golgi and endosomes are irregular structures that can appear quite different between cells and in different focal planes of the same cell, we sought a method that is inclusive of all staining in each cell and is not subject to focal plane bias. We used three dimensional image-based isosurface intensity (3D3I) analysis (Caster and Kahn 2012), that employs wide field imaging with deconvolution and Imaris software to quantify overlap of staining of any two antigens in fixed cells. In our studies we used 3D3I to generate isosurfaces defined by cargo or organelle marker staining and determined the extent to which adaptor or cargo staining is included in those defined isosurfaces. Results are expressed as a ratio of total pixel intensity of adaptor or cargo per unit volume of isosurface (defined by the cargo or marker) from each cell, in the units of sum staining intensity/μm^3. This method has a number of advantages: (1) isosurfaces are defined by a biologically relevant marker, (2) we monitor changes in co-localization throughout the entire volume of the cell and thus avoid sampling or focal plane bias, (3) we perform statistical analyses on a number of cells, comparing intensity per unit volume in control vs experimental conditions, as opposed to performing statistical analysis on mean correlational scores. We note that this method yields fold-differences that are typically smaller than those from simple pixel overlap approaches and that statistical testing allows high confidence in the conclusions.

To determine the location of each cargo at steady state (defined herein as HeLaM cells fixed 24 hr after transfection and maintained throughout at 37°C) we quantified the overlap of each cargo with that of a number of markers of the Golgi/TGN and endosomal compartments. The Golgi is a heterogeneous compartment with at least three regions, defined relative to import and export sites as cis-, medial-, and trans-Golgi, with the *trans*-Golgi network (TGN) emerging

from this last compartment and typically not resolved from the trans-Golgi at the level of light microscopy. We used p115 or GM130, giantin, mannosidase II and TGN46 as previously characterized markers of the early, middle, and late Golgi/TGN compartments.

When we compared the localization of each cargo to that of the different Golgi markers we found some marked and surprising differences. At steady state, most (71.3 +/- 14.8%) CD8-furin staining was found within TGN46 isosurfaces, with 51.3 +/- 11.7% also within giantin isosurfaces (Fig. 2A, filled bars). This reveals localization to multiple compartments but with a clear bias towards the TGN. Note that the sum can be greater than 100% when the markers themselves overlap. In contrast, only 19.0 +/- 6.4% of all CD8-M6PR staining was found within TGN46 isosurfaces, and 25.9 +/- 15.4% within giantin isosurfaces in cells maintained at 37°C (Fig. 2A, filled bars). This indicates that CD8-M6PR is more widely distributed and less concentrated in parts of the late Golgi/TGN containing these markers than is CD8-furin. These data were obtained from images such as those shown in Fig. 2B, where cells were stained for the cargos and Golgi markers indicated. Isosurfaces were generated for both the cargo and the Golgi marker. The cargo was falsely colored as a red/yellow heat map based on the amount of Golgi marker also present within the cargo isosurface (Fig. 2B, scale shown on right edge). The Golgi marker is displayed in green. CD8-furin is biased towards the TGN (compare the amount of yellow in the upper left panel vs. the right), while CD8-M6PR is more evenly distributed within giantin and TGN46 labeled compartments (compare lower left vs. right panels). These results are consistent with previously described roles for furin as an endopeptidase that localizes to the Golgi and is predominantly retained there and for M6PR as a carrier for lysosomal enzymes that cycles between the Golgi and TGN/endosomal compartments.

For comparison, we also used the more common measures of co-localization, by evaluating the distribution of CD8-M6PR within the Golgi by comparing the overlap (Mander's coefficients) of cargo staining from a single plane of a confocal image with markers of early (p115) medial (mannosidase II), and late (TGN46) Golgi (Fig. 2C). This method of quantification

essentially serves as a coincidence detector, indicating the co-localization of a Golgi marker and cargo signals. Using this approach, CD8-M6PR showed more overlap with TGN46 than it did with early or medial Golgi markers (p115 and mannosidase II, respectively). Thus, there is a clear bias of CD8-M6PR toward the later Golgi compartments/TGN. Note that the two different methods of quantifying co-localization of two antigens yield very different percentages; e.g., ~20% for CD8-M6PR within TGN46 isosurfaces and ~80% for CD8-M6PR and TGN46 using Mander's coefficients. We believe that the 3D3I method yields a much better indication of the location of the antigen within the cell while the latter gives useful information regarding the presence or absence of the antigen within an organelle, but can give a false impression of the overall distribution.

When we compared the distribution of CD8-M6PR to that of CD8-M6PRΔC we found statistically significant differences. The amount of CD8-M6PRΔC that overlapped with the markers of early, middle and late Golgi were all quite similar; p115, 32.3 +/- 1.8%, mannosidase II 45.2+/- 4.2%, and TGN46 staining 40.2+/- 3.8%. Thus, the truncation of the C-terminus resulted in the inability to concentrate within the later compartments of the Golgi, as seen for the full-length CD8-M6PR.

CD8-M6PR accumulates at the Golgi in response to a 20°C block

To test one aspect of our model, that cargo concentration is a determinant of adaptor recruitment; we sought a minimally invasive method for modulating cargo concentration at a functionally important site in anterograde traffic. We used the previously characterized 20°C block, in which cells are grown at 20°C for four hours, during which time protein synthesis and export from the ER continue but export from the late Golgi/TGN is inhibited (Lodish and Kong 1983, Saraste and Kuismanen 1984, Griffiths, Pfeiffer et al. 1985, Mottet, Tuffereau et al. 1986). Because M6PR acts to escort lysosomal hydrolases and other mannose 6-phosphate modified proteins to lysosomes, its traffic between the Golgi and the endosomal-lysosomal pathway is bi-

directional. Thus, a block in protein export from the Golgi in response to 20°C block is predicted to cause accumulation of M6PR at the Golgi. To confirm this, CD8-M6PR was expressed in HeLaM cells and the next day cells were either maintained at 37°C or incubated at 20°C for four hours prior to fixation. Visual inspection of CD8-M6PR staining confirmed that the cargo is increased at the Golgi during 20°C block, as evidenced by the increased perinuclear and decreased peripheral staining. To quantify this we used 3D3I to compare the percentage of CD8-M6PR staining that was seen within the isosurface defined by giantin staining and found double the amount; 25.9 +/- 15.4% at 37°C to 49.0 +/- 6.2% after the 20°C block (Fig. 2A). Similar results were obtained using cells stably transfected with CD8-M6PR (data not shown).

To determine whether the 20°C block resulted in changes in intra-Golgi localization of CD8-M6PR, we compared its co-localization with markers of early (p115), medial (giantin), or late (TGN46) Golgi in cells maintained at 37°C to those after 20°C block. While the levels of CD8-M6PR co-localization with each marker were increased, they were increased about equally across these three compartments (data not shown). Thus, we conclude that the absolute amount of CD8-M6PR within compartments of the Golgi was increased during 20°C block, but its distribution within the Golgi as a whole was maintained, with a clear bias toward later compartments.

When we looked at the effects of the temperature block on CD8-M6PRΔC we saw clear increases in cargo in all compartments of the Golgi, relative to controls (37°C), and again with no change in its distribution, which in this case is more uniform across Golgi compartments. Cells stably transfected with CD8-M6PRΔC showed similar, uniform distribution throughout the Golgi. Thus, the 20°C block causes both M6PR-based cargos to accumulate in the Golgi, and the cargos retain the same distribution across the Golgi seen in control cells.

Localization of full-length GFP-M6PR in response to temperature block was also tested. HeLaM cells transfected with GFP-M6PR were maintained at 37°C or temperature blocked for four hours. Cells were stained with antibodies against GFP and GM130. In cells maintained at

37°C, GFP-M6PR staining localized predominantly to punctate, endosomal-like structures throughout the cytosol (refer to Fig. 1C). After 20°C block, GFP-M6PR staining localized prominently in the perinuclear region, overlapping with GM130 staining (data not shown). Thus, the full-length cargo, GFP-M6PR, behaves similar to the CD8-M6PR, as it is sensitive to temperature block and re- localizes to the Golgi during incubation at 20°C.

Cargos are present in locations without adaptors

Because we hope to develop models for cargo-dependent adaptor recruitment we investigated further the site of adaptor concentration, relative to both the cargo and different compartments of the Golgi. We first asked where AP-1 is found in response to cargo expression. The expression of CD8-furin, CD8-M6PR, or CD8-M6PRΔC resulted in increased AP-1 staining in the perinuclear region when compared to mock transfected cells. We found that there was virtually no recruitment of AP-1 to early Golgi compartments in control cells or those expressing CD8-furin or either CD8-M6PR construct. The amount of AP-1 staining in p115-defined isosurfaces was so small that we did not quantify it. Instead, we compared cargo dependent concentration of AP-1 to giantin and TGN46 compartments and found a strong bias of AP-1 to these compartments for both CD8-furin and CD8-M6PR at steady state (Fig. 3A, black bars). As expected, the full cytoplasmic tail of M6PR or that portion that contains the AP-1 binding site each promotes localization of AP-1 to the Golgi. Thus, despite the presence of each of these cargos at early compartments within the Golgi, they are each capable of promoting the binding of AP-1 to only late Golgi compartments. Thus, at steady state the cargos used herein vary in relative abundances at different sites along the endomembrane system but promote the recruitment of adaptors to more spatially restricted sites. We conclude that cargo is necessary but not sufficient for adaptor recruitment and that other factor(s) are required to spatially restrict coat recruitment.

Adaptors are lost from M6PR isosurfaces in response to 20°C *block*

We predicted that the significant accumulation of CD8-M6PR at the Golgi during the 20°C block would be matched by increases in both AP-1 and GGA recruitment, as each has been proposed to function in export of M6PRs from that site (Doray, Bruns et al. 2002, Ghosh and Kornfeld 2004). Furthermore, we predicted that both cargo and adaptors would diminish in abundance during the recovery from the 20°C block, as carriers containing CD8-M6PR/adaptor pairs exited the Golgi and returned to steady state levels. Unexpectedly, we found that in cells expressing CD8-M6PR the staining of AP-1 (Fig. 3B) and GGA1 (Fig. 3C) were dramatically reduced during the 20°C block, to the extent that they were indistinguishable from control cells that don't express CD8-M6PR. Similarly, in cells expressing CD8-M6PRΔC, AP-1 staining was significantly decreased (Fig. 3E). We also evaluated adaptor recruitment in cells stably transfected with CD8-M6PR or CD8-M6PRΔC and found AP-1 recruitment to be lost following temperature block, recapitulating our observations using transiently transfected cells. The amount of AP-1 recruited to cargo volumes was quantified using 3D3I (Fig. 3G). Values were normalized to sum AP-1 intensity/cargo volume and analyzed by Student's t-test, comparing 37°C to 20°C block for each cargo. The decrease in AP-1 staining intensity was significant for both CD8-M6PR and CD8-M6PRΔC, with the latter being more dramatic as a result of the increase in AP-1 staining seen over that with CD8-M6PR in cells maintained at 37°C.

We also evaluated AP-1 at the Golgi (giantin isosurfaces) in cells expressing CD8-M6PR, CD8-M6PRΔC, or CD8-furin (Fig. 3H, quantified in Fig. 3A). Consistent with previous results, AP-1 staining at the Golgi is dramatically lowered in response to 20°C block in cells expressing CD8-M6PR or CD8-M6PRΔC. We also quantified GGA1 staining in cells stably or transiently expressing CD8-M6PR or CD8-M6PRΔC and found that temperature block had the same effect as it did on AP-1, causing its dissociation (Fig. 3I and data no shown). Thus, for CD8-M6PR the cargo and adaptors respond in opposite ways to the temperature block, with the cargo being significantly increased in abundance at the Golgi but AP-1 and GGA1 adaptors that presumably

facilitate its export from that compartment being lost. These results also support the conclusion that cargo is necessary but not sufficient to recruit adaptors, and confirm that additional factors regulate cargo-dependent ARF activation.

We used FAPP2 staining as a control for effects of the 20°C block on a cargo-independent, Arf-dependent effector at the Golgi and for general integrity of the Golgi. FAPP2 staining in control HeLaM cells (Fig. 3D) or cells over-expressing cargos (data not show) displayed a Golgi pattern of FAPP2 staining that was unchanged by 20°C block. This provides indirect evidence that neither phosphatidylinositol 4-phosphate levels, required for FAPP2 binding to Golgi (Godi, Pertile et al. 1999, Godi 2004), nor the "non-specific" levels of activated Arfs were grossly altered at the Golgi in response to cargo over-expression or temperature block. Our results are consistent with 20°C block causing only minimal perturbation to Golgi physiology and morphology, as previously reported using related assays (Ladinsky, Wu et al. 2002). In addition we have used mock transfections or homologous cargos, e.g., CD8 fused to the cytoplasmic tail of the amyloid precursor protein (CD8-APP) that do not bind AP-1 or GGAs, and found no significant changes in AP-1 (data not shown) or GGA1 recruitment at steady state or after temperature block (Fig. 3I). Together, our data show that CD8-M6PR and CD8-M6PRΔC are maintained or increased in abundance at the Golgi in response to 20°C block, but that AP-1 was lost from CD8-M6PR and CD8-M6PRDC when these proteins were arrested in traffic by a 20°C block.

Similar results were obtained when GFP-M6PR was expressed in HeLaM cells. GFP-M6PR expression resulted in the recruitment of AP-1 to the perinuclear region at steady state, but this recruitment was lost following temperature block (data not shown).

CD8-furin shows little change in localization, but AP-1 recruitment is increased in response to a 20°C block

The furin endoprotease acts at the Golgi and is retained there through a mechanism that involves the binding of Mint3 (Han, Wang et al. 2008). But furin also "escapes" to the endosomal system, using AP-1 in the process (Teuchert, Schafer et al. 1999). Thus, it was difficult to predict what impact the 20°C block might have on the localization of CD8-furin. The levels of CD8-furin at the Golgi before and after 20°C block were compared by doubly staining for CD8-furin and giantin (Fig. 2A). The percentages of CD8-furin found within the giantin-defined isosurface before and after 20°C block were 51.3 +/-11.7% and 66.0 +/- 5.8%, respectively (Fig. 2A). The percentages of CD8-furin found within TGN46-defined isosurfaces before and after 20°C block were 71.3 +/- 14.8% and 76.0 +/- 7.4%, respectively (Fig. 2A). The already high fraction of CD8-furin at the Golgi was seen to increase but not significantly ($p > 0.01$). Thus, we found that 20°C block is an effective inhibitor of M6PR export from the Golgi/TGN leading to its accumulation there, but has a far more limited effect on furin accumulation, likely because furin already accumulates in the Golgi.

In cells expressing FLAG-furin (data not shown), or CD8-furin, AP-1 staining was maintained throughout the 20°C block (Fig. 3F). AP-1 accumulation at CD8-furin defined isosurfaces was actually significantly *increased* following 20°C block, compared to cells maintained at 37°C (Fig. 3G). To ensure that the increased recruitment was still occurring on Golgi surfaces we also quantified the AP-1 staining present in giantin isosurfaces in cells with and without 20°C block (Fig. 3A). We found that the 20°C block increases AP-1 staining into giantin isosurfaces in CD8-furin expressing cells compared to controls ($p<0.01$), and rising to the level of statistical significance at the level of $p<0.05$ (though not $p<0.01$) when compared to CD8-furin expressing cells maintained at 37°C. The CD8-furin dependent increase in AP-1 is striking at both 37°C and 20°C, each significantly higher than controls (Fig. 3A) as well as from each other. Thus, the 20°C block increases the abundance of AP-1 in CD8-furin isosurfaces (Fig.

3F) as well as Golgi membranes, defined by giantin staining (Fig. 3A). Together with the FAPP2 control, these results highlight the specific and unexpected loss of adaptors from M6PR cargos during temperature block, including both full length GFP-M6PR and the CD8-M6PR fusion proteins.

BFA treatment also promotes loss of adaptors from M6PR and recovery is initiated at a site other than Golgi

We sought an assay independent of temperature changes and more rapid than the four hour 20°C block to assess sites of adaptor recruitment. We used the previously characterized ability of BFA to rapidly and reversibly inhibit a subset of Arf GEFs to inhibit Arf activation and Arf-dependent adaptor recruitment in live cells. This provides both a further confirmation that the adaptor recruitment being studied is in fact Arf-dependent, and also allows the synchronized re-recruitment of adaptors during recovery from the drug. Treatment with BFA blocks the activation of Arfs within seconds and strips endomembrane structures of Arf-dependent adaptors (Lippincott-Schwartz, Yuan et al. 1989, Wood, Park et al. 1991). After a two minute exposure to BFA (7.5 μg/ml; 0 min recovery) membrane staining of AP-1 (Fig. 4A, B), GGA1 (Fig. 4C), and Mint3 (data not shown) were completely lost. Only at longer times of BFA treatment (or higher doses) does the Golgi fragment, with retrograde movement of Golgi components to the ER (Lippincott-Schwartz, Yuan et al. 1989). After two minutes of BFA exposure we observed no changes in staining of the Golgi in general (Fig. 4A, B, C) with the exception that markers of the TGN may become more tubulated in appearance (not evident in the images shown in Fig. 4). And by about 15 min into the recovery phase, staining for Golgi markers typically became less reticular and more globular in appearance.

In CD8-furin expressing cells, the cargo-dependent recruitment of AP-1 (Fig. 4A) and Mint3 (data not shown) were each lost within 2 min of BFA treatment. Within 5 minutes of BFA washout, both AP-1 (Fig. 4A) and Mint3 (data not shown) adaptors were recruited back to the

Golgi, returning to control (vehicle only) levels within 10-15 min of washout. The staining of the re-recruited adaptors at each time point was characteristic of Golgi staining; i.e., perinuclear, often lamellar in appearance, and showing extensive overlap with giantin. The rapid return of both AP-1 and Mint3 to the Golgi after BFA washout is consistent with that being the initial site of recruitment of each adaptor in response to the presence of CD8-furin. FAPP2 staining was also lost in response to BFA and returned to the Golgi with kinetics indistinguishable from those of adaptors recruited by CD8-furin (data not shown). We conclude that AP-1 and Mint3 are each recruited to the Golgi by CD8-furin in an Arf-dependent, BFA-sensitive manner.

In cells either transiently or stably transfected to express CD8-M6PR, the Golgi re-recruitment of GGA1 and AP-1 after BFA washout was delayed, relative to that seen for CD8-furin dependent adaptors or FAPP2. Also, the pattern of AP-1 and GGA1 staining as they first re-appeared differed from that seen in cells that had not been exposed to BFA in that it was more punctate and peripheral. This punctate staining became apparent by ~15 min, while the more Golgi-like staining pattern seen in control cells was not evident until ~30 min of recovery from the drug. By 15 min of recovery from BFA, during which time AP-1 had clearly returned to the Golgi/TGN in CD8-furin expressing cells (Fig. 4A), we saw no evidence of Golgi localization of AP-1 in cells expressing CD8-M6PR (data not shown). Similarly, GGA1 was not re-recruited to the Golgi in cells expressing CD8-M6PR (Fig. 4C). Thus, the recruitment of both AP-1 and GGA1 in cells expressing CD8-M6PR during recovery from BFA were initiated at a compartment distinct from what was observed for AP-1 and Mint3 recruitment in cells expressing CD8-furin; i.e., the Golgi.

In cells expressing CD8-M6PRΔC, the re-recruitment of AP-1 was similar to that seen with CD8-M6PR expressing cells. AP-1 was recruited to peripheral puncta by about 15 min after washout. By 30 min, GGA1 was localized to Golgi compartments, similar in appearance to cells treated with vehicle only.

BFA treatment and recovery from drugs of cells expressing GFP-M6PR resulted in similar patterns of adaptor recruitment, with BFA treatment causing the loss of both GGA1 and AP-1 staining in the perinuclear region and only after 15 min washout was recruitment detected. The newly recruited adaptors were again seen first on sites that were clearly distinct from the Golgi as determined by GM130 staining, and identified as recycling endosomes by co-localization with TfR.

M6PR recruits AP-1 and GGA1 initially to recycling endosomes during recovery from BFA or temperature block

As shown in Fig. 4, by 15 minutes of recovery from BFA there was an indication of return of AP-1 and GGA1 staining to endomembranes in CD8-M6PR expressing cells, but no evident co-localization of adaptors with Golgi markers. To examine the possibility that CD8-M6PR recruits adaptors initially to endosomal compartments, we assessed the re-recruitment of adaptors during recovery from the 20°C block. As shown in Fig. 5, 20°C block caused the dissociation of GGA1 and AP-1 (data not shown) from the membranes in cells expressing CD8-M6PR. GGA1 was slowly re-recruited to membranes after shift from 20°C to 37°C, and was detected on membranes after 15 min of recovery (Fig. 5A, B). This amount of time has previously been shown to be sufficient for cargo to exit the Golgi and arrive at a proximal compartment (Griffiths, Pfeiffer et al. 1985). Recovery of AP-1 staining at endomembranes matched that of GGA1 with regard to kinetics and location throughout the recovery. Longer periods of recovery (~30-45 minutes) result in the return to distributions of CD8-M6PR, AP-1, and GGA1 seen in cells that had not undergone temperature block (i.e., steady state). Thus, the timing of GGA1 recruitment is consistent with the arrival of CD8-M6PR at a post-Golgi destination.

To identify the compartments to which GGA1 and AP-1 were initially recruited during recovery from the 20°C block, we co-localized GGA1 in CD8-M6PR expressing cells with cargo (Fig. 5A, C), transferrin receptors (TfR; Fig. 5B, E), GM130 (Fig. 5D), EEA1, Rab11, Lamp I,

and Lamp II (data not shown). The strongest co-localization was observed between GGA1 and TfR (Fig. 5B) and Rab11 (data not shown), well-characterized markers of recycling endosomes (Odorizzi and Trowbridge 1997, Gravotta, Deora et al. 2007). Quantification of deconvolved wide field images revealed the loss of GGA1 recruitment to CD8-M6PR after 20°C block but return of GGA1 staining at CD8-M6PR isosurfaces by about 15 min (Fig. 5C). Importantly, we also observed extensive co-localization between GGA1 and TfR isosurfaces by 15 min (Fig. 5E). In contrast, there was minimal co-localization between GGA1 and GM130 at that time (Fig. 5D).

Because our method of quantifying adaptor recruitment is not widely used yet, we compared results from 3D3I to the more common pixel overlap method of co-localization. Quantification of confocal images using Mander's coefficients was performed with similar results but with larger fold changes in co-localization. Both methods of quantification reveal a 20°C block-dependent loss of GGA1 at the Golgi in CD8-M6PR expressing cells that is not recovering at the Golgi by 15 minutes release from the block (Fig. 5D). Rather, GGA1 recruitment to TfR-positive structures is strongly increased at this time (Fig. 5E). AP-1 recruitment profiles and kinetics mimic those of GGA1 in that the adaptors almost completely co-localize and appear at TfR-positive structures at the same time after release from 20°C block (data not shown). Thus, the CD8-M6PR dependent recruitment of AP-1 and GGA1 in cells recovering from 20°C block doesn't occur first at the Golgi, as was seen with CD8-furin, but is primarily at recycling endosomes.

We then asked if the site of recovery of adaptor recruitment observed in cells recovering from 20°C block agreed or differed from that seen after BFA treatment. Cells expressing CD8-M6PR (Fig. 6), GFP-M6PR, or CD8-M6PRΔC (data not shown) were treated with BFA as in Fig. 5 and double-labeled with antibodies against GGA1 and TfR. GGA1 (Fig. 6) and AP-1 (data not shown) recruitment was seen at ~15 minutes after washout of BFA and occurred on TfR positive endosomes. Thus, the site of initial recruitment of GGAs (and AP-1) coincided with the appearance of CD8-M6PR or GFP-M6PR, following release from 20°C block or BFA, and was

found in each case to be recycling endosomes and not the Golgi. Adaptor re-recruitment to TfR positive endosomes was observed in both transiently and stably transfected cells. These results also suggest that the 20°C block did not result in gross, persistent changes to the rate of cargo export, either as a result of cargo accumulation or the exposure to lower temperature, as the arrival of new M6PR from the Golgi/TGN to recycling endosomes was about the same for release from 20°C block and BFA washout. These results are in marked contrast to those obtained with CD8-furin, in which AP-1 is recruited initially to the Golgi after BFA removal (Fig. 5). These results also serve as a control to confirm that the washout was effective and intracellular BFA concentrations were reduced to ineffective levels quickly.

NRK cell data

Temperature block (data not shown) and BFA recovery experiments were repeated in normal rat kidney (NRK) cells, the cell type originally used in different laboratories to describe GGA localization at the Golgi (Boman, Zhang et al. 2000, Dell'Angelica, Puertollano et al. 2000, Hirst, Lui et al. 2000), Control (non-transfected) NRK cells have more GGA1 and AP-1 staining in the perinuclear area than do HeLaM cells, as staining with antibodies at the same concentration resulted in greater intensity signal (compare Fig. 1A and 7A). Cells were fixed and stained with antibodies against GGA1 and AP-1 (Fig. 7, top two rows), or GGA1 and GM130 (Fig. 7, bottom two rows). Overlap in staining of the two adaptors and of GGA1 with the Golgi marker, GM130 is clearly evident. While the nature of the endogenous cargo(s) responsible for higher levels of GGA1 and AP-1 staining in NRK cells is unknown, the adaptors behave very similarly (see below) to those recruited by CD8-M6PR or GFP-M6PR in HeLaM cells. We interpret these findings as further evidence that neither protein over-expression nor the fusion proteins used in our studies alter responsiveness of adaptors.

GGA1 and AP-1 staining were each lost in response to the 20°C block in both control NRK cells (Fig. 7A) and those expressing CD8-M6PR (data not shown). Like in HeLaM cells,

GGA1 and AP-1 recruitment in NRK during recovery from 20°C block occurred onto structures that appeared quite different from Golgi, beginning ~15 minutes after washout (Fig. 7A). We confirmed that these are recycling endosomes based upon extensive overlap with TfR staining (data not shown).

BFA treatment of NRK cells (data not shown), or NRK cells expressing HA-GGA1 resulted in rapid GGA1 dissociation from membranes that failed to re-recruit directly onto Golgi membranes at early times during recovery from the drug (Fig. 7B). Rather, both GGA1 and AP-1 were first found on TfR^{+} endosomes. Thus, the endogenous cargo(s) in NRK cells responsible for higher steady state levels of AP-1 and GGAs at Golgi membranes, like M6PR, recruit these adaptors initially to recycling endosomes and only later to the Golgi.

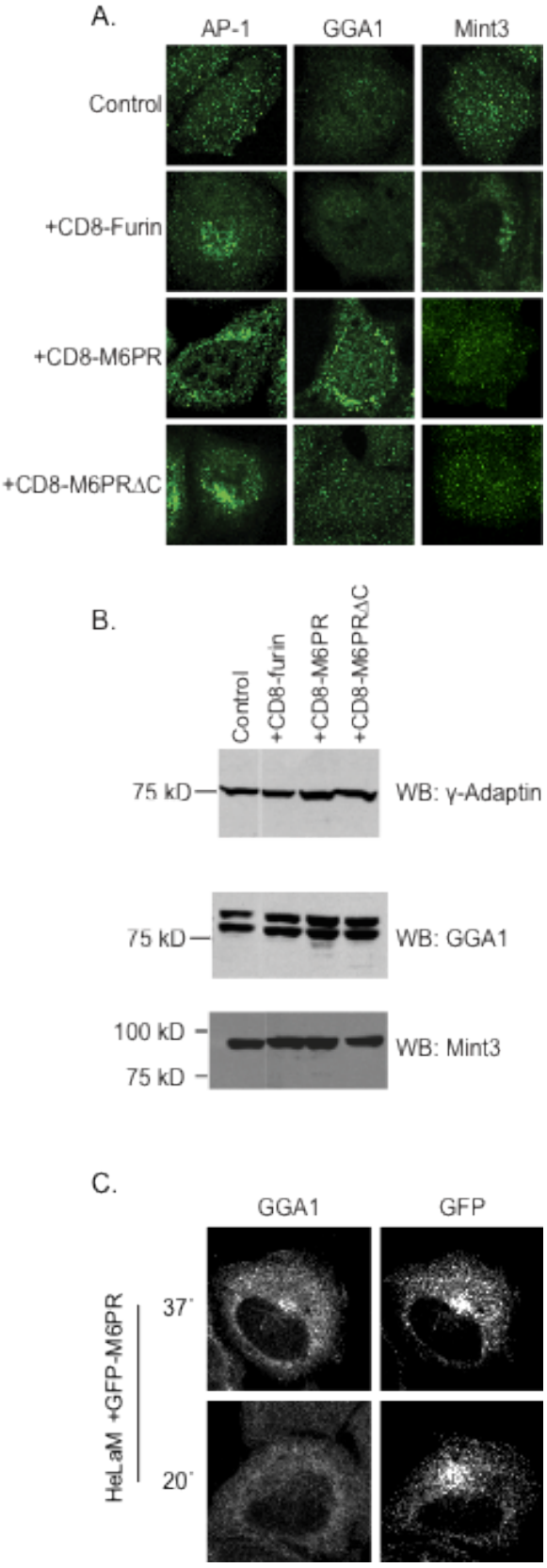
A.
AP-1
GGA1
Mint3
Control
+CD8-Furin
+CD8-M6PR
+CD8-M6PRΔC
B.
Control
+CD8-furin
+CD8-M6PR
+CD8-M6PRΔC
75 kD
WB: γ-Adaptin
75 kD
WB: GGA1
100 kD
75 kD
WB: Mint3
C.
GGA1
GFP
HeLaM +GFP-M6PR
37˚
20˚

Fig. 1: Cargo expression increases the recruitment of specific Arf-dependent adaptors to membranes. (**A**) HeLaM cells were transiently transfected with empty vector (control), or plasmids directing expression of the indicated cargo. The next day cells were fixed and stained for γ-adaptin (AP-1), GGA1 or Mint3. Confocal images are shown. (**B)** HeLaM cells were transiently transfected with plasmids that express the indicated cargos, prior to analyzing protein expression by immunoblotting for γ-adaptin, GGA1, or Mint3. GGA1 migrates as a doublet, presumably resulting from post-translational modification, e.g., phosphorylation. Results shown are typical of 5 independent experiments. **(C)** HeLaM cells expressing GFP-M6PR were maintained at 37°C, or at 20°C for four hr. Cells were then fixed and stained with antibodies against GFP and GGA1. GGA1 recruitment was comparable to that seen with CD8-M6PR and was lost during the temperature block.

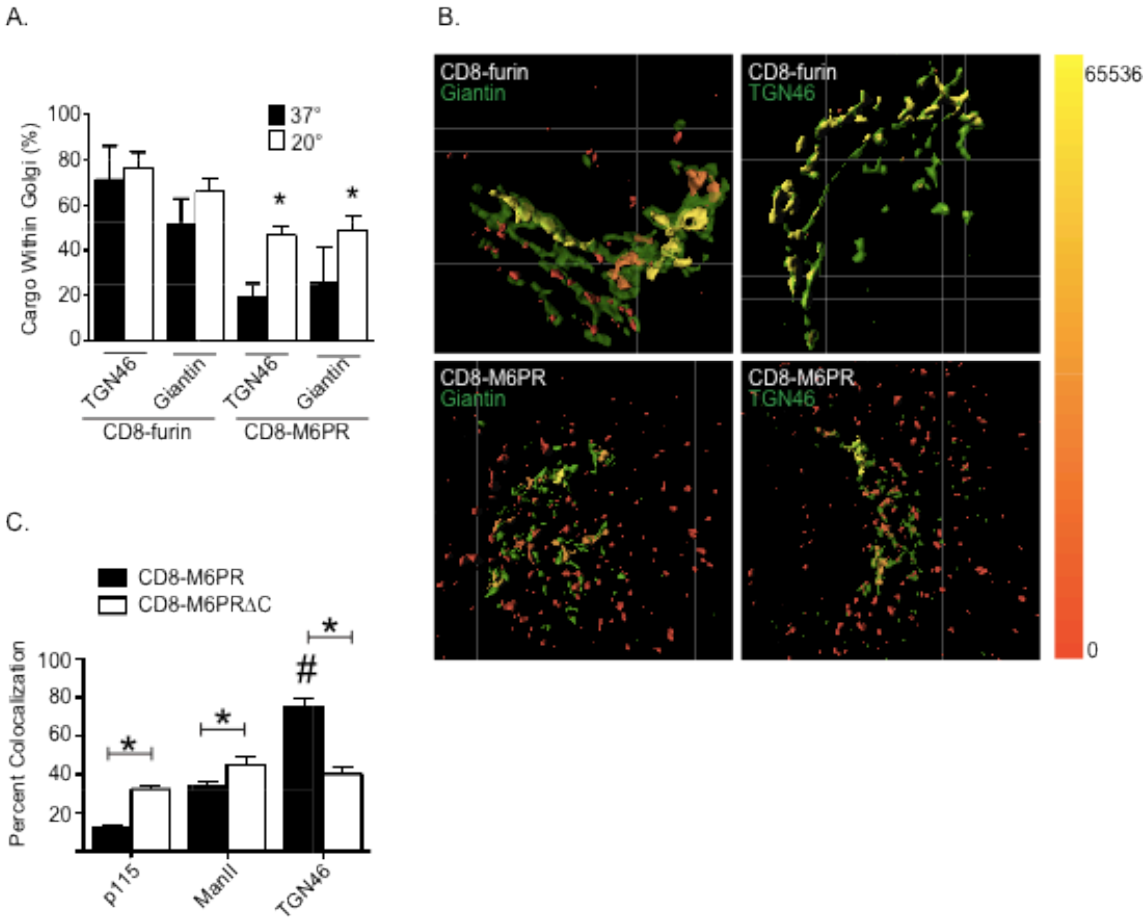

Fig. 2: Cargos localize to distinct Golgi compartments and respond to temperature block differently. HeLaM cells were transiently transfected with plasmids directing the expression of CD8-furin or CD8-M6PR. The next day (~16 hr), cells were fixed and labeled for CD8 and TGN46 or giantin. Stacks of images were collected using widefield imaging and were deconvolved, as described under Methods. (**A**) Deconvolved images were imported into Imaris and two isosurfaces were defined: one using the cargo (CD8-furin or CD8- M6PR) and the other using a TGN or Golgi marker (TGN46 or giantin). Total cargo fluorescence was calculated for each cell, and then the amount of cargo fluorescence within the Golgi marker isosurface was determined. The values shown indicate the percent of total cargo intensity found within the Golgi marker isosurface, and bars indicate standard errors of the mean (SEM, n=5). Student's t-test was

used to compare 37°C to 20°C for each cargo/Golgi marker pairing. Asterisks indicate $p<0.01$. Results are typical of at least three experiments. (**B**) Isosurfaces were generated for the indicated cargo and markers, as described under Methods. The cargo was falsely colored with a heat map indicating the amount of Golgi marker found within the cargo isosurface. The color range of intensities is shown as a bar on the right. (**C**) Cells expressing either CD8-M6PR or CD8-M6PRΔC were fixed and stained for CD8 and the indicated Golgi marker. Single-plane, confocal images were collected and the amount of Golgi marker signal that is also positive for cargo was calculated using Mander's coefficients. A Student's t-test was used to compare the overlap of each cargo with the Golgi marker indicated. An asterisk indicates statistical significance ($p<0.01$).

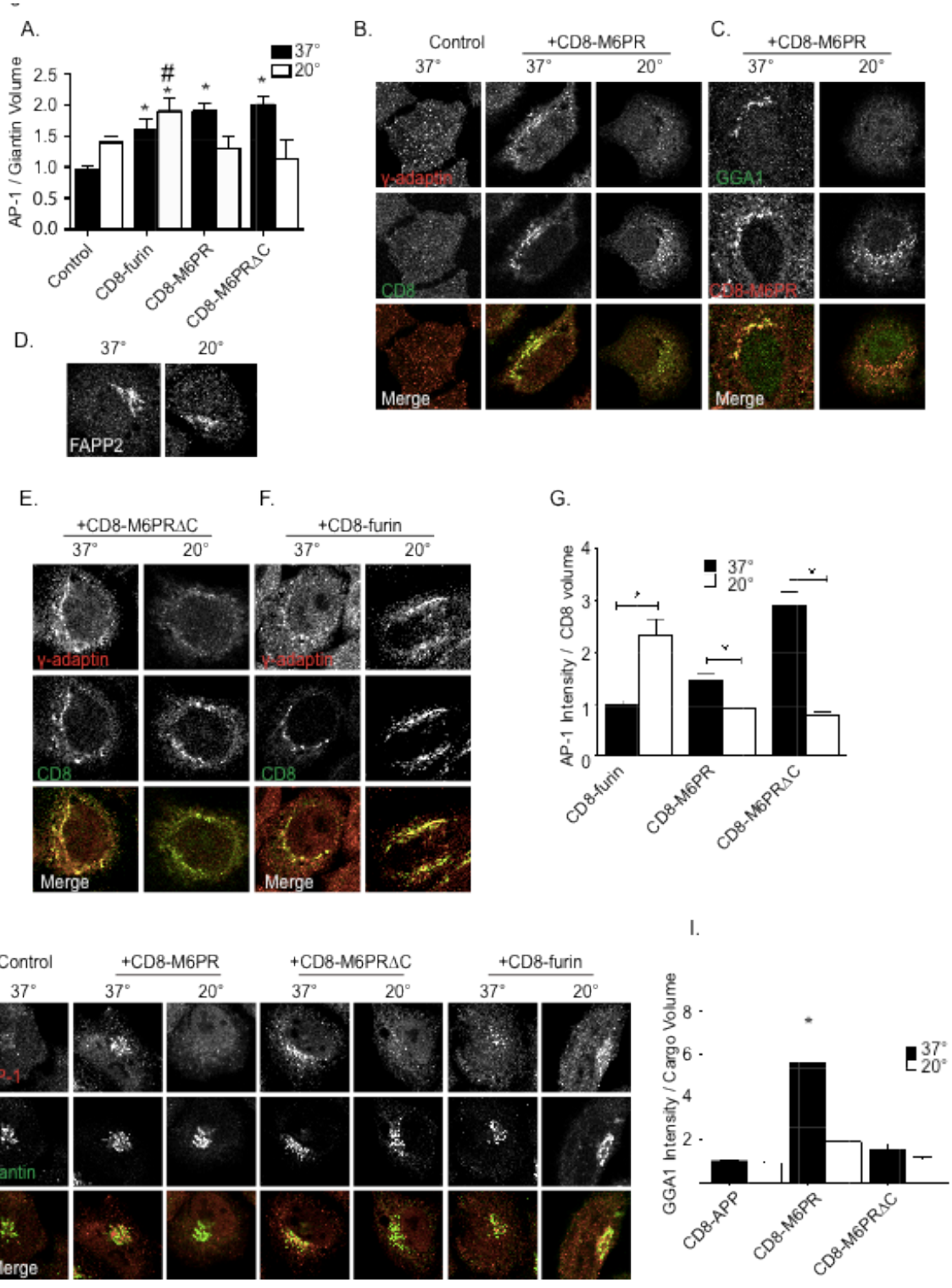
A.
AP-1 / Giantin Volume
37°
20°
Control
CD8-furin
CD8-M6PR
CD8-M6PRΔC
B.
Control
+CD8-M6PR
37°
37°
20°
γ-adaptin
CD8
Merge
C.
+CD8-M6PR
37°
20°
GGA1
CD8-M6PR
Merge
D.
37°
20°
FAPP2
E.
+CD8-M6PRΔC
37°
20°
γ-adaptin
CD8
Merge
F.
+CD8-furin
37°
20°
γ-adaptin
CD8
Merge
G.
AP-1 Intensity / CD8 volume
37°
20°
CD8-furin
CD8-M6PR
CD8-M6PRΔC
H.
Control
+CD8-M6PR
+CD8-M6PRΔC
+CD8-furin
37°
37°
20°
37°
20°
37°
20°
AP-1
Giantin
Merge
I.
GGA1 Intensity / Cargo Volume
37°
20°
CD8-APP
CD8-M6PR
CD8-M6PRΔC

Fig. 3: Adaptor recruitment to cargo and Golgi following 20°C block. (A) Quantification of AP-1 recruitment to giantin-defined isosurfaces in response to the presence of the indicated cargo. HeLaM cells were transfected with empty vector (control) or those directing expression of the indicated cargos. Eighteen hours later they were placed at 37°C or 20°C for four hours, fixed, and stained with antibodies against γ-adaptin (AP-1) and giantin. Wide field images were used to generate an isosurface based on cargo staining and the sum intensity of AP-1 staining within that isosurface was determined. Bars represent the mean ratio of AP-1 intensity within the cargo volume. Student's t-test was used to statistically compare cells at 37°C and 20°C for each cargo. Asterisks indicate statistical significance differences between cells at different temperatures ($p<0.01$), # indicates statistical significance between CD8-furin expressing cells incubated at 37°C and 20°C ($p<0.05$). **(B, E, F)** AP-1 or (**C**) GGA1 recruitment in response to cargo expression and temperature block is shown in confocal images. Cells were transfected with the indicated cargos and treated as described above. Cells were stained with antibodies against γ-adaptin and CD8 (B, E, F) or GGA1 and CD8 (C). **(D)** HeLaM cells were maintained at 37°C or 20°C for four hours, fixed, and stained for FAPP2. **(G)** Quantification of AP-1 recruitment to cargo-defined isosurfaces. Wide field images were used to generate an isosurface based on cargo staining and the sum intensity of AP-1 staining within that isosurface was determined. Bars represent the mean ratio of AP-1 intensity within the cargo volume. Student's t-test was used to statistically compare cells at 37°C and 20°C for each cargo. Asterisks indicate statistical significance differences in sum intensity of AP-1 within cargo isosurfaces ($p<0.01$). **(H)** AP-1 recruitment to Golgi in cells expressing various cargos, at 37°C and 20°C. Cells were prepared and treated as described in (A). Confocal images are shown. AP-1 recruitment is lost in response to 20°C block in cells expressing CD8-M6PR and CD8-M6PRΔC, but not CD8-furin. **(I)** Quantification of GGA1 recruitment to cargo volumes is shown. HeLaM cells were transfected with the indicated cargos, treated as described above, and stained with antibodies against GGA1

and CD8. Images were prepared as described above, and isosurfaces were generated based on CD8 staining. Sum intensity of GGA1 staining within each cargo isosurface is reported. Values are normalized to GGA1 intensity within CD8-APP defined isosurfaces at 37°C. Groups were analyzed using ANOVA, $n>5$ cells for each condition, error bars indicate standard error of the means, and asterisks indicate statistical significance ($p<0.01$).

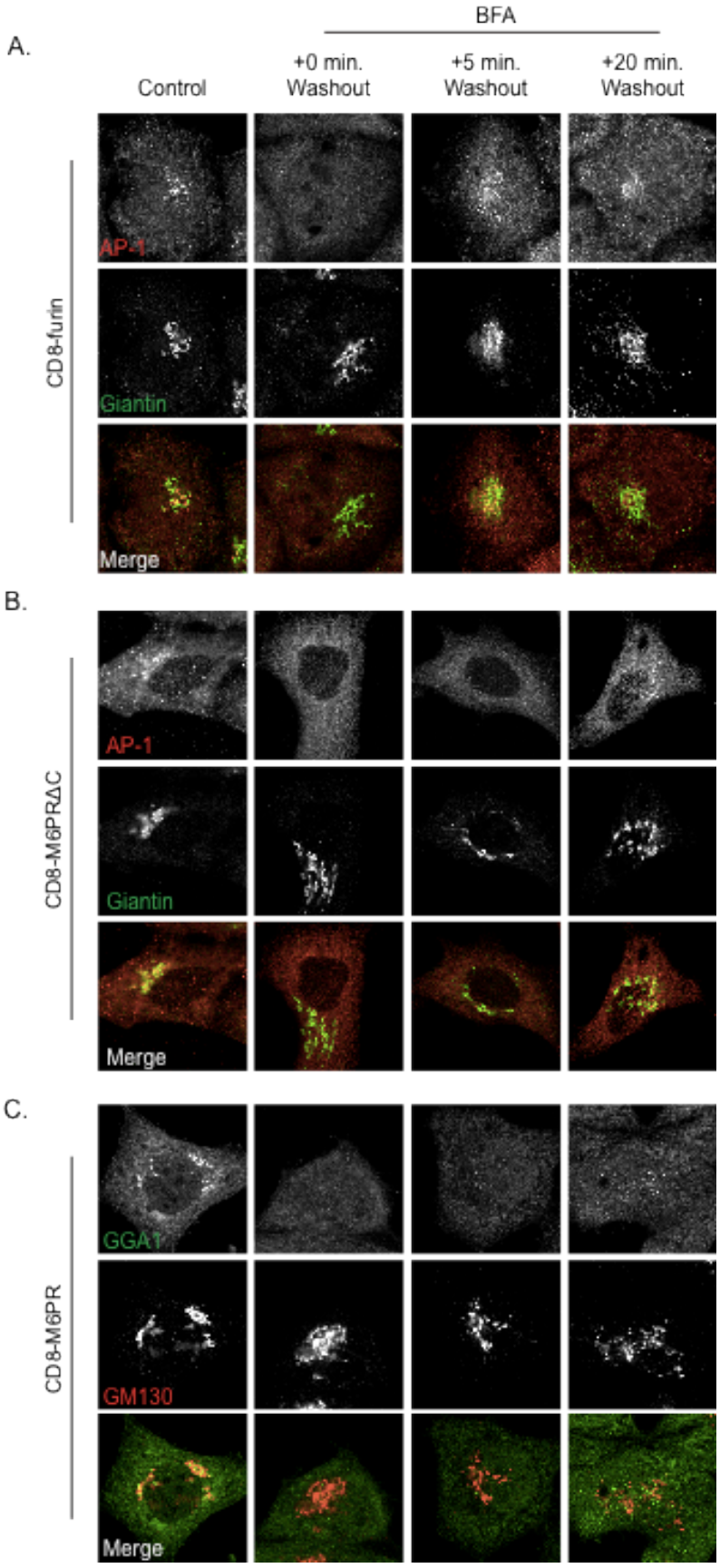
A.
BFA
Control
+0 min. Washout
+5 min. Washout
+20 min. Washout
CD8-furin
AP-1
Giantin
Merge
B.
CD8-M6PRΔC
AP-1
Giantin
Merge
C.
CD8-M6PR
GGA1
GM130
Merge

Fig. 4: Distinct AP-1 re-recruitment to different cargo during BFA recovery. HeLaM cells expressing **(A)** CD8-furin, **(B)** CD8-M6PRΔC, or **(C)** CD8-M6PR were treated with 7.5ug/mL BFA for two minutes, then the drug was removed, and cells were fixed at the indicated times and stained for (A, B) AP-1 and Giantin or (C) GGA1 and GM130. AP-1 recruitment to Golgi membranes is evident within 5 minutes of BFA washout in CD8-furin expressing cells. (B) AP-1 and (C) GGA1 re-recruitment is delayed in cells expressing (B) CD8-M6PRΔC or (C) M6PR and appears more punctate and peripheral.

Figure 5

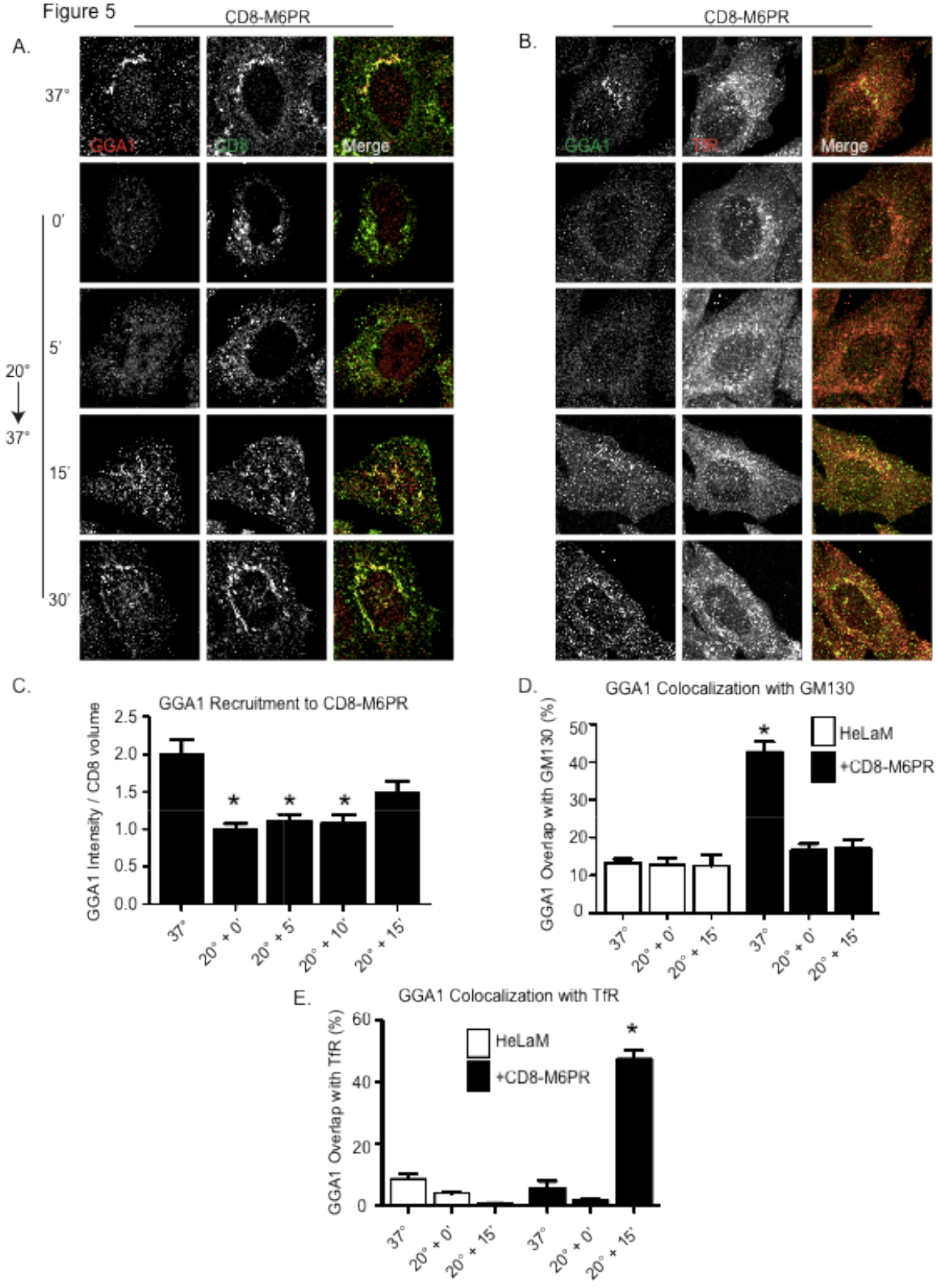
A.
CD8-M6PR
37°
GGA1
CD8
Merge
0'
5'
20°
37°
15'
30'
B.
CD8-M6PR
GGA1
TfR
Merge
C.
GGA1 Recruitment to CD8-M6PR
GGA1 Intensity / CD8 volume
2.5
2.0
1.5
1.0
0.5
0.0
*
*
*
37°
20° + 0'
20° + 5'
20° + 10'
20° + 15'
D.
GGA1 Colocalization with GM130
GGA1 Overlap with GM130 (%)
50
40
30
20
10
0
*
HeLaM
+CD8-M6PR
37°
20° + 0'
20° + 15'
37°
20° + 0'
20° + 15'
E.
GGA1 Colocalization with TfR
GGA1 Overlap with TfR (%)
60
40
20
0
*
HeLaM
+CD8-M6PR
37°
20° + 0'
20° + 15'
37°
20° + 0'
20° + 15'

Fig. 5: Re-recruitment of adaptors following 20°C block occurs initially on recycling endosomes in CD8-M6PR expressing cells. HeLaM cells expressing CD8-M6PR for 24 hr were untreated (37°C) or temperature blocked (20°C) for four hours before return to 37°C for the indicated times. Cells were stained for **(A, C)** CD8 and GGA1, **(B, E)** GGA1 and TfR, or **(D)** GGA1 and GM130. CD8-M6PR (**C**) staining was also imaged by wide field microscopy and used to generate isosurfaces into which GGA1 recruitment was quantified and normalized to cells kept at 20°C for four hours. GGA1 recruitment to CD8-M6PR was statistically significantly decreased during 20°C block and returned to control levels only 15 min into recovery. GGA1 intensity within CD8 defined isosurfaces was analyzed using ANOVA and asterisks indicate $p<0.01$, compared to steady state ($n>5$ cell analyzed). **(D, E)** Confocal images were acquired and quantified using M1 and M2 coefficient, as described under Methods. (D) Bar graphs represent mean Mander's coefficients of GGA1 intensity that is also GM130 positive, or (E) GGA1 intensity that is also TfR positive. Error bars indicate SEM. Asterisks indicate $p<0.01$ when evaluated with a one-way ANOVA and a Dunnet post-test. All comparisons were made to staining in HeLaM maintained at 37°C.

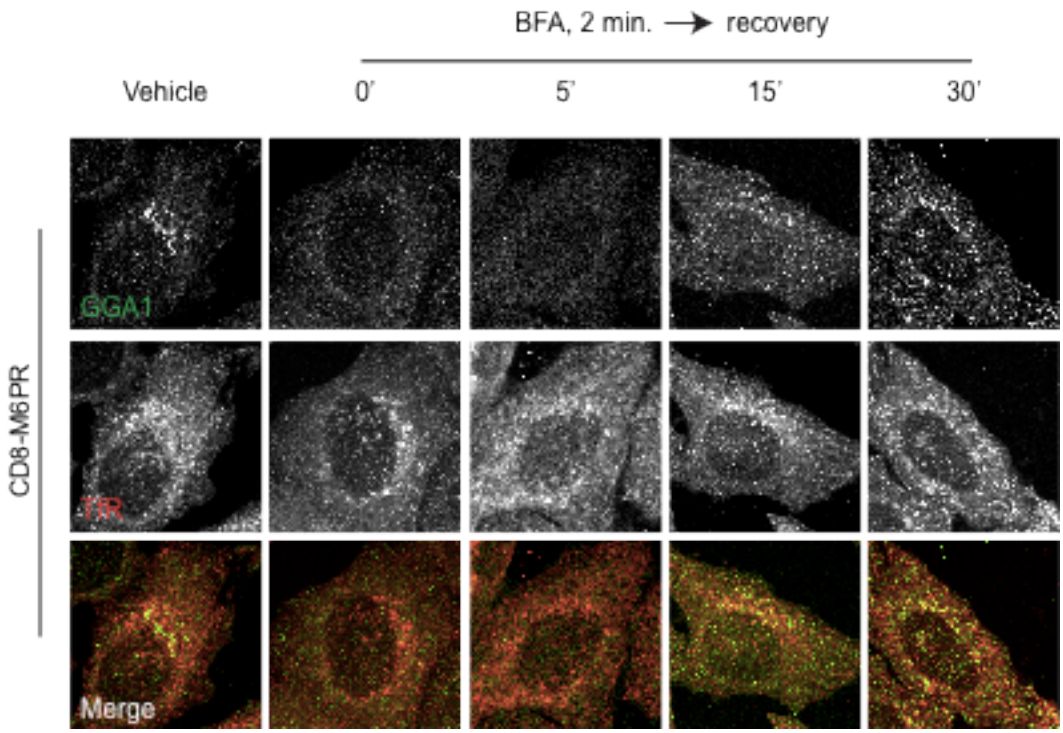

Fig. 6: GGA1 recruitment to M6PR is delayed after BFA washout, and co-localizes with TfR. HeLaM cells expressing CD8-M6PR were treated with vehicle (0.175% methanol) or 7.5 μg/ml BFA for two min, then BFA was removed and cells were allowed to recover for the times indicated, fixed and stained for GGA1 and TfR.

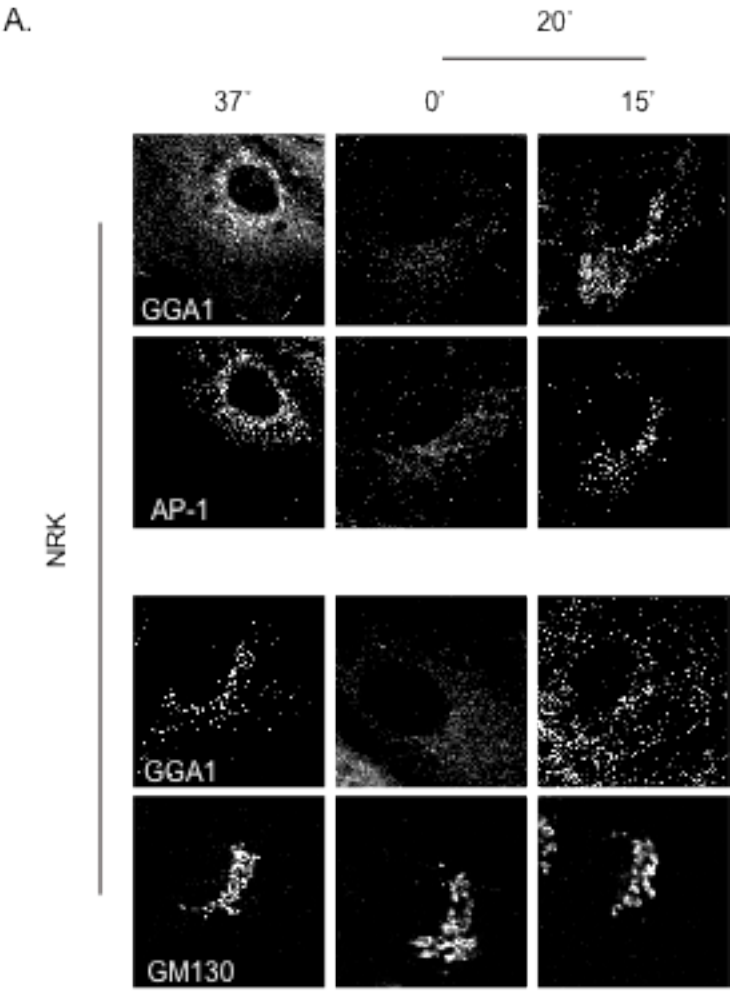
A.
20'
37'
0'
15'
GGA1
AP-1
NRK
GGA1
GM130
B.
BFA, 2 min. → recovery
Vehicle
0'
15'
30'
NRK + HA-GGA1
GGA1
GM130
Merge

Fig. 7: GGAs and AP-1 are lost during temperature block or BFA treatment in NRK cells and return first on endosomes. (A) NRK cells were maintained at 37°C (left panels) or subjected to 20°C temperature block for four hr (0', middle panels) or then recovery for 15 min at 37°C (15', right panels). Fixed cells were stained with antibodies against GGA1 and γ-adaptin (AP-1) (upper panels) or GGA1 and GM130 (lower panels). Like in HeLaM cells expressing CD8 fusions or full-length cargos, GGA1 and AP-1 are lost in response to temperature block and re-recruitment is delayed after release and occurs to small, peripheral puncta. (B) NRK cells were transfected with HA-GGA1 and the next day were treated with vehicle or BFA (2 min, 7.5 μg/ml) before washout and recovery for 15 or 30 min. Cells were fixed and stained with antibodies against GGA1 (top panels) and GM130 (middle panels) or false colored before merging (bottom panels). Confocal images are shown.

3.4. Discussion

Arfs and Arf-dependent adaptors regulate cargo traffic and/or retention in the secretory and endocytic pathways. Despite years of research we still lack clear molecular models for the nature of the signal that leads to Arf activation and adaptor recruitment. Our goal was to define an experimental model to begin dissecting aspects of Arf activation and adaptor recruitment that retain the specificity and biological relevance seen in intact cells. We used fluorescence imaging of HeLaM cells after transient expression of model cargos combined with two independent manipulations, temperature block and BFA treatment, for evaluating the Arf- and cargo-dependent recruitment of adaptors at Golgi and recycling endosomes by monitoring recovery from each treatment. These provided consistent results and strengthen the conclusions drawn from each. Our results demonstrate that the specificities of cargo-adaptor interactions documented using *in vitro* assays are faithfully preserved in cells. We also discovered that the cytoplasmic tail of M6PR recruits both AP-1 and GGAs first to recycling endosomes after recovery from either BFA treatment or cold temperature blockade and only later displays a prominent Golgi distribution pattern. That AP-1 and GGAs behaved the same in M6PR expressing cells is consistent with the proposal that they work together (Doray, Bruns et al. 2002), though not necessarily to coordinate the packaging of cargos for export from the Golgi. Because the same results were obtained with CD8-M6PR, GFP-M6PR in HeLaM cells and endogenous proteins in NRK cells we believe these are generally true of a subset of physiologically important cargos, including M6PR. The initial recruitment of AP-1 to recycling endosomes by M6PR is in clear contrast to its recruitment at the Golgi by CD8-furin. These results point to the clear need to define the roles of the different adaptors by both cargo and location, as there is increasing evidence that adaptors may have the capacity to act at different sites to carry out different and even opposing actions in cells. Finally, the specificity of adaptor recruitment by different cargos is evidence against a model in which activated Arfs are freely available on membrane surfaces. Rather, we conclude that Arfs must

remain coupled in some way to the Arf GEF or cargo responsible for their activation. This is predicted but unproven to be a direct, physical coupling.

Our goal was to test the hypothesis that cargo acts upstream of Arf activation, perhaps analogous to the roles of ligands in GPCR- or RTK-mediated activation of G proteins and Ras, respectively. Ras is likely the better analogy as cargos lack Arf GEF activity, while GPCRs serve that role themselves. Adaptors studied here are Arf-dependent because they have been shown in one or more biochemical assays to bind directly to Arfs in a GTP-sensitive fashion, rapidly dissociate from Golgi membranes upon exposure of cells to BFA, and activated Arfs increase their binding to biological membranes or synthetic liposomes in reconstitution assays (Zhu, Drake et al. 1999, Kuai and Kahn 2002, Nakayama and Takatsu 2005, Yoon, Bonifacino et al. 2005). We believe that adaptor recruitment was confirmed as a legitimate surrogate for Arf activation in our studies as each of the adaptors are Arf-dependent and BFA sensitive, are recruited in a cargo dependent fashion to different sites, and adaptor recruitment was only ever observed at locations containing cargo. The role of activated Arfs in the recruitment of adaptors is incompletely understood but is typically modeled as facilitating adaptor-cargo association by direct binding to adaptor and orienting it on the surface of the membrane to promote binding to cargo. The observations that increasing the density of different cargo at endomembranes (through specific over-expression with or without temperature block) resulted in the recruitment of some adaptors, but not others, leads us to propose that the cargos are likely to play a more direct role in adaptor recruitment and Arf activation than previously appreciated. For example, it appears unlikely that activation of an Arf GEF would lead to the generation of Arf-GTP that is diffusible within the two dimensional space of a membrane and recruit adaptors independently of an associated cargo, as this would predict the recruitment of all Arf-dependent adaptors at that site.

A model for Arf6 acting at sites quite distant from its site of activation has recently been proposed (Montagnac, de Forges et al. 2011) but the actions of Arf6 at the cell surface differ substantially from those of Arfs 1-5 on endomembranes so it is not clear how comparable these

studies will prove to be. We currently lack direct evidence of specific cargo-GEF-Arf complex formation and must also consider additional components acting between the cargo and the Arf GEFs. We believe the experimental system developed here will be useful in studies to explore the role of different cargos in facilitating activation of specific Arf GEF, recruitment and activation of specific Arf isoforms (Volpicelli-Daley, Li et al. 2005), Arf GAPs, and other regulators of carrier biogenesis.

The choice of furin as one of the cargos studied was fortuitous as it shares the ability to bind AP-1 with M6PR, has a short cytoplasmic tail, localizes strongly to the Golgi, and was found to behave as predicted in response to BFA or temperature block, thus serving as a very important control for other cargos. We found that CD8-furin or FLAG-furin localized to the Golgi where it bound AP-1 in a BFA-sensitive manner. We showed that CD8-furin is predominantly found on Golgi membranes at steady state so that there was relatively little enhancement in cargo staining in response to 20°C block. With only small increases in cargo it was surprising to observe the increase in Golgi staining of AP-1 upon 20°C block of CD8-furin expressing cells. One explanation for these results is that during 20°C block a subset of CD8-furin "escapes" the retention mechanism and becomes available for export and AP-1 binding, but is prevented from export by the 20°C block. This is consistent with the previously described role of AP-1 in exit of furin from the Golgi and the idea that this represents a small subset of the cargo that escapes retention mechanisms there. In future studies it may be possible to determine the localization of AP-1 under these conditions by electron microscopy, to determine if two pools of CD8-furin may be identified, bound to distinct adaptors and possibly at distinct domains of the Golgi/TGN. Importantly, furin constructs and the AP-1 that was recruited by them behaved in every other respect as predicted in that AP-1 was (i) recruited to the Golgi in response to furin expression, (ii) rapidly lost upon exposure to BFA, (iii) returned directly onto Golgi membranes at the earliest time points during recovery from the drug, and (iv) was retained, even increased, during temperature blockade. Thus, this cargo retained the ability to bind AP-1 throughout the

temperature block and recovery. While we had assumed this would be standard for all cargos it was not the case for M6PR and led to quite different results. The retention of adaptors in furin expressing cells and of FAPP2 in all cells subjected to temperature block indicate that the lower temperature likely does not itself change Arf activities.

M6PR traffic is bi-directional, between the Golgi and endosomes/lysosomes, though it can also appear on the cell surface (Diaz and Pfeffer 1998, Puertollano, Aguilar et al. 2001, Medigeshi and Schu 2003). We propose recycling endosomes as the initial site of action of AP-1 and GGA1 in regulating sorting and packaging of M6PRs into carriers, though we cannot predict from our data whether the destination of those carriers is the TGN, plasma membrane, or an alternate organelle. Our conclusion is based upon four observations: (i) the delay in recruitment of AP-1 and GGAs during recovery from temperature block of CD8-M6PR expressing cells, in comparison to CD8-furin or FLAG-furin recruitment of AP-1 to the Golgi, (ii) transient but robust co-localization of GGAs and AP-1 with TfR and Rab11 as the initial site of re-recruitment during recovery from temperature block, (iii) identification of recycling endosomes as the site of initial recruitment of GGAs and AP-1 after washout of BFA, and (iv) demonstration that AP-1 is recruited initially to the Golgi during recovery from either temperature block or BFA exposure in CD8-furin expressing cells. This last point essentially serves as a control in that it emphasizes the fact that AP-1 *can* be recruited to the Golgi/TGN in HeLaM cells under the conditions used but that CD8-M6PR fails to do so.

That CD8-M6PR was effectively concentrated at the Golgi/TGN during temperature block was expected but the observation that the adaptors dissociate in the process was novel and quite surprising. During recovery from temperature block the accumulated CD8-M6PR returns back toward levels seen in control cells with kinetics that resemble those of export from the Golgi/TGN. Those rates are consistent with CD8-M6PR leaving the TGN and going directly to recycling endosomes. However, we note that this step did not appear to require the recruitment of detectible AP-1 or GGAs to the Golgi/TGN. A role for AP-1 and GGA1 recruitment to CD8-

M6PR at recycling endosomes and not at the Golgi/TGN was further supported by BFA experiments, in which adaptors were recruited initially to CD8-M6PR at recycling endosomes and appeared on Golgi/TGN only later. BFA treatment has been previously shown to cause a redistribution of M6PR resulting in its increased levels at the cell surface, though that study used higher concentrations and longer times of BFA treatment that caused Golgi breakdown and redistribution to the ER (Wood, Park et al. 1991), neither of which occurred in our study. Thus, it is possible that the increase in AP-1 and GGA1 staining seen first at recycling endosomes after recovery from BFA could result from arrival of CD8-M6PR from the cell surface, rather than that exiting the Golgi, though we consider this less likely. And even if true, it does not change our conclusion that AP-1 and GGA1 are recruited initially to recycling endosomes after recovery from BFA.

Early reports of the discovery of GGAs as Arf-dependent adaptors reported recruitment to the Golgi and BFA sensitivity. We have verified our results and those of others (Boman, Zhang et al. 2000, Dell'Angelica, Puertollano et al. 2000, Hirst, Lui et al. 2000, Takatsu, Yoshino et al. 2000) in finding that steady state staining of GGAs in cells expressing GGA-binding cargo appears to overlap more closely with Golgi markers than with endosomal markers. The differences we describe here cannot be ascribed to cell type specificities as we obtained the same results in HeLaM and NRK cells. In a more recent study of GGA and AP-1 localization at both the light and EM level in Drosophila Dmel2 and HeLa cells, Hirst et al (Hirst, Sahlender et al. 2009) described cargo-dependent recruitment and discovered that AP-1 and GGA staining are in close apposition, though are not superimposable. The authors point out the difficulties in clearly discriminating between Golgi and endosomal staining and acknowledge that both AP-1 and GGA staining is equally likely to be endosomal. Thus, we cannot exclude the possibility that at steady state, GGAs are on either membrane, or both. This striking difference with results of our co-localization of GGA1 or AP-1 with recycling endosome markers may be explained by the transient nature of this initial recruitment that was only revealed in our protocols that led to the

removal of previously bound adaptors and allowed a focus on the pool of newly recruited adaptors in CD8-M6PR expressing cells.

Another formal possibility for the apparent differences in GGA recruitment in steady state cells and those recovering from 20°C block or BFA treatments is that steady state staining of adaptors may not represent predominantly those involved in carrier biogenesis. If adaptors are retained on mature carriers and the process of uncoating at their destination is slower than that of coating at their source, then the steady state staining could give an erroneous impression of the site of adaptor recruitment. Recent reports of complexes involved in tethering of carriers at destination organelles are consistent with our suggestion that vesicle fusion may be the rate limiting step in movement of a carrier from one site to another (e.g., see Cai, et al (Cai 2007)). Of course, the observation that CD8-M6PR recruits AP-1 and GGAs first to recycling endosomes in no way challenges the conclusion that each of these adaptors may also be recruited to the TGN, or other sites, by other cargos. Indeed, we showed that CD8-furin recruits AP-1 initially to the Golgi.

We find a number of findings in the literature that further support our conclusion that AP-1 and GGAs are recruited initially to recycling endosomes in response to the presence of CD8-M6PR or M6PR itself. AP-1 has been reported previously to bind endosomes and to function in the retrograde traffic of cargos from endosomes to the TGN (Le Borgne, Schmidt et al. 1993, Mallard, Antony et al. 1998, Meyer, Zizioli et al. 2000, Valdivia, Baggott et al. 2002), including that of the M6PRs. There is also evidence that GGA3 can be recruited to recycling endosomes (Wahle, Prager et al. 2005) and even by the tail of M6PR (Puertollano and Bonifacino 2004). These earlier reports suggest specificity for GGA3, but we observed an almost complete pairing of AP-1 recruitment and all three GGAs in CD8-M6PR expressing HeLaM cells. Even the earliest reports of GGA localization included suggestions of binding to or actions at endosomes (Boman, Zhang et al. 2000, Hirst, Lui et al. 2000). GGAs, but more specifically GGA3, also have been reported to be recruited to endosomes by BACE1 (He, Li et al. 2005, Wahle, Prager et al. 2005,

Tesco, Koh et al. 2007). Interestingly, He, et al (He, Li et al. 2005) also compare BACE1 localization to that of a BACE1 fusion protein that swaps out the cytoplasmic tail of the CD8-M6PR and found striking similarities. Depletion of GGAs or expression of a BACE1 mutant that cannot bind GGAs resulted in accumulation of BACE1 at endosomes, leading those authors to propose roles for GGA in both directions of TGN-endosome BACE1 traffic. We speculate that more cargos will be found to recruit GGAs, alone or in parallel with AP-1, to endosomes though we emphasize that simply demonstrating that a particular adaptor binds to a cargo can no longer be taken as evidence for its role at a particular site. Together, our findings demonstrate that the recruitment of the adaptors to regulate carrier biogenesis is cargo dependent, and that adaptors are not limited to a single site of action.

There is currently no molecular model to explain why one cargo-adaptor pair is retained during temperature block (CD8-furin or FLAG-furin with AP-1) and another is lost (CD8-M6PR or GFP-M6PR with AP-1 or GGA1). This behavior and others, including differences in localization within the Golgi of CD8-M6PR and CD8-M6PRΔC, argue strongly for the existence of additional steps in the regulation or "activation" of cargo that leads to downstream actions that include Arf GEF activation. Such regulation likely includes phosphorylation of cargo tail or adaptor (McKay and Kahn 2004, Pulvirenti, Giannotta et al. 2008, Vieira, Rebelo et al. 2009), other post-translational modifications, changes in lipid composition or binding of regulatory components. We believe that dissection of these complex processes and the spatially and temporally controlled changes involved will require the integration of biochemical, high-resolution structural, and cell-based studies and that the cell based models developed herein will allow these questions to be addressed in the near future.

3.5. Experimental Procedures

Cell Culture: HeLaM and NRK cells were maintained in 10% fetal bovine serum (GemCell Cat# 100-500, Sacramento, CA, USA) in DMEM medium (GIBCO Cat# 11965 Carlsbad, CA, USA). Stably transfected cells were supplemented with 50 μg/mL G418. Cells used for imaging were grown on Matrigel-coated coverslips (BD Biosciences, Bedford, MA, USA).

Plasmids and cell transfections: pIRESneo2-CD8-M6PR and pIRES-neo2-CD8-M6PRΔC were generous gifts from Dr. Margaret Robinson (University of Cambridge) and are described in Hirst, et al(Hirst, Seaman et al. 2007). They express the lumenal and transmembrane regions of CD8 fused to the full 163 residues of the cytoplasmic tail of cation independent mannose 6-phosphate receptor (M6PR) or only the juxtamembrane 74 residues, respectively. pIRESneo2-CD8-furin was kindly provided by Dr. Matthew Seaman (University of Cambridge). The cytoplasmic tail of furin is 58 residues in length. pGEM FLAG-furin was a generous gift from Dr. Gary Thomas (Oregon Health & Science University) (Molloy, Thomas et al. 1994). Plasmids were transfected using Fugene6 (Roche Cat# 11814443001 Indianapolis, IN, USA), according to manufacturer's instructions. Cells were placed at 37°C for four hours, rinsed once, and trypsinized to remove them from the well. Cells were suspended in 3mL of normal growth media, and 1mL of the suspension was transferred to a new well of 6-well plates, containing Matrigel coated coverslips. Cargos were allowed to express for a total of 24 hours.

Antibodies and dilutions used for immunocytochemistry: γ-adaptin (AP-1), 1:100 (BD/Transduction cat # 610502, Bedford, MA, USA); CD8, 1:1000 (Ancell Corp. cat #153-020 Bayport, MN, USA); CD8-FITC, 1:500 (Ancell Corp. cat #153-040 Bayport, MN, USA), GGA1 1:1000 (Boman et al., 2000); giantin, 1:1000 (Covance cat # prb-114c Emeryville, CA, USA), GM130, 1:1000 (BD/Transduction cat #610823 Bedford, MA, USA); FAPP2, 1:1000 (D'Angelo

et al., 2007), a generous gift from Dr. Antonella de Matteis; TGN46, 1:1000 (Serotec Cat#AHP500 Oxford, UK), Rab11, 1:200, a kind gift from Dr. James Goldenring (Calhoun and Goldenring, 1996); Transferrin receptor, 1:1000 (Zymed cat# 136800 Carlsbad, CA, USA), and Mint3, 1:100 (BD/Transduction cat #611380). Antibodies and dilutions used in immunoblotting: γ-adaptin, 1:100 (BD/Transduction cat #610502 Bedford, MA, USA); GGA1, 1:500 (Boman et al., 2000); and Mint3, 1:500 (BD/Transduction cat #611380 Bedford, MA, USA).

Temperature (20°C) block and Immunocytochemistry: Medium was replaced with 4mL 20mM HEPES/10% FBS in DMEM. Cells were placed in a water bath and maintained at 19.5°C for four hours, then either immediately fixed, or returned to 37°C for varying times of "release", prior to fixation. Release was performed by replacing medium with fresh, pre-warmed (37°C) medium without HEPES and dishes were placed in a gassed incubator. Cells were fixed in 2% paraformaldehyde in phosphate buffered saline (PBS; 137 mM NaCl, 2.7 mM KCl, 10 mM Na2HPO4, 2 mM KH2PO4, pH 7.4) for 20 min at room temperature. Following fixation, cells were rinsed with PBS for 5 min, a total of four times. Individual coverslips were then placed on a parafilm coated 24-well dish, and ~200 μL blocking solution (1% bovine serum albumin (BSA, Sigma cat #A3059 St. Louis, MO, USA) and 0.05% saponin (Sigma #S5881 St. Louis, MO, USA) in PBS) for 20 min at room temperature. Primary antibodies in blocking solution were added to coverslips and placed at 4°C overnight. Coverslips were then washed four times with 0.05% saponin in PBS for 5 min each. Coverslips were mounted using Mowiol (CalBiochem #475904 Darmstadt, Germany), prepared as described in Valnes and Brandtzaeg (Valnes and Brandtzaeg 1985).

BFA treatment: BFA (7.5 μg/mL) or methanol vehicle were prepared freshly in culture medium, pre-warmed to 37°C and applied to cells for 2 min. Cells were then quickly rinsed with pre-warmed medium and fresh medium applied before fixing as above.

Confocal Image Acquisition: Images were collected on an Olympus IX81 Fluoview FV1000 using a 100X oil immersion objective with a NA of 1.4. Images were imported into ImageJ, converted to 16-bit images, and intensities scaled to a maximal signal intensity of 255 (Bolte and Cordelieres 2006, North 2006).

Wide Field Image Acquisition: Stacks of images were collected using a Nikon Bx51 microscope with a 60x 1.4NA oil immersion objective with a Photometrics Quantix camera. Images were captured at 1316x1035 pixel ratio and a 16-bit image depth. Where indicated, z-series were deconvolved with Huygens SVI software (Hilversum, Netherlands), using an iterative maximum likelihood function for a maximum of 40 iterations.

Wide Field Image Quantification: We developed a method for the quantification of three-dimensional wide field fluorescence data that identifies structures and evaluates signal intensity information within those structures and named the technique three dimensional (3D) image-based isosurface generation and intensity analysis (3D3I). The 3D3I method differs from traditional co-localization methods of quantification. Co-localization methods typically use two-dimensional datasets and a manually defined region of interest (ROI) for analysis. The ROI is then analyzed for how well signal in one channel correlates with signal in another. In contrast, 3D3I establishes an ROI, or 3D isosurface, using a biologically relevant signal from one channel (e.g., giantin staining), and quantifies the total intensity of signal from the other channel (e.g., adaptor staining) within it. Thus, the values generated (intensity per μm^3) are non-correlative. For additional details and discussion see Caster and Kahn (Caster and Kahn 2012). The use of 3D3I eliminates the potential for focal plane bias by using data from the entire cell. It is optimal for quantifying staining in irregularly shaped objects, particularly ones that differ in size and number between cells in a population; e.g., Golgi components and endosomes.

Deconvolved images were opened in Imaris (Bitplane, South Windsor, CT, USA) and isosurfaces were generated for the staining of interest. Isosurfaces representing Golgi or cargo staining were generated using 'automatic iterative selection'. The total fluorescence intensity of the channel of interest was then totaled, within the volume defined by the isosurface. Values were then exported into Excel for each individual cell. At least five cells were quantified in each case.

Statistical Analysis: Sum intensities from the channel of interest were totaled and divided by the total volume of the surface, resulting in a ratio of sum intensity/isosurface μm^3. This value was determined for each cell for statistical analysis. One-way ANOVA or Student's t-test was used with the indicated post-test. Every experiment described was repeated at least three times with consistent results. Images shown are representative of the cell population, determined by quantification of the phenotypes observed.

3.6. Acknowledgements

This work was supported by a grant from the National Institute of General Medical Sciences (GM067226) and in part by the Imaging Core of the Emory Neuroscience NINDS Core Facilities grant, P30NS055077.

Aguilar, R. C., H. Ohno, K. W. Roche and J. S. Bonifacino (1997). "Functional domain mapping of the clathrin-associated adaptor medium chains mu1 and mu2." J Biol Chem **272**(43): 27160-27166.
Aridor, M. and L. M. Traub (2002). "Cargo selection in vesicular transport: the making and breaking of a coat." Traffic **3**(8): 537-546.
Arighi, C. N., L. M. Hartnell, R. C. Aguilar, C. R. Haft and J. S. BONIFACINO (2004). Role of the mammalian retromer in sorting of the cation-independent mannose 6-phosphate receptor. J Cell Biol. **165:** 123-133.
Bolte, S. and F. P. Cordelieres (2006). "A guided tour into subcellular colocalization analysis in light microscopy." J Microsc **224**(Pt 3): 213-232.
Boman, A. L., C. Zhang, X. Zhu and R. A. Kahn (2000). "A family of ADP-ribosylation factor effectors that can alter membrane transport through the trans-Golgi." Mol Biol Cell **11**(4): 1241-1255.
Bonifacino, J. S. and J. Lippincott-Schwartz (2003). "Coat proteins: shaping membrane transport." Nat Rev Mol Cell Biol **4**(5): 409-414.
Borg, J. P., J. Ooi, E. Levy and B. Margolis (1996). "The phosphotyrosine interaction domains of X11 and FE65 bind to distinct sites on the YENPTY motif of amyloid precursor protein." Mol Cell Biol **16**(11): 6229-6241.
Cai, H., Reinisch, K., and Ferro-Novick, S. (2007). "Coats, tethers, Rabs and SNARES work together to mediate the intracellular destination of a transport vesicle." Dev Cell **12**: 671-682.
Caster, A. H. and R. A. Kahn (2012). "Computational method for calculating fluorescence intensities within three-dimensional structures in cells." Cellular Logistics **2**(4): 176-188.
Cockcroft, S., G. M. Thomas, A. Fensome, B. Geny, E. Cunningham, I. Gout, I. Hiles, N. F. Totty, O. Truong and J. J. Hsuan (1994). "Phospholipase D: a downstream effector of ARF in granulocytes." Science **263**(5146): 523-526.
Cosson, P. and F. Letourneur (1994). "Coatomer interaction with di-lysine endoplasmic reticulum retention motifs." Science **263**(5153): 1629-1631.
Dell'Angelica, E. C., R. Puertollano, C. Mullins, R. C. Aguilar, J. D. Vargas, L. M. Hartnell and J. S. Bonifacino (2000). "GGAs: a family of ADP ribosylation factor-binding proteins related to adaptors and associated with the Golgi complex." J Cell Biol **149**(1): 81-94.
Diaz, E. and S. R. Pfeffer (1998). "TIP47: a cargo selection device for mannose 6-phosphate receptor trafficking." Cell **93**(3): 433-443.
Donaldson, J. G., J. Lippincott-Schwartz, G. S. Bloom, T. E. Kreis and R. D. Klausner (1990). "Dissociation of a 110-kD peripheral membrane protein from the Golgi apparatus is an early event in brefeldin A action." J Cell Biol **111**(6 Pt 1): 2295-2306.
Doray, B., K. Bruns, P. Ghosh and S. Kornfeld (2002). "Interaction of the cation-dependent mannose 6-phosphate receptor with GGA proteins." J Biol Chem **277**(21): 18477-18482.
Fiedler, K., M. Veit, M. A. Stamnes and J. E. Rothman (1996). "Bimodal interaction of coatomer with the p24 family of putative cargo receptors." Science **273**(5280): 1396-1399.
Geuze, H. J., W. Stoorvogel, G. J. Strous, J. W. Slot, J. E. Bleekemolen and I. Mellman (1988). "Sorting of mannose 6-phosphate receptors and lysosomal membrane proteins in endocytic vesicles." J Cell Biol **107**(6 Pt 2): 2491-2501.

Ghosh, P. and S. Kornfeld (2004). "The cytoplasmic tail of the cation-independent mannose 6-phosphate receptor contains four binding sites for AP-1." Arch Biochem Biophys **426**(2): 225-230.
Godi, A., Di Campli, A., Konstantakopoulos, A., Di Tullio, G., Alessi, DR., Kular, GS., Daniele, T., Marra, P., Lucocq, JM., De Matteis, A. (2004). "FAPPs control Golgi-to-cell-surface membrane traffic by binding to ARF and PtdIns(4)P." Nat Cell Biol **6**: 393-404.
Godi, A., P. Pertile, R. Meyers, P. Marra, G. Di Tullio, C. Iurisci, A. Luini, D. Corda and M. A. De Matteis (1999). "ARF mediates recruitment of PtdIns-4-OH kinase-beta and stimulates synthesis of PtdIns(4,5)P2 on the Golgi complex." Nat Cell Biol **1**(5): 280-287.
Gravotta, D., A. Deora, E. Perret, C. Oyanadel, A. Soza, R. Schreiner, A. Gonzalez and E. Rodriguez-Boulan (2007). "AP1B sorts basolateral proteins in recycling and biosynthetic routes of MDCK cells." Proc Natl Acad Sci U S A **104**(5): 1564-1569.
Griffiths, G., S. Pfeiffer, K. Simons and K. Matlin (1985). "Exit of newly synthesized membrane proteins from the trans cisterna of the Golgi complex to the plasma membrane." J Cell Biol **101**(3): 949-964.
Han, J., Y. Wang, S. Wang and C. Chi (2008). "Interaction of Mint3 with Furin regulates the localization of Furin in the trans-Golgi network." Journal of Cell Science **121**(Pt 13): 2217-2223.
He, X., F. Li, W.-P. Chang and J. Tang (2005). GGA proteins mediate the recycling pathway of memapsin 2 (BACE). J Biol Chem. **280:** 11696-11703.
Heilker, R., U. Manning-Krieg, J. F. Zuber and M. Spiess (1996). "In vitro binding of clathrin adaptors to sorting signals correlates with endocytosis and basolateral sorting." EMBO J **15**(11): 2893-2899.
Hirst, J., W. W. Lui, N. A. Bright, N. Totty, M. N. Seaman and M. S. Robinson (2000). "A family of proteins with gamma-adaptin and VHS domains that facilitate trafficking between the trans-Golgi network and the vacuole/lysosome." J Cell Biol **149**(1): 67-80.
Hirst, J., D. A. Sahlender, M. Choma, R. Sinka, M. E. Harbour, M. Parkinson and M. S. Robinson (2009). "Spatial and functional relationship of GGAs and AP-1 in Drosophila and HeLa cells." Traffic **10**(11): 1696-1710.
Hirst, J., M. N. Seaman, S. I. Buschow and M. S. Robinson (2007). "The role of cargo proteins in GGA recruitment." Traffic **8**(5): 594-604.
Honing, S., J. Griffith, H. J. Geuze and W. Hunziker (1996). "The tyrosine-based lysosomal targeting signal in lamp-1 mediates sorting into Golgi-derived clathrin-coated vesicles." EMBO J **15**(19): 5230-5239.
Jacobsen, L., P. Madsen, M. S. Nielsen, W. P. Geraerts, J. Gliemann, A. B. Smit and C. M. Petersen (2002). "The sorLA cytoplasmic domain interacts with GGA1 and -2 and defines minimum requirements for GGA binding." FEBS Lett **511**(1-3): 155-158.
Jian, X., M. Cavenagh, J. M. Gruschus, P. A. Randazzo and R. A. Kahn (2010). "Modifications to the C-terminus of Arf1 alter cell functions and protein interactions." Traffic **11**(6): 732-742.
Jones, D. H., J. B. Morris, C. P. Morgan, H. Kondo, R. F. Irvine and S. Cockcroft (2000). "Type I phosphatidylinositol 4-phosphate 5-kinase directly interacts with ADP-ribosylation factor 1 and is responsible for phosphatidylinositol 4,5-bisphosphate synthesis in the golgi compartment." J Biol Chem **275**(18): 13962-13966.

Karlsson, K. and S. R. Carlsson (1998). "Sorting of lysosomal membrane glycoproteins lamp-1 and lamp-2 into vesicles distinct from mannose 6-phosphate receptor/gamma-adaptin vesicles at the trans-Golgi network." J Biol Chem **273**(30): 18966-18973.
Klumperman, J., R. Kuliawat, J. M. Griffith, H. J. Geuze and P. Arvan (1998). "Mannose 6-phosphate receptors are sorted from immature secretory granules via adaptor protein AP-1, clathrin, and syntaxin 6-positive vesicles." J Cell Biol **141**(2): 359-371.
Kuai, J. and R. A. Kahn (2002). "Assays of ADP-ribosylation factor function." Methods Enzymol **345**: 359-370.
Kuge, O., C. Dascher, L. Orci, T. Rowe, M. Amherdt, H. Plutner, M. Ravazzola, G. Tanigawa, J. E. Rothman and W. E. Balch (1994). "Sar1 promotes vesicle budding from the endoplasmic reticulum but not Golgi compartments." J Cell Biol **125**(1): 51-65.
Ladinsky, M. S., C. C. Wu, S. McIntosh, J. R. McIntosh and K. E. Howell (2002). "Structure of the Golgi and distribution of reporter molecules at 20 degrees C reveals the complexity of the exit compartments." Mol Biol Cell **13**(8): 2810-2825.
Le Borgne, R., A. Schmidt, F. Mauxion, G. Griffiths and B. Hoflack (1993). Binding of AP-1 Golgi adaptors to membranes requires phosphorylated cytoplasmic domains of the mannose 6-phosphate/insulin-like growth factor II receptor. J Biol Chem. **268:** 22552-22556.
Lee, M. C., E. A. Miller, J. Goldberg, L. Orci and R. Schekman (2004). "Bi-directional protein transport between the ER and Golgi." Annu Rev Cell Dev Biol **20**: 87-123.
Letourneur, F., E. C. Gaynor, S. Hennecke, C. Demolliere, R. Duden, S. D. Emr, H. Riezman and P. Cosson (1994). "Coatomer is essential for retrieval of dilysine-tagged proteins to the endoplasmic reticulum." Cell **79**(7): 1199-1207.
Lippincott-Schwartz, J., L. C. Yuan, J. S. Bonifacino and R. D. Klausner (1989). "Rapid redistribution of Golgi proteins into the ER in cells treated with brefeldin A: evidence for membrane cycling from Golgi to ER." Cell **56**(5): 801-813.
Liu, Y., R. A. Kahn and J. H. Prestegard (2010). "Dynamic structure of membrane-anchored Arf*****GTP." Nat Struct Mol Biol **17**(7): 876-881.
Lodish, H. F. and N. Kong (1983). "Reversible block in intracellular transport and budding of mutant vesicular stomatitis virus glycoproteins." Virology **125**(2): 335-348.
Luttrell, L. M., Y. Daaka and R. J. Lefkowitz (1999). "Regulation of tyrosine kinase cascades by G-protein-coupled receptors." Curr Opin Cell Biol **11**(2): 177-183.
Mallard, F., C. Antony, D. Tenza, J. Salamero, B. Goud and L. Johannes (1998). "Direct pathway from early/recycling endosomes to the Golgi apparatus revealed through the study of shiga toxin B-fragment transport." J Cell Biol **143**(4): 973-990.
Matlin, K. S. and K. Simons (1983). "Reduced temperature prevents transfer of a membrane glycoprotein to the cell surface but does not prevent terminal glycosylation." Cell **34**(1): 233-243.
McKay, M. M. and R. A. Kahn (2004). "Multiple phosphorylation events regulate the subcellular localization of GGA1." Traffic **5**(2): 102-116.
Medigeshi, G. R. and P. Schu (2003). "Characterization of the in vitro retrograde transport of MPR46." Traffic **4**(11): 802-811.
Meyer, C., D. Zizioli, S. Lausmann, E. L. Eskelinen, J. Hamann, P. Saftig, K. von Figura and P. Schu (2000). mu1A-adaptin-deficient mice: lethality, loss of AP-1 binding and rerouting of mannose 6-phosphate receptors. EMBO J. **19:** 2193-2203.

Molloy, S. S., L. Thomas, J. K. VanSlyke, P. E. Stenberg and G. Thomas (1994). "Intracellular trafficking and activation of the furin proprotein convertase: localization to the TGN and recycling from the cell surface." EMBO J **13**(1): 18-33.
Montagnac, G., H. de Forges, E. Smythe, C. Gueudry, M. Romao, J. Salamero and P. Chavrier (2011). "Decoupling of activation and effector binding underlies ARF6 priming of fast endocytic recycling." Curr Biol **21**(7): 574-579.
Mottet, G., C. Tuffereau and L. Roux (1986). "Reduced temperature can block different glycoproteins at different steps during transport to the plasma membrane." J Gen Virol **67 (Pt 9)**: 2029-2035.
Nakano, A. and M. Muramatsu (1989). "A novel GTP-binding protein, Sar1p, is involved in transport from the endoplasmic reticulum to the Golgi apparatus." J Cell Biol **109**(6 Pt 1): 2677-2691.
Nakayama, K. and H. Takatsu (2005). "Analysis of Arf interaction with GGAs in vitro and in vivo." Methods Enzymol **404**: 367-377.
North, A. J. (2006). "Seeing is believing? A beginners' guide to practical pitfalls in image acquisition." J Cell Biol **172**(1): 9-18.
Odorizzi, G. and I. S. Trowbridge (1997). "Structural requirements for basolateral sorting of the human transferrin receptor in the biosynthetic and endocytic pathways of Madin-Darby canine kidney cells." J Cell Biol **137**(6): 1255-1264.
Owen, D. J. and P. R. Evans (1998). "A structural explanation for the recognition of tyrosine-based endocytotic signals." Science **282**(5392): 1327-1332.
Puertollano, R., R. C. Aguilar, I. Gorshkova, R. J. Crouch and J. S. Bonifacino (2001). "Sorting of mannose 6-phosphate receptors mediated by the GGAs." Science **292**(5522): 1712-1716.
Puertollano, R. and J. S. Bonifacino (2004). "Interactions of GGA3 with the ubiquitin sorting machinery." Nat Cell Biol **6**(3): 244-251.
Pulvirenti, T., M. Giannotta, M. Capestrano, M. Capitani, A. Pisanu, R. S. Polishchuk, E. San Pietro, G. V. Beznoussenko, A. A. Mironov, G. Turacchio, V. W. Hsu, M. Sallese and A. Luini (2008). "A traffic-activated Golgi-based signalling circuit coordinates the secretory pathway." Nat Cell Biol **10**(8): 912-922.
Robinson, M. S. and J. S. Bonifacino (2001). "Adaptor-related proteins." Curr Opin Cell Biol **13**(4): 444-453.
Rothman, J. E. and L. Orci (1992). "Molecular dissection of the secretory pathway." Nature **355**(6359): 409-415.
Rothman, J. E. and F. T. Wieland (1996). "Protein sorting by transport vesicles." Science **272**(5259): 227-234.
Saraste, J. and E. Kuismanen (1984). "Pre- and post-Golgi vacuoles operate in the transport of Semliki Forest virus membrane glycoproteins to the cell surface." Cell **38**(2): 535-549.
Saraste, J., G. E. Palade and M. G. Farquhar (1986). "Temperature-sensitive steps in the transport of secretory proteins through the Golgi complex in exocrine pancreatic cells." Proc Natl Acad Sci U S A **83**(17): 6425-6429.
Seaman, M. N. (2004). "Cargo-selective endosomal sorting for retrieval to the Golgi requires retromer." J Cell Biol **165**(1): 111-122.
Seaman, M. N. (2007). "Identification of a novel conserved sorting motif required for retromer-mediated endosome-to-TGN retrieval." J Cell Sci **120**(Pt 14): 2378-2389.

Sohn, K., L. Orci, M. Ravazzola, M. Amherdt, M. Bremser, F. Lottspeich, K. Fiedler, J. B. Helms and F. T. Wieland (1996). "A major transmembrane protein of Golgi-derived COPI-coated vesicles involved in coatomer binding." J Cell Biol **135**(5): 1239-1248.
Takatsu, H., Y. Katoh, Y. Shiba and K. Nakayama (2001). "Golgi-localizing, gamma-adaptin ear homology domain, ADP-ribosylation factor-binding (GGA) proteins interact with acidic dileucine sequences within the cytoplasmic domains of sorting receptors through their Vps27p/Hrs/STAM (VHS) domains." J Biol Chem **276**(30): 28541-28545.
Takatsu, H., K. Yoshino and K. Nakayama (2000). "Adaptor gamma ear homology domain conserved in gamma-adaptin and GGA proteins that interact with gamma-synergin." Biochem Biophys Res Commun **271**(3): 719-725.
Tesco, G., Y. H. Koh, E. L. Kang, A. N. Cameron, S. Das, M. Sena-Esteves, M. Hiltunen, S. H. Yang, Z. Zhong, Y. Shen, J. W. Simpkins and R. E. Tanzi (2007). "Depletion of GGA3 stabilizes BACE and enhances beta-secretase activity." Neuron **54**(5): 721-737.
Teuchert, M., W. Schafer, S. Berghofer, B. Hoflack, H. D. Klenk and W. Garten (1999). "Sorting of furin at the trans-Golgi network. Interaction of the cytoplasmic tail sorting signals with AP-1 Golgi-specific assembly proteins." J Biol Chem **274**(12): 8199-8207.
Thomas, G. (2002). "Furin at the cutting edge: from protein traffic to embryogenesis and disease." Nat Rev Mol Cell Biol **3**(10): 753-766.
Tikkanen, R., S. Obermüller, K. Denzer, R. Pungitore, H. J. Geuze, K. von Figura and S. Höning (2000). "The dileucine motif within the tail of MPR46 is required for sorting of the receptor in endosomes." Traffic **1**(8): 631-640.
Traub, L. M., J. A. Ostrom and S. Kornfeld (1993). "Biochemical dissection of AP-1 recruitment onto Golgi membranes." J Cell Biol **123**(3): 561-573.
Valdivia, R. H., D. Baggott, J. S. Chuang and R. W. Schekman (2002). "The yeast clathrin adaptor protein complex 1 is required for the efficient retention of a subset of late Golgi membrane proteins." Dev Cell **2**(3): 283-294.
Valnes, K. and P. Brandtzaeg (1985). "Retardation of immunofluorescence fading during microscopy." J Histochem Cytochem **33**(8): 755-761.
Vieira, S. I., S. Rebelo, S. C. Domingues, E. F. da Cruz e Silva and O. A. da Cruz e Silva (2009). "S655 phosphorylation enhances APP secretory traffic." Mol Cell Biochem **328**(1-2): 145-154.
Volpicelli-Daley, L. A., Y. Li, C. J. Zhang and R. A. Kahn (2005). "Isoform-selective effects of the depletion of ADP-ribosylation factors 1-5 on membrane traffic." Mol Biol Cell **16**(10): 4495-4508.
Wahle, T., K. Prager, N. Raffler, C. Haass, M. Famulok and J. Walter (2005). "GGA proteins regulate retrograde transport of BACE1 from endosomes to the trans-Golgi network." Mol Cell Neurosci **29**(3): 453-461.
Wood, S. A., J. E. Park and W. J. Brown (1991). "Brefeldin A causes a microtubule-mediated fusion of the trans-Golgi network and early endosomes." Cell **67**(3): 591-600.
Yoon, H. Y., J. S. Bonifacino and P. A. Randazzo (2005). "In vitro assays of Arf1 interaction with GGA proteins." Methods Enzymol **404**: 316-332.
Zhu, Y., M. T. Drake and S. Kornfeld (1999). "ADP-ribosylation factor 1 dependent clathrin-coat assembly on synthetic liposomes." Proc Natl Acad Sci U S A **96**(9): 5013-5018.

CHAPTER 4

RECRUITMENT OF THE MINT3 ADAPTOR IS NECESSARY FOR EXPORT OF THE AMYLOID PRECURSOR PROTEIN (APP) FROM THE GOLGI COMPLEX

4.1. Summary

The amyloid precursor protein (APP) is a ubiquitously expressed, single-pass transmembrane protein that undergoes proteolytic processing by secretases to generate the pathogenic Aβ peptide, the major component in Alzheimer's plaques. The traffic of APP through the cell determines its exposure to secretases, and consequently the cleavages that generate the pathogenic or non-pathogenic peptide fragments. Despite the likely importance of APP traffic to Alzheimer's disease we still lack clear models for the routing and regulation of APP in cells. Like traffic of most transmembrane proteins, the binding of adaptors to its cytoplasmic tail, which is 47 residues long and contains at least four distinct sorting motifs, regulates that of APP. We tested each of these for effects on the traffic of APP from the Golgi by mutating key residues within them and examining adaptor recruitment at the Golgi and traffic to post-Golgi site(s). We demonstrate strict specificity for recruitment of the Mint3 adaptor by APP at the Golgi, a critical role for Y682 (within the *Y*ENPTY motif) in Mint3 recruitment and export of APP from the Golgi, and identify $LAMP1^{+}$ structures as the proximal destination of APP after leaving the Golgi. Together, these data provide a detailed view of the first sorting step in its route to the cell surface and processing by secretases and further highlight the critical role played by Mint3.

4.2. Introduction

The amyloid precursor protein (APP[7]) is a ubiquitously expressed, single-pass transmembrane protein of unknown function in mammals. APP is important in the brain as its proteolytic processing can generate the Aβ peptide, which contributes to the pathogenesis of Alzheimer's disease (Selkoe 1998, Rajendran and Annaert 2012). APP is synthesized in the rough endoplasmic reticulum (ER), travels to the Golgi where it is glycosylated into its mature form,

[7] Abbreviations used in the text include: 3D3I, three-dimensional isosurface image intensity; APP, amyloid precursor protein; BFA, Brefeldin A; ER, endoplasmic reticulum; LAMP, lysosomal associated membrane protein; M6PR, mannose 6-phosphate receptor; Mint3, Munc18 interacting protein 3; PBS, phosphate buffered saline; TfR, transferrin receptor.

and then exits the Golgi before arriving at the plasma membrane. From the plasma membrane it can be internalized through the endocytic pathway (Selkoe 1994, Selkoe 1998) and traffic to endosomes. Throughout this journey APP may be cleaved by α- and γ-secretases to generate non-toxic protein fragments or by β- and γ-secretases to generate the pathogenic fragment Aβ. These peptide fragments oligomerize and later can be deposited into extracellular amyloid plaques, the pathogenic hallmark of Alzheimer's disease (Selkoe, Yamazaki et al. 1996, Greenfield, Tsai et al. 1999, Lah and Levey 2000). The different secretases responsible for the cleavage of APP have distinct distributions throughout the cell. Non-amyloidogenic processing of APP occurs predominantly at the plasma membrane where APP is exposed to α-secretase (Sisodia 1992). Although still controversial, the amyloidogenic processing is thought to occur predominantly in the endomembrane system (for a review of APP processing, see (Thinakaran and Koo 2008)). Both the routing and the kinetics of APP traffic through the cell are thought to determine the extent of exposure to the different secretases and thereby the rate and extent of processing into amyloidogenic or non-amyloidogenic species.

The sorting of APP at each membrane and its traffic through the cell is influenced by its binding to adaptor proteins that are recruited from cytosol to initiate carrier biogenesis (Rothman and Wieland 1996, Robinson and Bonifacino 2001, Bonifacino and Lippincott-Schwartz 2003, Bonifacino and Glick 2004). Adaptors interact with cargo via sorting motifs contained in the cytoplasmic tail. Adaptors can bind directly to the cargo and facilitate both the concentration of the cargo into nascent carriers as well as recruit other proteins that together form a coated carrier (Rothman and Orci 1992, Rothman and Wieland 1996, Robinson and Bonifacino 2001, Bonifacino and Lippincott-Schwartz 2003, Lee, Miller et al. 2004, Donaldson and Jackson 2011). The mature carrier requires machinery to pinch it off from the donor membrane, as well as information ensuring its movement to a specific membrane destination and machinery involved in

uncoating and fusion at that site. Thus, the recruitment of specific protein adaptors to APP is directly linked to its routing throughout the endomembrane system.

The cytoplasmic tail of APP is 47 residues long and contains at least four distinct sorting motifs ((Borg, Ooi et al. 1996, Marks, Woodruff et al. 1996, Nordeng and Bakke 1999), see Fig. 3A), each with the potential to regulate APP traffic at one or more sites (Lee, Kao et al. 2003). APP is expressed in mammals in several splice variants of different lengths. The most prominent variant in human brain is 695 residues long and this variant was used in all of our studies. The numbering of residues is based on this variant. The membrane-proximal YXXϕ (where X is any amino acid and ϕ is a hydrophobic one) adaptin binding motif (^{653}YTSI^{656}) functions in the basolateral sorting of APP in at least some cell types (Haass, Koo et al. 1995, Icking, Amaddii et al. 2007), as well as in internalization at the plasma membrane (Perez, Soriano et al. 1999). The more membrane-distal portion of the tail contains an YXNPXY motif (^{682}YENPTY^{687}) that binds to the Munc18-interacting proteins (Mint1-3 (Borg, Yang et al. 1998)). We have previously shown that the monomeric adaptor Mint3 is important for export from the Golgi, as depletion of Mint3 or truncation of the tail of APP to remove the YENPTY motif alter APP traffic (Shrivastava-Ranjan, Faundez et al. 2008). The shorter NPXY motif is found within the YENPTY motif and binds to Fe65 and Dab2 (Borg, Ooi et al. 1996), though reports vary as to the effect of Fe65 on the processing of APP (Sabo, Lanier et al. 1999, Saito, Akiyama et al. 2011). Snx17 also binds to APP through the YENPTY motif at early endosomes to affect Aβ production (Lee, Retamal et al. 2008). Finally, the membrane-distal YKFFE motif (^{686}YKFFE^{690}) mediates the binding of the tetrameric adaptin, AP-4, and can affect the processing of APP to pathogenic species (Burgos, Mardones et al. 2010, Choy, Cheng et al. 2012). AP-4 also has been implicated in regulating traffic of APP from the Golgi. Indeed, it was reports that AP-4 is the mediator of export of APP from the Golgi (Burgos, Mardones et al. 2010) that prompted the current study to assess the contribution of Mint3 to this process.

Because of the importance of membrane traffic to the localization and processing of APP this protein has been the subject of a large number of studies (Thinakaran and Koo 2008). Importantly, while there appears to be strong evidence that the generation of the pathogenic Aβ occurs largely in endosomes, there are several reports claiming that the Golgi is also an important site of processing (Xu, Sweeney et al. 1997, Siman and Velji 2003, Burgos, Mardones et al. 2010, Choy, Cheng et al. 2012). The Golgi is the first site of sorting divergence for membrane proteins, allowing their export to distinct destinations. While the mechanisms by which this sorting decision is made and carried out are not completely understood it is likely that the adaptors have a large influence on the destination of each transmembrane cargo. That is, if APP has more than a single means for exit from the Golgi the nature of the adaptor(s) it recruits will likely result in different routes to the plasma membrane. This has the potential for delivering APP to different sites for processing, resulting in differences in the location and extent of Aβ generation. Clearly, a better understanding of the regulation of export of APP from the Golgi will provide not only a better understanding of the regulation of this process but may also provide targets for clinically relevant intervention.

Previous work from our lab demonstrated that APP recruits Mint3 for export from the Golgi, and a truncation of the cytoplasmic tail of APP to eliminate the YENPTY motif eliminated Mint3 recruitment and altered APP export (Shrivastava-Ranjan, Faundez et al. 2008). However, this truncation also eliminated other known adaptor binding motifs, most importantly to our interpretation, the motif that binds to AP-4. Thus, we wanted to refine these studies using site-directed mutagenesis to determine the impact on binding and functionality of a much more discrete number of binding partners. To evaluate the effect of the sorting motifs on the export of APP from the Golgi and proximal destination, we mutated key residues within the cytosolic tail of APP and evaluated effects on adaptor recruitment at the Golgi, and traffic to post-Golgi sites. We also took advantage of previously described protocols that can arrest protein export from the

Golgi and accumulate a bolus of cargo that is more easily tracked (20°C temperature block) or strip the Golgi of Arf-dependent adaptors (short term exposure to the drug Brefeldin A (BFA)) to ask specific questions about the impact of specific residues in the cytoplasmic tail of APP on adaptor recruitment and Golgi export and proximal destination.

4.3. Results

Mint3 is specifically recruited in response to APP expression

The cytoplasmic tail of APP is 47 residues in length and contains four previously described sorting motifs that bind different proteins and potentially contribute to APP traffic from the Golgi: YXXϕ, YENPXY, NPXY (contained within the larger YENPTY motif), and KFFE. We mutated key residues in these motifs to evaluate their effect on (i) the recruitment of adaptors, (ii) the rate of export of APP from the Golgi, and (iii) the proximal destination of APP after leaving the Golgi.

The APP gene is expressed in humans as a number of alternatively spliced transcripts, resulting in different length proteins. We based our constructs and numbering of residues on the transcript that encodes a protein of 695 residues, as it is the major isoform expressed in the brain and is most commonly studied by Alzheimer's disease researchers. The lumenal domain of APP has been shown to interact with other proteins, notably the transmembrane protein LR11/SORLA (Andersen, Reiche et al. 2005) and this has been predicted to influence the retention, sorting, and kinetics of its export from the Golgi. To allow us to discriminate between cytoplasmic tail and combined lumenal plus cytoplasmic tail interactions, we generated a fusion protein consisting of the lumenal and transmembrane domain of CD8 with only the cytoplasmic tail of APP. Homologous CD8 fusion proteins have been used in several labs and found to retain key sorting information for protein cargos including the mannose 6-phosphate receptor and furin (Seaman 2004, Hirst, Seaman et al. 2007). The CD8-APP proteins expressed are each 257 amino acids in length, with an apparent molecular weight of ~28kD. Thus, our studies were performed with both

full length APP and the CD8-fusion constructs and the results were quite consistent, indicating only minimal, if any, effects of lumenal interactions on APP in our assays.

APP or CD8-APP proteins were transiently expressed in HeLaM cells to allow quantification and localization using immunofluorescence. This cell line was chosen due to its flattened morphology when grown on cover slips, providing advantages for imaging, and low background of adaptor staining on endomembranes, facilitating quantification. The use of fusion proteins and protein over-expression required that attention be given to the potential for artifactual results. To minimize these concerns the following steps were taken: (i) results from CD8 fusions were always compared to those from use of the full length (untagged) APP, (ii) we selected for analysis only those cells that displayed clear but minimal protein expression, (iii) we confirmed by visual inspection that cells expressing higher levels of exogenous protein than those used in quantification yielded the same qualitative results, and (iv) DNA concentrations in transfections were optimized such that each mutant in the series was expressed to the same extent as the non-mutated proteins (we found that this could vary with the DNA preparation but was not consistently different among the mutants). Additional controls included untransfected cells, empty vector transfections, and CD8 lumenal and transmembrane domain with no cytoplasmic tail. This last control displayed diffuse staining throughout the cell so confirmed the functional importance of the cytoplasmic tail but was not used in quantification due to its completely diffuse nature (not shown).

We evaluated each of the well-characterized Golgi adaptors for membrane recruitment in response to expression of our APP constructs and found that only Mint3 was differentially affected. HeLaM cells were transfected with the indicated cargo, fixed ~20 hr later and stained with antibodies against either APP or CD8 and COPI, GGA1, AP-1, AP-3, AP-4 or Mint3. Endogenous APP staining in HeLaM cells is punctate and widely distributed throughout the cytoplasm, with a higher density of staining in the perinuclear region that overlaps with Golgi markers (Fig. 1A). With expression of APP or CD8-APP, staining with the antibody directed

against the C-terminus of APP or to CD8, respectively, resulted in brighter staining that is otherwise the same as that of endogenous APP (Fig. 1A). Each of the adaptors tested exist in a cytosolic pool from which they are recruited to membranes as a result of direct interactions with some combination of a transmembrane cargo, activated Arfs, and phospholipids (Cockcroft, Thomas et al. 1994, Godi, Pertile et al. 1999, Jones, Morris et al. 2000, Aridor and Traub 2002, Bonifacino and Traub 2003). The levels of adaptors in the cells did not change in response to cargo expression (e.g., see Caster, et al (Caster, Sztul et al. 2013) or Fig. 3F). Thus, increased adaptor staining at a membrane is interpreted as evidence of recruitment to that organelle from the soluble pool. We observed no changes in the staining of COPI, GGAs, AP-3 (data not shown), AP-1 (Fig. 1A), or AP-4 (Fig. 1A) in response to increased expression of APP or CD8-APP. In marked contrast, Mint3 staining was seen to specifically increase (Fig. 1A) and the intensity of Mint3 staining correlated, by visual inspection, with the level of APP or CD8-APP staining in the perinuclear region (data not shown).

The cytoplasmic tail of APP also binds a number of other proteins, most of which have no clear role in membrane traffic. The NPXY motif is directly involved in binding to Fe65 and Dab2 (Borg, Ooi et al. 1996, Lee, Retamal et al. 2008) and each of these have been found capable of changing the amount of Aβ secreted by cells, though through unknown mechanisms or sites of action within cells. Like the adaptors assessed in the previous section, each of these proteins reside in the cytosol from which they can be recruited to binding sites on different membranes. We also tested FAPP2, which localizes at the late Golgi in an Arf- and PI(4)P-dependent fashion and serves as a control for non-specific Golgi recruitment as there is no published evidence linking FAPP2 to APP or other transmembrane cargos transiting the Golgi. We expressed APP or CD8-APP in HeLaM cells, fixed cells ~20 hr later and then stained with antibodies against APP and Fe65, Dab2, or FAPP2. As FAPP2 served as our negative control, it was not surprising to find that FAPP2 staining was not changed in cells expressing even the highest levels of APP or CD8-APP. Similarly, Dab2 and Fe65 staining is localized to small puncta throughout the periphery of

the cell and each was unaltered by APP or CD8-APP expression (data not shown). Thus, of the known adaptors acting at the Golgi and previously described proteins that bind the cytoplasmic tail of APP, only Mint3 was recruited to the Golgi in an APP-dependent fashion in HeLaM cells.

Both APP and Mint3 are further enriched at the Golgi in response to temperature block

APP traffics the secretory and endocytic pathway at different rates in different cells and its steady state distributions are quite different among cell types (Selkoe 1994). Our goal was to focus on APP traffic at the Golgi, and we developed a method termed three dimensional isosurface image intensity or 3D3I for quantification of immunofluorescence imaging data, described in detail in Experimental Procedures and previous publications (Caster and Kahn 2012, Caster, Sztul et al. 2013). Briefly, we use wide field fluorescence imaging to collect a z-stack that is deconvolved using Huygen's SVI software. Deconvolved stacks are imported into Imaris, and an isosurface is generated based upon the staining of a previously characterized marker of an organelle. The fluorescence intensity of the APP or CD8-APP staining within that isosurface is then calculated. Alternatively, we can quantify any changes in adaptor localization within a cargo-defined isosurface. We also took advantage of a temperature block (20°C, four hr) that inhibits export from the Golgi (while ER to Golgi traffic continues) and results in an increase in the amount of cargo at the Golgi. The temperature block is rapidly reversible and allows us to monitor the abundance of adaptors recruited in response to specific cargos in a temporally and spatially highly controlled fashion.

APP or CD8-APP displayed punctate staining throughout the cytoplasm with little evidence of localization to the Golgi in HeLaM cells (Fig. 1A) without imposition of the temperature block. This low steady state localization at the Golgi contributed to a large fold-increase in the staining of APP or CD8-APP there in response to the 20°C block (Fig. 1B). In this experiment, one day after transfection, fixed cells were stained with antibodies against the C-terminus of APP and GM130, or CD8-APP and giantin. Isosurfaces were generated based on GM130 or giantin

staining (Fig. 1B) and the fluorescence intensity of APP (Fig. 1B, upper) or CD8-APP (Fig. 1B, lower) within the GM130 or giantin isosurfaces, respectively, was calculated. This switch in Golgi marker was necessary to facilitate double labeling of our fixed cells as the APP and CD8 antibodies were raised in different species. Each of the Golgi markers was color coded as a heat map in Figure 1B, to indicate the amount of APP or CD8-APP within the isosurface at 37°C or 20°C. The scale of sum intensities per volume (μm^3) is shown on the right of Fig. 1B. Incubation at 20°C significantly increased the amount of APP or CD8-APP in GM130 or giantin isosurfaces. We also calculated the percent of total APP present within giantin-defined isosurfaces. To do this, two isosurfaces were defined: first, one was generated based on the total APP fluorescence within the cell, then an isosurface based on giantin staining was identified and the amount of APP within it was calculated. At steady state, 10.5 +/- 2.8% of total APP fluorescence was found within giantin-defined isosurfaces. Following the four hr incubation at 20°C, APP fluorescence within giantin-defined isosurfaces increased to 75.2 +/- 4.1% (results typical of 3 independent experiments, >5 cells per condition). Thus, as expected and shown previously for M6PR or CD8-M6PR (Caster, Sztul et al. 2013), the amount of APP and CD8-APP at the Golgi were significantly increased by temperature block in HeLaM cells.

As shown above in Fig. 1A, expression of APP or CD8-APP resulted in increased recruitment of Mint3 to the perinuclear region. To establish the site of Mint3 recruitment we performed double labeling with markers of several different endomembranes (including ER, recycling endosomes, lysosomes, and early, medial and late Golgi) and found the strongest overlap with those of the Golgi. We next quantified the amount of Mint3 recruited to giantin positive isosurfaces in response to CD8-APP expression using 3D3I (Fig. 1C). Temperature block has little or no effect on the amount of Mint3 within a giantin-defined isosurface in control (mock-transfected) cells (Fig. 1C, left). Expression of CD8-APP significantly increased the amount of Mint3 within giantin-defined isosurfaces at 37°C and this was further increased by the four hr incubation at 20°C (Fig. 1C, right). Similar results were obtained using APP (not shown). We also

examined the recruitment of other adaptors to APP accumulated at the Golgi by the temperature block. We observed no changes in the recruitment of other proteins or adaptors such as AP-1, GGAs, FAPP2, Dab2, or Fe65 in APP-expressing cells following temperature blockade, despite the increased presence of APP or CD8-APP (see below). We conclude that increasing the amount of cellular APP or CD8-APP results in a higher concentration of either cargo at the Golgi, with parallel increases in Mint3, and that imposition of a temperature block further increases the levels of these cargos and Mint3 at the Golgi, but not those of the other adaptors or binding partners examined.

Increasing APP at the Golgi leads to greater recruitment of Mint3 that retains BFA sensitivity

Mint3 has been shown to bind directly to active (GTP-bound) Arf GTPases through the C-terminal portion of their PTB domains and C-terminal of two PDZ domains (Hill, Li et al. 2003). Mint1 and Mint2 are neuron-specific adaptors (Duclos, Boschert et al. 1993), while Mint3 is ubiquitously expressed (Okamoto, Nakajima et al. 2001, Hill, Li et al. 2003), localizes to the TGN in multiple cells lines, and is the only Mint paralog expressed in HeLa cells (Okamoto and Sudhof 1998, Hill, Li et al. 2003). Like many other protein adaptors at the Golgi, Mint3 is recruited to membranes in an Arf-dependent fashion (Hill, Li et al. 2003). To ensure that the pool of Mint3 recruited to the Golgi is predominantly recruited in an Arf-dependent fashion, we treated cells with the membrane-permeable inhibitor BFA that strips endomembranes of activated Arf, and subsequently Arf-dependent adaptors, within minutes of addition to live cells (Donaldson, Lippincott-Schwartz et al. 1990, Robinson and Kreis 1992, Szul, Garcia-Mata et al. 2005, Hirst, Seaman et al. 2007). These responses to short-term exposure to BFA are in marked contrast to the much more dramatic and well known loss of Golgi integrity and retrograde movement of many Golgi components back to the ER, seen with longer exposures or higher concentrations of the drug (Lippincott-Schwartz, Yuan et al. 1989, Strous, Berger et al. 1991). APP-expressing HeLaM cells were treated with vehicle or 7.5µg/mL BFA for two min and then either fixed, or the drug

was washed out and cells were allowed to recover for the times indicated (Fig. 1D). APP localization was unaltered by addition of BFA compared to vehicle treated cells (data not shown), but Mint3 staining at the Golgi was undetectable after 2 min of BFA treatment. Recovery of Mint3 staining at the Golgi was evident by 5 min after washout of the drug, and continued to increase back toward steady state levels over the first 15 min.

APP traffics to a LAMP1^{+} compartment from the Golgi

As noted above, temperature block led to a significant accumulation of APP cargos and Mint3 at the Golgi and this afforded us the opportunity to follow a bolus of APP as it leaves the Golgi and assess the proximal destination. We used temperature block and release of APP over-expressing cells, fixing at 5 min intervals after return to 37°C. Cells were double labeled with antibodies against the C-terminus of APP and organelle markers (including EEA1, TfR, LAMP1, and LAMP2) and evaluated for overlap in staining. Early endosomes (EEA1), recycling endosomes (TfR)(data not shown), and a subset of lysosomes (LAMP2, Fig. 2C)) showed very little overlap with APP at any of the early times after release from temperature block. In contrast, LAMP1 staining displayed a high level of overlap with that of APP at 5 and 10 min after release (Fig. 2 A, B, D). Note that at 0 minutes release, APP and LAMP1 co-localization is quite low, though LAMP1 staining is more centralized compared to cells maintained at 37°C (Fig. 2A, compare 37°C to 0'). The co-localization of APP and LAMP1 was transient as it was clearly reduced by 15 min and not evident in cells that had never been exposed to the block. We were surprised that APP staining co-localized with one lysosomal membrane marker, LAMP1 (Fig. 2A, B, D), but not another, LAMP2 (Fig. 2C), under the same conditions. While these two lysosomal membrane proteins are often used interchangeably and described as staining lysosomes, there is little or no evidence we could find that they necessarily are found in the same lysosomes. Because we do see some changes in LAMP1 staining profiles before and after temperature block, it is possible that the changes observed result from alterations in either the traffic of APP, LAMP1, or

both following release from temperature block. However, note that LAMP1 staining did not increase in overlap with Golgi markers at any time or with APP prior to release from the blockade. Thus, we conclude that there exists two distinct compartments, with different lysosomal markers, and APP moves only through the LAMP1 positive structures at early times after exit from the Golgi. Similar results were obtained using CD8-APP (see below).

We were surprised to observe APP and CD8-APP traffic directly from the Golgi to a potentially degradative compartment as we do not observe a decrease in total cellular APP levels post-release from temperature block. In efforts to better characterize the relationship of APP to LAMP1 we used the higher resolution, structured illumination microscopy to visualize this compartment. As seen in Fig. 2D, there is little overlap of the two markers at steady state but this is quite different at early times after release from temperature blockade. These images reveal close apposition of LAMP1 and APP or CD8 staining that appear adjacent to one another, at times appearing to represent two parts of the same structure, with different extents of overlap (yellow staining) among the closely related structures (Fig. 4D, small arrowheads). Other structures even appear to have staining of one marker wrapping around the other (Fig. 4D, large arrowheads). We currently interpret these data as evidence of a transient mixing and quick resolution of two compartments.

The Y2A mutant of APP specifically fails to recruit Mint3 to the Golgi

To assess the importance of each of the four previously described sorting signals in the cytoplasmic tail of APP to its localization and export from the Golgi we generated a series of mutants in APP and CD8-APP. Each of the constructs that were used in our studies are depicted in Figure 3A. Because of the importance of tyrosines in sorting motifs and the presence of three of these in the cytoplasmic tail of APP, we refer to Y653 within the YTSI motif as Y1, Y682 within the larger YENPXY motif as Y2, and Y687 within the NPXY motif as Y3 (Fig. 3A). Mutation of ^{688}FFE^{690} to AAA is referred to as FFE/AAA.

We tested each of the Y→A and FFE/AAA mutations for their effect on the recruitment of Mint3 to the Golgi (Fig. 3). Expression of APP (Fig. 3B) or CD8-APP (Fig. 3C) with the mutants Y1A, Y3A, or FFE/AAA resulted in Mint3 staining that was indistinguishable as far as intensity of Mint3 staining or its location in cells. In contrast, the Y2A mutants failed to promote Mint3 recruitment and instead showed staining comparable to that of untransfected cells or those transfected with the vector that lacked insert (Fig. 3B, C). Recruitment of Mint3 to each cargo was quantified using 3D3I. Wide field images of at least seven cells in each case were analyzed. Computational isosurfaces were generated based on APP (Fig. 3D) or CD8-APP (Fig. 3E) staining and the sum intensity of Mint3 within the isosurfaces was determined. The Mint3 staining within the APP-Y2A defined isosurface was not statistically different from control cells that expressed no exogenous proteins (Fig. 3D). Similarly, CD8-Y2A displayed significantly less ($p<0.05$) Mint3 staining within cargo-defined isosurfaces, compared to CD8-APP or the other three mutants (Fig. 3E). Note that in this case we could not compare to mock- or un-transfected controls, as they display no CD8 staining. The Y3A mutant fully supported Mint3 recruitment that was indistinguishable from the non-mutated tail, despite being found within the larger YENPXY motif that includes Y2.

The cytoplasmic tail of APP is expected to be largely or wholly unstructured (Ramelot, Gentile et al. 2000) so a point mutation is unlikely to cause changes in protein stability. Nevertheless, we wanted to ensure we were comparing adaptor recruitment under comparable conditions of protein expression. Transfected cells were collected 18 hr later and cell homogenates analyzed for Mint3 (Fig. 3F) or CD8-APP (Fig. 3G) expression by immunoblots from denaturing SDS gels. When the cell lysates were immunoblotted using a commercially available (Chemicon) antibody to the N-terminus of APP, all the proteins were found to be expressed to comparable levels (Fig. 3H). The same pattern was found for the CD8-APP constructs (Fig. 3G).

The failure of APP-Y2A to recruit Mint3 is correlated with a delay in its export from the Golgi

With the near complete lack of Mint3 recruitment to the Y2A mutant of APP or CD8-APP we asked if the lack of Mint3 binding caused a defect in export from the Golgi. This was deemed risky because it is common for transmembrane protein cargos to have alternative routes of traffic and so the lack of one route is typically compensated by an alternate. Nevertheless, we compared the rate of exit from the Golgi, and the subsequent time it took to arrive at $LAMP1^+$ structures after release from temperature block, for the CD8-APP and CD8-Y2A constructs. Isosurfaces were generated using TGN46 staining (Fig. 4A, B) and the amount of CD8 fluorescence within those structures was determined. CD8-APP accumulated in the TGN following temperature block (Fig. 4A) and then returned to levels comparable to those seen at 37°C by 10 min post-release. CD8-Y2A accumulated in the TGN to essentially the same levels as CD8-APP during temperature block (Fig. 4B). However, CD8-Y2A failed to exit the TGN during the 15 min recovery period, as seen by the unchanging overlap with TGN46 (Fig. 4B), and in contrast to the result with CD8-APP (Fig. 4A).

The kinetics of CD8-APP or CD8-Y2A arrival at $LAMP1^+$ structures were also evaluated. Isosurfaces were generated based on LAMP1 staining, and the amount of CD8 fluorescence within those isosurfaces was determined. The amount of CD8-APP within $LAMP1^+$ structures was unchanged by temperature block (Fig. 4C, compare 37°C to 0' release), as it was quite low under each condition. The amount of CD8-APP in $LAMP1^+$ isosurfaces was significantly increased 5 min post-release from blockade. This value was increased even further at 10 min post-release and returned to levels indistinguishable from control (37°C) by 15 min, consistent with our observations using APP described above. In contrast, CD8-Y2A displayed greater overlap in staining within $LAMP1^+$ isosurfaces at 37°C (Fig. 4D), prior to temperature block. In this case, the block reduced the amount of CD8-Y2A in $LAMP1^+$ isosurfaces and did not return during the 15 min recovery. These results are consistent with Y2A having a defect in the rate of export from the Golgi.

We followed up on the observation that APP-Y2A displayed a greater extent of overlap with $LAMP1^+$ structures than did APP in cells maintained at 37°C (Fig. 4C, D) by including each of our mutants in these analyses of steady state distributions. We found no differences between APP and mutants in their overlap with EEA1 (Fig. 5A) or transferrin receptor (Fig. 5B). However, the APP-Y2A and to an even greater extent APP-Y3A staining displayed enhanced overlap with that of LAMP1 (Fig. 5C). These data are consistent with both Y2 and Y3 playing roles in traffic of APP in HeLaM cells, potentially through interactions with other adaptors though not necessarily at the Golgi based on this result alone. Together the data support the conclusion that Y2 and Mint3 recruitment are critical to the export of APP from the Golgi and that the greater YENPTY motif, or at least Y3 at its C-terminus, has at least one additional role in traffic to or from the $LAMP1^+$ compartment. Of course, in this case the traffic to that site is not limited to late Golgi/TGN but could include other sources of APP. The fact that we also observe overlap in LAMP1 and APP or CD8 staining at steady state with the Y2A and Y3A mutants suggests that this co-localization at the $LAMP1^+$ compartment is not an artifact of temperature block or release.

APP and Furin each recruit Mint3 to the Golgi but with opposing outcomes

Arf-dependent adaptors regulate membrane traffic specifically in the initiation of nascent vesicular carriers for export from a donor compartment. In contrast to the critical role played by Mint3 in export of APP from the Golgi, Mint3 has been shown previously to play an equally important role in the retention of another cargo at the Golgi, furin. To compare the characteristics of the recruitment of Mint3 to these two different cargos, which result in opposing outcomes as far as export, we used FLAG-furin or CD8-furin expression in HeLaM cells. Furin is an endoprotease that acts at the Golgi, being retained there via a mechanism that includes direct binding of the cytoplasmic tail to Mint3 (Han, Wang et al. 2008). The residues involved in furin binding to Mint3 are less well characterized than those in the APP tail but are thought to include a stretch of acidic residues ^{773}SDSEEDE^{779} (numbered using the human furin sequence), based

upon deletion analysis (Han, Wang et al. 2008). We generated a plasmid that directs expression of a CD8 fusion protein containing the entire 56 residue cytoplasmic tail of human furin, homologous to the CD8-APP construct. Expression of CD8-furin in HeLaM cells led to a steady state distribution that was highly enriched in Golgi structures (Caster, Sztul et al. 2013), clearly more so than was seen for CD8-APP. This is despite the fact that immunoblotting with anti-CD8 revealed very similar levels of CD8-APP and CD8-furin were expressed in HeLaM cells (Fig. 6A). CD8-furin expression resulted in enhanced Mint3 recruitment to the Golgi at steady state, and this recruitment is only slightly enhanced following temperature block (Caster, Sztul et al. 2013).When we quantified total cellular staining for CD8-APP and CD8-furin and then determined the fraction that was within isosurfaces identified by TGN46 staining we found 12.8% of CD8-APP and 64.3% of CD8-furin in this region of the Golgi. Imposition of the temperature block only slightly enhanced CD8-furin (76.0%, (33)) at that site but dramatically increased the fraction of cellular CD8-APP (68.1%) there. We attribute the less dramatic changes in CD8-furin localization in response to temperature block to the already high percentage of CD8-furin there prior to the block, but it also suggests that the rate of export may be substantially lower than that of APP.

Like APP and CD8-APP, expression of furin or CD8-furin resulted in increased staining of Mint3 at the Golgi, as defined here by giantin isosurfaces (Fig. 6B). No changes were seen in total cellular Mint3 (not shown), indicating that the adaptor is recruited from cytosol. One day (~18 hr) after transfections, we compared the relative abilities of these two cargos to recruit Mint3 to the Golgi (giantin isosurfaces) at steady state and after temperature block (Fig. 6B). Transfected cells were maintained at 37°C (black bars) or switched to 20°C (white bars) for four hours, then fixed and stained for Mint3 and giantin. CD8-APP and CD8-furin resulted in similar levels of Mint3 recruitment to giantin-defined isosurfaces at 37°C, each significantly higher than control cells (CD8-empty). CD8-APP dependent recruitment of Mint3 was further and

significantly increased during temperature block but CD8-furin mediated recruitment was not (Fig. 6B).

Finally, we evaluated the BFA sensitivity of Mint3 recruited to the Golgi by CD8-furin expression. HeLaM cells were transfected with plasmids directing expression of CD8-furin (Fig. 6C) and after ~20 hours were treated with vehicle (methanol) or 7.5µg/mL BFA for two minutes. The drug was then washed out with pre-warmed medium and cells were allowed to recover for 0', 5' (Fig. 6C), 10', or 15 min (data not shown). Treatment with BFA caused the essentially complete loss of Mint3 staining that returned to the Golgi, evident already at five min and increasing back to steady state levels by 15 min. We conclude that the cytoplasmic tails of APP and furin each recruit Mint3 to the Golgi in an Arf-dependent manner despite the fact that the consequences differ, with one cargo (APP) being dependent on it for export and the other (furin) for its retention.

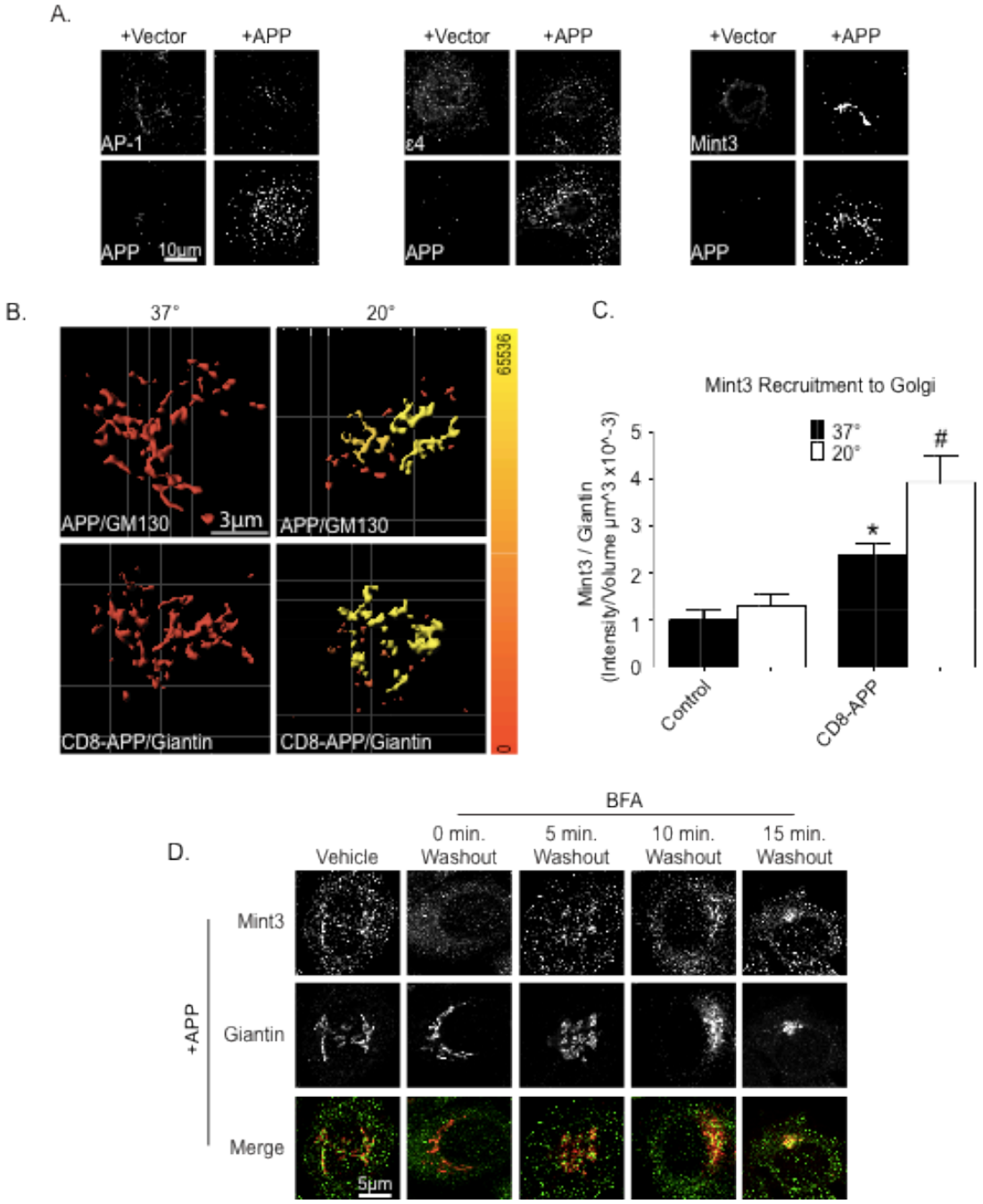

Figure 1. *APP specifically recruits Mint3 to the Golgi in an Arf-dependent fashion.* **(A)** Cells were transfected with empty vector (pFUGW) or pFUGW-APP as indicated. Cells were fixed one day later and stained with antibodies against the C-terminus of APP and γ-adaptin (AP-1), ε4 (AP-4), or Mint3. Maximum intensity projections of wide field images are shown. **(B)**. Cells were

transfected with APP or CD8-APP, as indicated, and stained with antibodies to APP and GM130 (top panels), or CD8 and giantin (bottom panels). Isosurfaces were built based on GM130 (upper), or giantin (lower) staining, and the total intensity of APP (upper), or CD8 (lower) within the isosurface was calculated. A heat map of intensities ranging from 0 to 65536 was generated (color bar on right). **(C)** Mock transfected cells, or cells expressing CD8-APP, were treated as described in (B), and stained with antibodies against Mint3 and giantin. Wide field stacks of images were collected, deconvolved, and imported into Imaris where isosurfaces were built based on giantin staining, the total amount of Mint3 within the isosurface recorded, and expressed as a ratio of intensity/giantin volume (intensity/μm^3 $x10^{-3}$). Values were normalized to control cells maintained at 37°C. Statistical significance is indicated with #, $p<0.01$, and *, $p<0.05$, when analyzed using ANOVA. **(D)** APP-dependent Mint3 recruitment is BFA-sensitive and rapidly reversible. HeLaM cells expressing APP were treated with either vehicle or BFA for 2 min (see Experimental Procedures). Fresh, pre-warmed medium was then used to wash out the drug and cells allowed to recover for the times indicated, before fixation and staining with antibodies against Mint3 and giantin. Confocal images are shown.

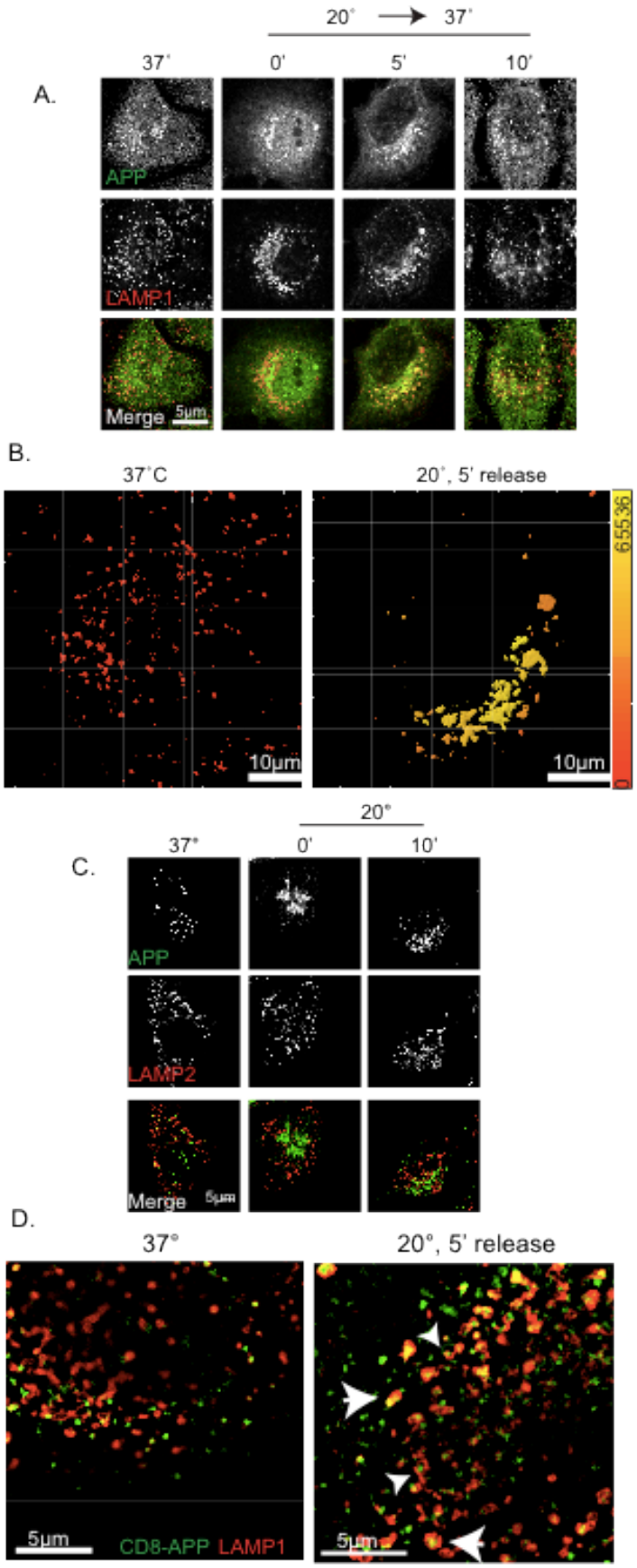
20˚ → 37˚
A.
37˚
0'
5'
10'
APP
LAMP1
Merge
5μm
B.
37˚C
20˚, 5' release
655.36
0
10μm
10μm
20°
C.
37°
0'
10'
APP
LAMP2
Merge
5μm
D.
37°
20°, 5' release
5μm
CD8-APP LAMP1
5μm

Figure 2. *APP exits from the Golgi and arrives at LAMP1^{+} structures*. HeLaM cells were transfected with **(A, B, C)** APP, or **(D)** CD8-APP. The next day cells were maintained at 37°C or 20°C for 4 hr, then returned to 37°C for the times indicated. **(A)** Cells were fixed and stained with antibodies against the C-terminus of APP, and LAMP1. Maximum intensity projections of widefield images are shown. **(B)** Isosurfaces were generated based on the LAMP1 staining shown in **A,** described under Experimental Procedures. Isosurfaces were then color coded using a heatmap, indicating the sum intensity of APP within the LAMP1+ isosurfaces. Color range is indicated in the vertical bar on the right. **(C)** Cells expressing APP were treated as described in (A), fixed, and stained with antibodies against APP and LAMP2. APP does not overlap with LAMP2 at steady state, or at any point after release from temperature blockade. Maximum intensity projections of widefield images are shown. **(D)** Cells expressing CD8-APP, and treated as described above were stained with antibodies against CD8 and LAMP1 were fixed and stained at the times indicated. Cells were imaged on a Nikon Structured Illumination Microscope (see Experimental Methods), and images reconstructed. Large arrowheads indicate examples of overlapping CD8-APP and LAMP1 compartment, while smaller arrowheads indicate examples of CD8-APP that is closely apposed to LAMP1 staining. Cells were imaged on a Nikon Structured Illumination Microscope (see Experimental Methods), and images reconstructed. 5 min. after release from blockade, CD8-APP overlap with LAMP1 is increased.

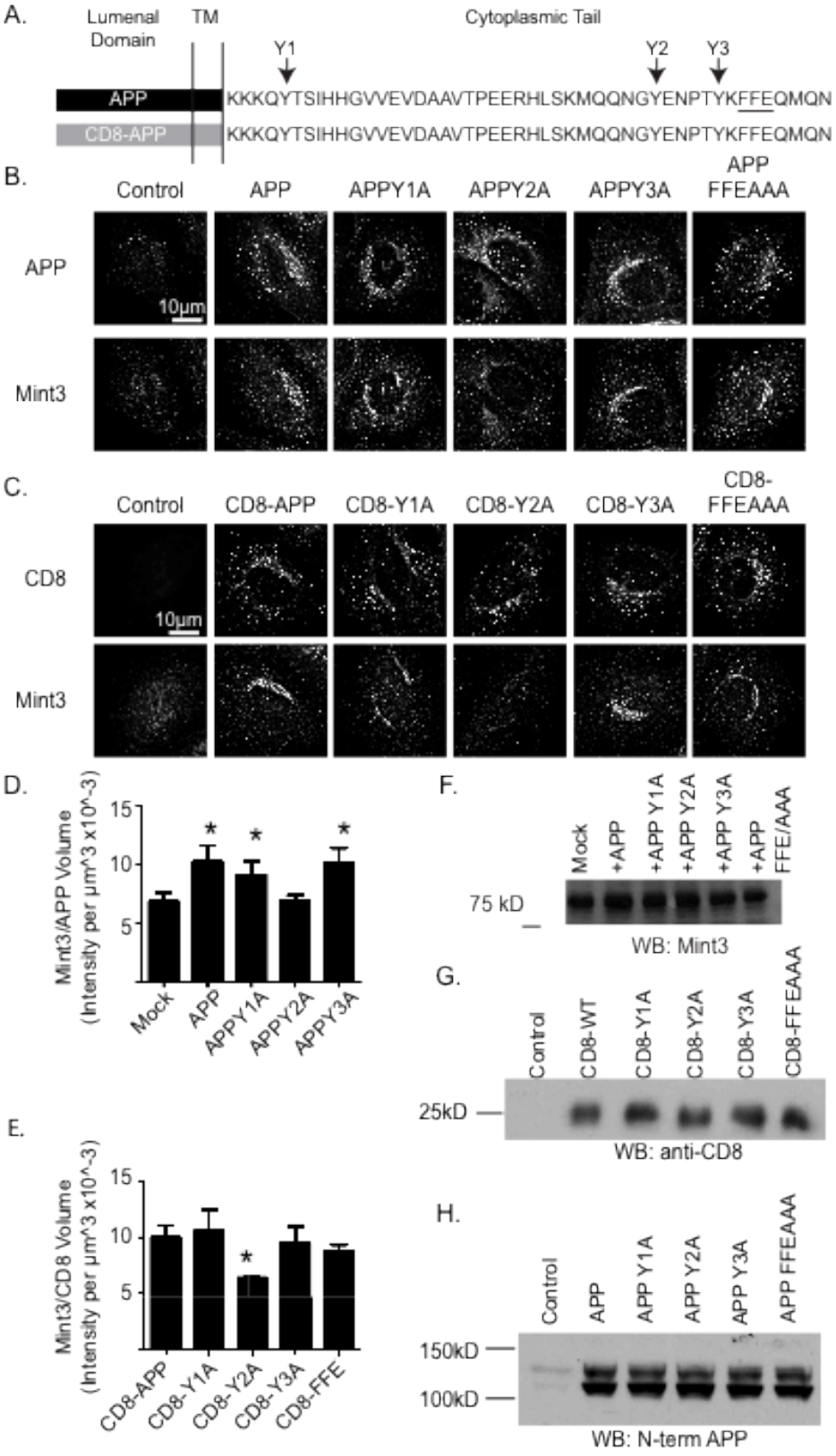
A.
Lumenal Domain
TM
Cytoplasmic Tail
Y1
Y2
Y3
APP
KKKQYTSIHHGVVEVDAAVTPEERHLSKMQQNGYENPTYKFFEQMQN
CD8-APP
KKKQYTSIHHGVVEVDAAVTPEERHLSKMQQNGYENPTYKFFEQMQN
B.
Control
APP
APPY1A
APPY2A
APPY3A
APP FFEAAA
APP
Mint3
10μm
C.
Control
CD8-APP
CD8-Y1A
CD8-Y2A
CD8-Y3A
CD8-FFEAAA
CD8
Mint3
10μm
D.
Mint3/APP Volume (Intensity per μm^3 x10^-3)
15
10
5
Mock
APP
APPY1A
APPY2A
APPY3A
E.
Mint3/CD8 Volume (Intensity per μm^3 x10^-3)
15
10
5
CD8-APP
CD8-Y1A
CD8-Y2A
CD8-Y3A
CD8-FFE
F.
Mock
+APP
+APP Y1A
+APP Y2A
+APP Y3A
+APP FFE/AAA
75 kD
WB: Mint3
G.
Control
CD8-WT
CD8-Y1A
CD8-Y2A
CD8-Y3A
CD8-FFEAAA
25kD
WB: anti-CD8
H.
Control
APP
APP Y1A
APP Y2A
APP Y3A
APP FFEAAA
150kD
100kD
WB: N-term APP

Figure 3. *Mutation of Y2 to alanine results in the inability to recruit Mint3 in CD8-APP or APP.* **(A)** Schematic representation of APP, consisting of the lumenal, transmembrane (TM), and cytosolic (tail) domains showing the primary sequence of only the cytoplasmic tail. The three tyrosines mutated (to alanines) are shown above as Y1, Y2, or Y3 and the three-residue FFE motif, mutated to AAA, is underlined. The lower construct indicates that the lumenal and transmembrane domains of APP were replaced with those of CD8. HeLaM cells were transfected with the cargos indicated and 18 hr later were fixed and stained with antibodies against **(B)** APP and Mint3, or **(C)** CD8 and Mint3. Confocal images are shown. Wild type and all other mutants recruit Mint3 comparably but the Y2A mutation uniquely loses Mint3 recruitment. **(D, E)** Mint3 recruitment was quantified in cells treated as described above. Stacks of wide field images were collected, deconvolved and isosurfaces were generated based on **(D)** APP staining, or **(E)** CD8 staining. The total pixel intensity within each isosurface was calculated and expressed as a ratio of Mint3 intensity/cargo volume. N>7 cells were used per condition. ANOVA was use to compare groups to (D) mock transfected cells, or (E) CD8-APP. Asterisks indicate statistical significance compared to (D) mock transfected, or (E) CD8-APP ($p<0.05$). **(F)** Total cellular Mint3 is unaffected by expression of APP mutants. HeLaM cells were transfected with the mutants indicated and 18 hr later cells were lysed and proteins (20 μg) were resolved in 10% PAGE gels, prior to immunoblotting with Mint3 antibody, as described under Experimental Procedures. **(G)** HeLaM cells were transfected with the CD8-APP constructs indicated and treated as described in (F). Immunoblots probed with an antibody against CD8, as described under Experimental Procedures. Overall, none of the mutations cause a change in the level of expression in total cell homogenates.

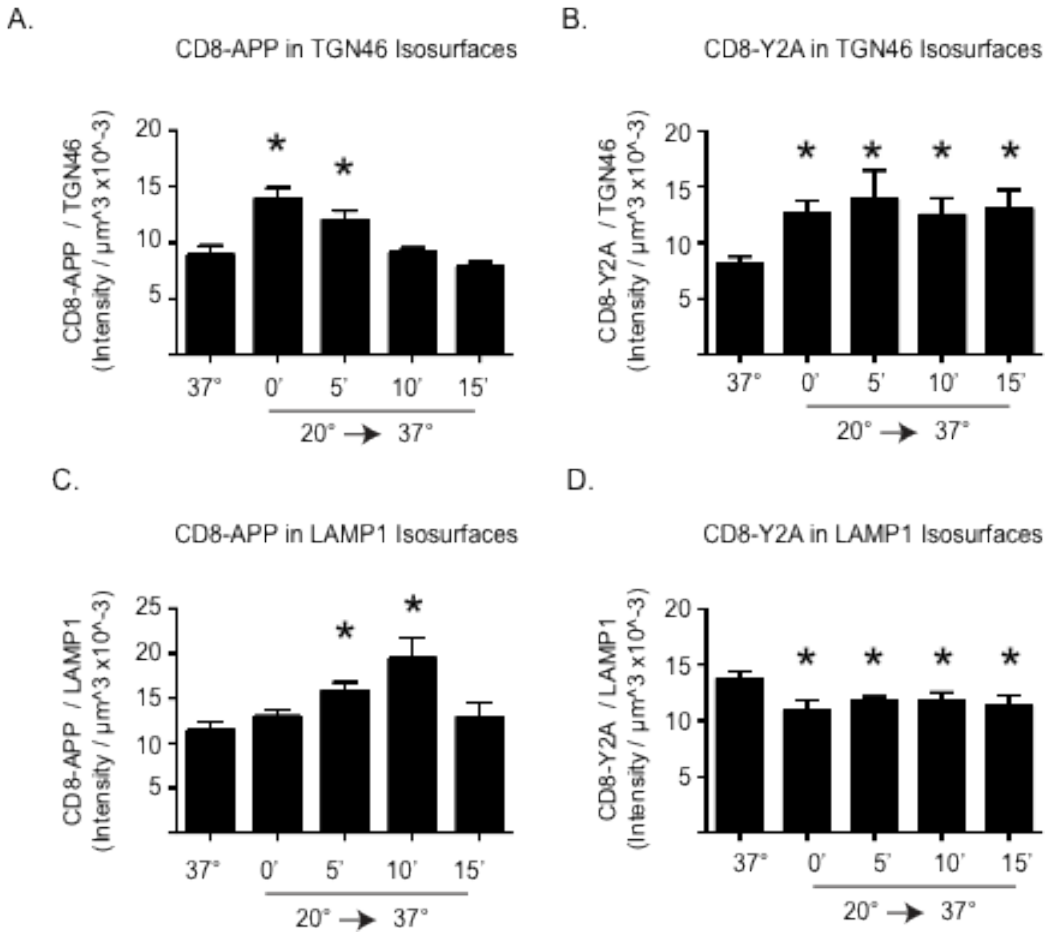

Figure 4. *Mutation of Y2A alters APP exit from the Golgi and arrival at LAMP1$^+$ structures*. The amount of **(A, C)** CD8-APP, or **(B, D)** CD8-Y2A in **(A, B)** TGN46 isosurfaces, or **(C, D)** LAMP1 isosurfaces was quantified using 3D3I analysis. Cells treated as described above were stained with antibodies against **(A, B)** CD8 and TGN46, or **(C, D)** CD8 and LAMP1. Isosurfaces were generated based on **(A, B)** TGN46, or **(C, D)** LAMP1 staining. The intensity of CD8 staining within each isosurface was totaled, and expressed as a ratio of CD8 intensity per isosurface volume. Asterisks indicate statistical significance ($p<0.05$) using ANOVA, comparing each group to cells maintained at 37°C.

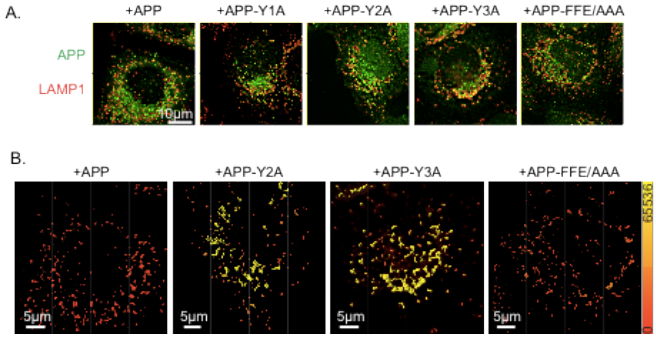

Figure 5. *APP-Y3A or APP- Y2A display increased overlap with LAMP1 at steady state.* HeLaM cells were transfected with the APP mutants indicated. The next day cells were fixed and stained with antibodies against APP and LAMP1. **(A)** Maximum intensity projections of widefield images are shown. **(B)** Images shown in (A) were imported into Imaris, and isosurfaces generated based on LAMP1 staining. Isosurfaces were then falsely colored with a heat map (shown on right, ranging from 0 to 65536) indicating the sum intensity of APP staining within the isosurfaces.

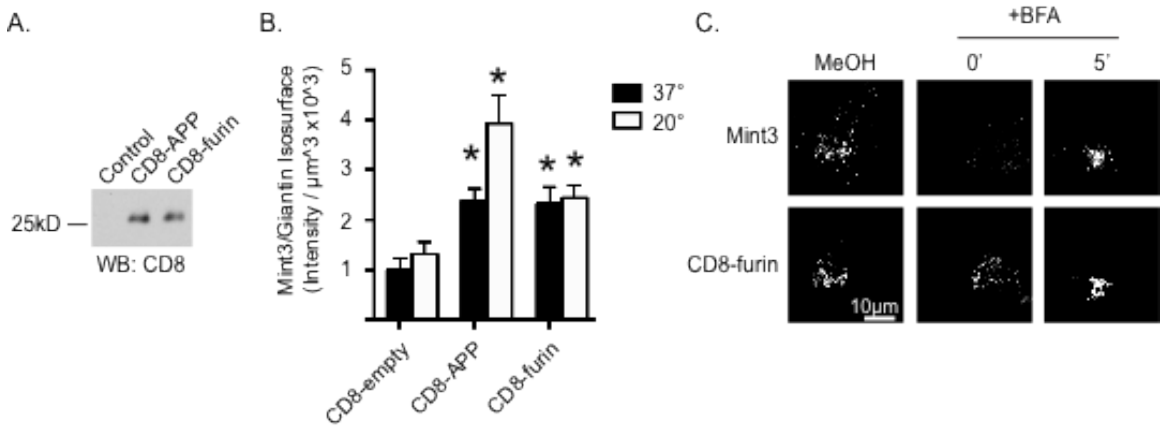

Figure 6. *CD8-furin recruits Mint3 to the Golgi in a BFA-sensitive fashion.* **(A)** HeLaM cells or those expressing CD8-APP or CD8-furin, as indicated, were collected one day after transfection and total cell homogenates (20 µg) analyzed by immunoblotting with anti-CD8. (**B**) HeLaM cells expressing CD8-empty (no cytoplasmic tail), CD8-APP, or CD8-furin were maintained at 37°C or subjected to 20°C block, before fixation and staining for Mint3 and giantin. Isosurfaces based on giantin staining were generated and the sum intensity of Mint3 staining within those isosurfaces determined. Graphs represent an average (N ≥ 7 cells per condition) and are representative of at least three independent experiments. Error bars indicate SEM and bars are normalized to Mint3 recruitment to giantin isosurfaces in cells not over-expressing CD8-empty at 37°C. Asterisks indicate a $p<0.01$ when analyzed using ANOVA, each compared to control staining. **(C)** HeLaM cells were transfected with a plasmid directing the expression of CD8-furin. The next day cells were treated with methanol vehicle (methanol) or BFA for 2 min. Drug was then washed from cells with pre-warmed medium and incubated for the times indicated. Cells were then fixed and stained with antibodies against CD8 and Mint3. Confocal images are shown.

4.4. Discussion

In this study we investigated the role of specific residues within sorting motifs in the cytoplasmic tail of APP to assess the specificity for and roles of adaptors involved in export from the Golgi. Parallel studies using full length, untagged APP and CD8-APP ensured that the results were both dependent upon the cytoplasmic tail and representative of the native protein. The combined use of minimal exogenous protein expression, point mutations in the tail, temperature block and release, and BFA treatment and recovery afforded us the opportunity to assess the role of Mint3 in APP export specifically from the Golgi and also allowed us to identify $LAMP1^+$ structures as the proximal destination of those carriers. We found that: (i) Mint3 is specifically recruited to the Golgi in response to increases in the levels of APP/CD8-APP there, (ii) Y2, the first tyrosine within the YENPXY motif, is critical for APP-dependent Mint3 recruitment to the Golgi, (iii) mutation of Y2 to alanine results in a strong delay in export of APP from the Golgi, (iv) APP moves to $LAMP1^+$ structures soon after leaving the Golgi, and (v) Mint3 can be recruited to the Golgi by different cargos, using different sorting motifs, and resulting in different outcomes as far as cargo export or retention.

We conclude that Mint3 recruitment and Y2 are critical for export of APP from the Golgi in HeLaM cells based upon the following observations: (i) APP or CD8-APP carrying the Y2A mutation fail to recruit Mint3 to the Golgi, (ii) the Y2A mutants showed a delay in export after the block, and (iii) the Y2A mutants failed to demonstrate the transient wave of localization to $LAMP1^+$ structures after release from block, compared to wild type. These results are consistent with our previous observations, that APP and Mint3 were found together on post-Golgi vesicles (Shrivastava-Ranjan, Faundez et al. 2008) and that truncation of the 10 amino acids near the cytoplasmic tail of APP (that includes both YENPXY and FFE motifs) failed to recruit Mint3 (Han, Wang et al. 2008, Shrivastava-Ranjan, Faundez et al. 2008). This truncation mutant exited the Golgi by 15 min after temperature block, but we did not identify the destination in the earlier study. The fact that the truncated APP still exited the Golgi is consistent with alternative routes

for egress. Our earlier study used 15 min. post-release as the earliest time point evaluated, and found that the truncated form of APP resulted in enlarged carriers. Additionally, depletion of Mint3 was evaluated under steady state conditions and found increased overlap with syntaxin6 (a SNARE protein that localizes to the Golgi and endosomes) and EEA1. The current work enhances the previous findings in that we look at earlier time points after release from temperature block and identify an earlier structure (LAMP1) to which APP localizes after release. We also add context to the earlier work in that the overall effects of Mint3 depletion were likely due to traffic events occurring at sites other than the Golgi. Alternatively, it is possible that residue(s) within the C-terminal 10 amino acid deletion are involved in retention of APP at the Golgi. Although there is currently scant experimental evidence for such speculation, such a mechanism could have important ramifications to APP traffic and human disease. Note that a strength of this study is the specific examination of directional traffic from a single site, as induced by imposition and release of the temperature block or BFA treatment. By generating a bolus of cargo in the Golgi as it is released, we can monitor subsequent changes in localization of cargo and associated traffic components. However, as the period of release increases, it is increasingly difficult to assign changes in traffic as resulting solely from the cargo leaving the Golgi.

AP-4 has also been reported to affect APP traffic at the Golgi in HeLa cells (Burgos, Mardones et al. 2010). In their studies, a change in the steady state distribution of APP-CFP was observed either when the APP-CFP construct contained the FFE/AAA mutations or when the μ4 subunit of AP-4 was knocked down by siRNA. The APP-CFP changed from dispersed puncta (presumably $EEA1^{+}$ endosomes) to perinuclear staining displaying increased overlap with TGN46. They also show that AP-4 is concentrated in the perinuclear region of HeLa cells and partially overlaps with TGN46 staining. The authors interpreted these data as evidence that AP-4 is important for APP export from the Golgi in HeLa cells. In contrast, we were unable to find any APP- or CD8-APP-dependent changes in the staining of AP-4 in HeLaM cells. Neither did we

find evidence of perinuclear clustering of AP-4, using the commercially available (BD Biosciences) antibody directed against the ε4 subunit (Burgos, Mardones et al. 2010) of AP-4 (Fig. 1A). We obtained an aliquot of the antibody directed against the μ4 subunit of AP-4, kindly provided by Dr. Juan Bonifacino (Hirst, Bright et al. 1999, Burgos, Mardones et al. 2010), but again did not detect any APP-dependent changes in the staining of AP-4 in HeLaM cells nor staining that overlapped to any appreciable extent with Golgi markers (data not shown). As a positive control the same antibody was used to stain primary cultures of mouse cortical neurons and we observed very clear perinuclear staining that overlapped extensively with Golgi markers. Thus, we believe that AP-4 expression is quite low in HeLaM cells and quite possibly lower than in HeLa cells. We also treated APP expressing HeLaM cells with BFA and found no changes to AP-4 staining patterns with either antibody. This suggests either that the staining observed with AP-4 antibodies is not Arf-dependent or that the AP-4 recruited to endomembranes in HeLaM cells is mediated by an Arf GEF that is not sensitive to BFA. We interpret these data as evidence that AP-4 is not recruited to the Golgi in response to increased levels of APP in HeLaM cells and as a consequence is unlikely to serve as the protein adaptor for carrier biogenesis or export. Thus, of the Arf-dependent adaptors functional in carrier biogenesis at the Golgi only Mint3 was found to concentrate there in response to increased APP expression.

A trivial explanation for these differences could be that HeLa and HeLaM differ in some important way to affect APP traffic, e.g., levels of AP-4 expressed, though this would be surprising for cell lines that have common origins. While we believe that our studies address fundamental aspects of membrane traffic relevant to all eukaryotic cells, the traffic of APP is particularly important in the brain because changes in traffic can alter exposure to secretases, increase Aβ generation, and promote neurodegeneration (Thinakaran and Koo 2008). Thus, it will be important to expand our observations into other cell types and specifically test the extent to which levels of expression of different binding partners or post-translational modifications to APP

or partners may influence outcomes. Burgos, et al (Burgos, Mardones et al. 2010) did not report on AP-4 distribution with and without APP over-expression, neither did they look at time resolved traffic of APP constructs in their cells. Thus, detailed comparisons of datasets are not possible. Nevertheless, based upon our results we believe that Mint3 is the adaptor involved in APP export from the Golgi, though we cannot conclude that AP-4 plays a role in its export in other cells.

These data are consistent with the model that a BFA-sensitive Arf guanine nucleotide exchange factor (GEF) at the Golgi is responsible for activation of the Arf(s) that recruit the adaptor Mint3 to that site for binding to the cytoplasmic tail of APP. This is in notable contrast to results obtained with CD8-M6PR which lost its Arf-dependent adaptors, GGAs and AP-1, during exposure to BFA but recovery was delayed by almost 15 min and occurred initially at recycling endosomes (Caster, Sztul et al. 2013). When combined with results from this closely related study (Caster, Sztul et al. 2013), we find that at least three different cargos (the cation-independent mannose 6-phosphate receptor, furin, and APP) each display a high level of specificity in Arf-dependent adaptor recruitment to the Golgi or endosomes. As the number of cargos that are discovered to share these properties rises, and the number of Arf GEFs there is limited, we speculate that the cargo itself contains within it the information that dictates specificity in adaptor recruitment. We believe the simplest model to explain this would be if cargo activates an Arf GEF, leading to activation and recruitment of one or more Arfs at the Golgi, which leads to recruitment of adaptor(s) that bind both activated Arf and motifs in the cytoplasmic tail of the cargo. This idea of dual binding sites is a form of coincidence detection that can provide the level of specificity found in cells. This speculative model suggests the formation of a multi-subunit complex of cargo-GEF-Arf-adaptor that is likely to be quite transient and difficult to document in cells. The later role of an Arf GAP and consequent dissociation of the Arf GEF and Arfs is also predicted as carriers mature but were not addressed at all in the current studies.

Our data also lend support to the conclusion that at least one other APP binding partner plays a significant role in its traffic, other than Mint3 or AP-4. This comes from the observation that the

Y3A and Y2A mutants each display increased staining at $LAMP1^+$ structures at steady state (no temperature block). Both Y3 and FFE have been implicated in AP-4 binding but the fact that the FFE/AAA mutant did not increase at the $LAMP1^+$ compartment indicates that this effect of Y3A is likely not mediated by AP-4. The observation that these two mutants each cause increased steady state accumulation at $LAMP1^+$ structures also seems to suggest that this compartment is perhaps more than a transient stop for APP exiting the Golgi. The finding that APP-Y3A is concentrated there, relative to the wild type protein, should also allow the means to identify the binding partner responsible for what we tentatively interpret as a delay in exit from this organelle.

What is the nature of the $LAMP1^+$ compartment to which APP traffics after leaving the Golgi? We do not believe they represent lysosomes as the association with LAMP1 is transient and the levels of APP fluorescence and protein do not decrease in synchrony with its traffic to/through that compartment, despite the fact that more than 50% of cellular APP was predicted to do so. Thus, we believe it to represent a sorting compartment that happens to also contain LAMP1 but not LAMP2. These are often used interchangeably as markers of lysosomes, though they are known to traffic to endosomes and to the TGN (Pols, van Meel et al. 2013). Note, however, that we did not observe increased staining of either LAMP with markers of the Golgi or TGN during temperature block. Rather, the overlap in APP staining was decidedly after release. The higher resolution images provided by SIM (e.g., Fig. 2D) indicate a close apposition of markers with at least some mixing and are encouraging that further studies may provide more details and potentially functions of this novel compartment. The fact that the Y2A and Y3A mutants each displayed increased overlap in staining with LAMP1 at steady state is evidence that the presence of APP at this compartment cannot be dismissed as an unexplained artifact resulting from the temperature block. Future studies of this organelle, and the binding partners involved in APP's import and export, are planned to further expand our detailed understanding of the routes and mechanisms of APP traffic.

Finally, we were interested in comparing results in our assays for two different cargos that each recruits Mint3 to the Golgi, though using distinct sorting motifs and with opposing consequences to cargo traffic. We focused on the CD8-fusion proteins to allow more direct and comparable quantitative data but the same (qualitative) results were obtained with the full-length proteins. In comparison to CD8-APP a much higher fraction of cellular CD8-furin is present at the Golgi in steady state cells and this fraction does not change with temperature block. Indeed, because the two cargos are expressed to comparable levels and recruit very similar percentages of cellular Mint3 to the Golgi, yet several fold more CD8-furin is at the Golgi than is CD8-APP, it appears that CD8-APP has a higher "specific activity" as far as Mint3 recruitment to the Golgi. This is consistent with the fact that furin also binds AP-1 and PACS-1 at the Golgi and thus may have a lower percentage of Mint3 sites accessible for binding. We believe the commonalities between cargo-dependent Mint3 recruitment for export and retention suggest the possibility that other cargos may be recruiting Arf-dependent adaptors for retention that are currently interpreted solely as a role in export. This highlights a point that will require much more detailed follow up studies than can be included here but is one that we believe will be important in the evolution of models of the regulation of membrane traffic.

4.5. Experimental Procedures

Cell Culture

HeLaM (generous gift from Dr. Margaret Robinson) cells were maintained in 10% fetal bovine serum (Atlanta Biologicals, cat #S11150) in DMEM (GIBCO #11965, v/v) in a water-jacketed incubator, maintained at 5% CO2 and 37°C.

Plasmids and Transfections

Generation of the CD8-tail constructs is described in Caster and Kahn (Caster, Sztul et al. 2013). Each of these constructs expresses the ectodomain and transmembrane domain of CD8

fused to the cytoplasmic tail of APP with the indicated mutations. Mutations were introduced by amplifying the region encoding the cytoplasmic tail of APP using primers that incorporated the desired changes. All constructs were sequenced to confirm the mutation desired and ensure against additional changes. pFUW-APP was described in Shrivastava-Ranjan et al (Shrivastava-Ranjan, Faundez et al. 2008) and directs expression of the 695 residue variant of human APP, under control by the ubiquitin C promoter.

Plasmids were transfected using Fugene6 transfection reagent (Roche catalog #11814443001). Cells were plated onto 6-well dishes one day prior to transfection at a density resulting in 80% confluence at the time of transfection. Each well of a 6-well plate received 1 μg DNA in 100μL warmed OPTI-MEM medium (GIBCO catalog # 11058). After a 5 min incubation, 6 μL FuGene6 was added to the DNA/OPTI-MEM mixture and incubated at room temperature for 20 min. During this incubation, cells were rinsed once with 1 mL of pre-warmed OPTI-MEM, and then placed in 1 mL of pre-warmed OPTI-MEM. At the conclusion of the 20 min incubation, the DNA/FuGene/OPTI-MEM solution was added drop-wise to the well. Cells were then returned to 37°C for 4 hr. Cells were then split by taking up cells with 0.5 ml 0.05% Trypsin-EDTA (GIBCO catalog # 25300), adding 3 ml medium and plating onto 6 cm dishes containing Matrigel-coated coverslips (BD Biosciences, catalog # 356234). Cells were allowed to attach overnight.

Antibodies

Primary antibodies reported in this manuscript are: C-terminus APP (Synaptic Systems catalog #127002) at 1:1000 (WB) and 1:500 (ICC), N-terminus APP (Chemicon, catalog #MAB348) at 1:1000 for ICC; CD8 (Santa Cruz Biotechnologies, catalog #SC7188) was used at 1:500 for immunoblotting; CD8 (Ancell Corp., catalog #153020) was used for ICC at 1:1000; Mint3 (BD Transduction Laboratories, catalog #611380) was used at 1:500 for WB and 1:200 for ICC; Mint3 (Santa Cruz Biotechnologies, Inc., catalog #SC-28970) was used at 1:500 for ICC; ε4

(AP-4, BD Bioscience, catalog #612018) was used at 1:100 for ICC; pre-immune serum and μ4 (AP-4) antibody were generous gifts from Dr. Juan Bonifacino (NICHD) used at 1:200 (ICC); Fe65 (Upstate EMD Millipore, catalog #05-758) at 1:1000 (ICC); FAPP2 (gift from Antonella DeMatteis) was used at 1:1000; giantin (Covance, catalog #PRB-114C) was used at 1:1000; GM130 (BD Transduction Laboratories, catalog #610823) was used at 1:1000; EEA1 (Abcam, catalog #ab2900) used at 1:1000; transferrin receptor (TfR, Invitrogen, catalog #13-680) was used at 1:1000; LAMP1 (catalog #H4A3), LAMP2 (catalog #H4B4), and AP-3 (delta SA4) were purchased from the Developmental Studies Hybridoma Bank, University of Iowa and used at 1:1000 (ICC); TGN46 (AbD Serotec (BioRad Laboratories, Inc.), catalog #AHP500) was used at 1:1000; AP-1 (γ-adaptin, BD Transduction Laboratories, catalog #610502) was used at 1:100. Secondary antibodies reported in this manuscript are: Alexa488 and Alexa594 (both from Invitrogen) were used at 1:500 for ICC.

Immunoblotting

Cells were lysed in RIPA buffer (50 mM Tris, pH 8.0, 150 mM NaCl, 0.1% SDS, 0.5% deoxycholate, 1% NP-40) containing a mixture of protease inhibitors (Sigma Chemical Co, catalog #P2714-1PTL). Protein concentrations were determined using the Bradford Protein Assay (BioRad #500-0113). Proteins (20 μg) were resolved in SDS-PAGE gels prior to transfer to nitrocellulose, which were later placed in blocking solution consisting of phosphate buffered saline (PBS; 137 mM NaCl, 2.7 mM KCl, 10 mM sodium phosphate dibasic, 2 mM potassium phosphate monobasic, pH 7.4) with 5% powdered milk and 0.02% sodium azide for one hr. Primary antibodies were diluted in blocking solution and applied to the blot overnight at 4°C. Blots were then washed three times in PBS containing 0.01% Tween 20. Secondary antibodies were diluted in blocking solution and applied to the blot for one hour at room temperature. Blots were developed using SuperSignal (Thermo Scientific, catalog #34075) and films exposed for the times indicated in the figures.

BFA Treatment

Cells were maintained and transfected as described above were plated onto 6cm dishes containing Matrigel coated coverslips. BFA was diluted in methanol to a 10x working stock, and applied to cells so the final concentration was 7.5µg/mL. Two minutes after application of drug, cells were rinsed once with pre-warmed medium, 4 mL of medium was applied to cells for the remainder of the recovery period and cells were fixed as described below. Cells treated with methanol (final concentration 1% v/v) vehicle control were morphologically indistinguishable from untreated cells (data not shown).

Temperature Block and Immunocytochemistry

Medium was aspirated from cells and replaced with 4mL 20mM HEPES/10% fetal bovine serum in DMEM (GIBCO cat #11965). Cells were then placed in the 19.5°C water bath for four hr. Following this temperature block, cells were either immediately fixed, or returned to 37°C for varying times of "release", prior to fixation. Release was performed by replacing medium with fresh, pre-warmed (37°C) medium without HEPES and dishes were placed in a gassed incubator. Cells were fixed in 2% paraformaldehyde in PBS for 20 min at room temperature. Following fixation, cells were rinsed with PBS for 5 min, a total of four times. Individual coverslips were then placed on a parafilm coated 24-well dish, and ~200 µL blocking solution, 1% bovine serum albumin and 0.05% saponin in PBS, for 20 min at room temperature. Primary antibodies were diluted in blocking solution and ~100µL added to a coverslip, covered, and placed at 4°C overnight. Coverslips were then washed four times with washing solution (0.05% saponin in PBS) for 5 min each wash. Secondary antibodies were diluted in blocking solution at a 1:500 dilution and applied to cells for 1 hr at room temperature. Coverslips were then washed twice with washing solution for 5 min. Hoechst 33342 (Invitrogen) was diluted 1:5000 in blocking solution and applied to cells for 5 min. Cells were washed twice for 5 minutes with washing

solution, and then placed in PBS for 5 minutes. Coverslips were mounted using Mowiol (CalBiochem, catalog #475904), prepared as described in Valnes and Brandtzaeg (Valnes and Brandtzaeg 1985) .

Image Acquisition and Quantification

Confocal images were acquired on an Olympus IX81 microscope using a 100x objective, NA 1.45. Each channel was manually thresholded using red/blue intensity indicators. Channels were excited and imaged sequentially. Wide field images were collected on a Nikon TE300 using a 63x objective lens with a numerical aperture of 1.4 and a Quantix cooled CCD camera. Stacks of images were collected with a 1316 x1035 pixel aspect ratio, a 16-bit file depth, and with a step size of 0.2um.

Structured illumination microscopy images were collected on a Nikon Eclipse Ti microscope using a 100X objective with NA 1.49 and an Andor DU-897 camera. The 594 nm and 488 nm channels were collected with a 100 ms and 300 ms exposure time, respectively; each with a conversion gain of 1x. Images were reconstructed using Nikon Elements software with the following parameter settings: structured illumination contrast of 1.5, apodization filter parameter of 1.0, and width of 3D-SIM filter of 0.15.

Quantitative Image Analysis

Stacks of wide field images were deconvolved using Huygens SVI deconvolution software. Each channel was deconvolved using the theoretical point spread function appropriate for the fluorophore indicated. Each stack of images was iteratively deconvolved until a threshold of 0.1 total image change was achieved. Deconvolved images were imported into Imaris where isosurfaces were defined based on cell marker staining. Note that once an isosurface is defined, Imaris generates many parameters that describe the structure, including but not limited to volume, and surface area. We chose to use sum pixel intensity within an isosurface volume, rather than

surface area, due to concerns that invaginations or extensions of membrane surfaces or adjacent planar membranes may contribute more to errors in the latter. This method and surrounding issues are described in more detail in Caster and Kahn (Caster and Kahn 2012).

Andersen, O. M., J. Reiche, V. Schmidt, M. Gotthardt, R. Spoelgen, J. Behlke, C. A. von Arnim, T. Breiderhoff, P. Jansen, X. Wu, K. R. Bales, R. Cappai, C. L. Masters, J. Gliemann, E. J. Mufson, B. T. Hyman, S. M. Paul, A. Nykjaer and T. E. Willnow (2005). "Neuronal sorting protein-related receptor sorLA/LR11 regulates processing of the amyloid precursor protein." Proc Natl Acad Sci U S A **102**(38): 13461-13466.
Aridor, M. and L. M. Traub (2002). "Cargo selection in vesicular transport: the making and breaking of a coat." Traffic **3**(8): 537-546.
Bonifacino, J. S. and B. S. Glick (2004). "The mechanisms of vesicle budding and fusion." Cell **116**(2): 153-166.
Bonifacino, J. S. and J. Lippincott-Schwartz (2003). "Coat proteins: shaping membrane transport." Nat Rev Mol Cell Biol **4**(5): 409-414.
Bonifacino, J. S. and L. M. Traub (2003). "Signals for sorting of transmembrane proteins to endosomes and lysosomes." Annu Rev Biochem **72**: 395-447.
Borg, J. P., J. Ooi, E. Levy and B. Margolis (1996). "The phosphotyrosine interaction domains of X11 and FE65 bind to distinct sites on the YENPTY motif of amyloid precursor protein." Mol Cell Biol **16**(11): 6229-6241.
Borg, J. P., Y. Yang, M. De Taddeo-Borg, B. Margolis and R. S. Turner (1998). "The X11alpha protein slows cellular amyloid precursor protein processing and reduces Abeta40 and Abeta42 secretion." J Biol Chem **273**(24): 14761-14766.
Burgos, P. V., G. A. Mardones, A. L. Rojas, L. L. daSilva, Y. Prabhu, J. H. Hurley and J. S. Bonifacino (2010). "Sorting of the Alzheimer's disease amyloid precursor protein mediated by the AP-4 complex." Dev Cell **18**(3): 425-436.
Caster, A. H. and R. A. Kahn (2012). "Computational method for calculating fluorescence intensities within three-dimensional structures in cells." Cellular Logistics **2**(4): 176-188.
Caster, A. H., E. Sztul and R. A. Kahn (2013). "A Role for Cargo in the Activation of ADP-Ribosylation Factors (Arf) and Adaptor Recruitment." J Biol Chem.
Choy, R. W., Z. Cheng and R. Schekman (2012). "Amyloid precursor protein (APP) traffics from the cell surface via endosomes for amyloid beta (Abeta) production in the trans-Golgi network." Proc Natl Acad Sci U S A **109**(30): E2077-2082.
Cockcroft, S., G. M. Thomas, A. Fensome, B. Geny, E. Cunningham, I. Gout, I. Hiles, N. F. Totty, O. Truong and J. J. Hsuan (1994). "Phospholipase D: a downstream effector of ARF in granulocytes." Science **263**(5146): 523-526.
Donaldson, J. G. and C. L. Jackson (2011). "ARF family G proteins and their regulators: roles in membrane transport, development and disease." Nat Rev Mol Cell Biol **12**(6): 362-375.
Donaldson, J. G., J. Lippincott-Schwartz, G. S. Bloom, T. E. Kreis and R. D. Klausner (1990). "Dissociation of a 110-kD peripheral membrane protein from the Golgi apparatus is an early event in brefeldin A action." J Cell Biol **111**(6 Pt 1): 2295-2306.
Duclos, F., U. Boschert, G. Sirugo, J. L. Mandel, R. Hen and M. Koenig (1993). "Gene in the region of the Friedreich ataxia locus encodes a putative transmembrane protein expressed in the nervous system." Proc Natl Acad Sci U S A **90**(1): 109-113.
Godi, A., P. Pertile, R. Meyers, P. Marra, G. Di Tullio, C. Iurisci, A. Luini, D. Corda and M. A. De Matteis (1999). "ARF mediates recruitment of PtdIns-4-OH kinase-beta and stimulates synthesis of PtdIns(4,5)P2 on the Golgi complex." Nat Cell Biol **1**(5): 280-287.
Greenfield, J. P., J. Tsai, G. K. Gouras, B. Hai, G. Thinakaran, F. Checler, S. S. Sisodia, P. Greengard and H. Xu (1999). "Endoplasmic reticulum and trans-Golgi network generate distinct populations of Alzheimer beta-amyloid peptides." Proc Natl Acad Sci U S A **96**(2): 742-747.

Haass, C., E. H. Koo, A. Capell, D. B. Teplow and D. J. Selkoe (1995). "Polarized sorting of beta-amyloid precursor protein and its proteolytic products in MDCK cells is regulated by two independent signals." J Cell Biol **128**(4): 537-547.
Han, J., Y. Wang, S. Wang and C. Chi (2008). "Interaction of Mint3 with Furin regulates the localization of Furin in the trans-Golgi network." Journal of Cell Science **121**(Pt 13): 2217-2223.
Hill, K., Y. Li, M. Bennett, M. McKay, X. Zhu, J. Shern, E. Torre, J. J. Lah, A. I. Levey and R. A. Kahn (2003). "Munc18 interacting proteins: ADP-ribosylation factor-dependent coat proteins that regulate the traffic of beta-Alzheimer's precursor protein." J Biol Chem **278**(38): 36032-36040.
Hirst, J., N. A. Bright, B. Rous and M. S. Robinson (1999). "Characterization of a fourth adaptor-related protein complex." Mol Biol Cell **10**(8): 2787-2802.
Hirst, J., M. N. Seaman, S. I. Buschow and M. S. Robinson (2007). "The role of cargo proteins in GGA recruitment." Traffic **8**(5): 594-604.
Icking, A., M. Amaddii, M. Ruonala, S. Honing and R. Tikkanen (2007). "Polarized transport of Alzheimer amyloid precursor protein is mediated by adaptor protein complex AP1-1B." Traffic **8**(3): 285-296.
Jones, D. H., J. B. Morris, C. P. Morgan, H. Kondo, R. F. Irvine and S. Cockcroft (2000). "Type I phosphatidylinositol 4-phosphate 5-kinase directly interacts with ADP-ribosylation factor 1 and is responsible for phosphatidylinositol 4,5-bisphosphate synthesis in the golgi compartment." J Biol Chem **275**(18): 13962-13966.
Lah, J. J. and A. I. Levey (2000). "Endogenous presenilin-1 targets to endocytic rather than biosynthetic compartments." Mol Cell Neurosci **16**(2): 111-126.
Lee, J., C. Retamal, L. Cuitino, A. Caruano-Yzermans, J. E. Shin, P. van Kerkhof, M. P. Marzolo and G. Bu (2008). "Adaptor protein sorting nexin 17 regulates amyloid precursor protein trafficking and processing in the early endosomes." J Biol Chem **283**(17): 11501-11508.
Lee, M. C., E. A. Miller, J. Goldberg, L. Orci and R. Schekman (2004). "Bi-directional protein transport between the ER and Golgi." Annu Rev Cell Dev Biol **20**: 87-123.
Lee, M. S., S. C. Kao, C. A. Lemere, W. Xia, H. C. Tseng, Y. Zhou, R. Neve, M. K. Ahlijanian and L. H. Tsai (2003). "APP processing is regulated by cytoplasmic phosphorylation." J Cell Biol **163**(1): 83-95.
Lippincott-Schwartz, J., L. C. Yuan, J. S. Bonifacino and R. D. Klausner (1989). "Rapid redistribution of Golgi proteins into the ER in cells treated with brefeldin A: evidence for membrane cycling from Golgi to ER." Cell **56**(5): 801-813.
Marks, M. S., L. Woodruff, H. Ohno and J. S. Bonifacino (1996). "Protein targeting by tyrosine- and di-leucine-based signals: evidence for distinct saturable components." J Cell Biol **135**(2): 341-354.
Nordeng, T. W. and O. Bakke (1999). "Overexpression of proteins containing tyrosine- or leucine-based sorting signals affects transferrin receptor trafficking." J Biol Chem **274**(30): 21139-21148.
Okamoto, M., Y. Nakajima, T. Matsuyama and M. Sugita (2001). "Amyloid precursor protein associates independently and collaboratively with PTB and PDZ domains of mint on vesicles and at cell membrane." Neuroscience **104**(3): 653-665.
Okamoto, M. and T. C. Sudhof (1998). "Mint 3: a ubiquitous mint isoform that does not bind to munc18-1 or -2." Eur J Cell Biol **77**(3): 161-165.
Perez, R. G., S. Soriano, J. D. Hayes, B. Ostaszewski, W. Xia, D. J. Selkoe, X. Chen, G. B. Stokin and E. H. Koo (1999). "Mutagenesis identifies new signals for beta-amyloid precursor protein endocytosis, turnover, and the generation of secreted fragments, including Abeta42." J Biol Chem **274**(27): 18851-18856.
Pols, M. S., E. van Meel, V. Oorschot, C. ten Brink, M. Fukuda, M. G. Swetha, S. Mayor and J. Klumperman (2013). "hVps41 and VAMP7 function in direct TGN to late endosome transport of lysosomal membrane proteins." Nat Commun **4**: 1361.

Rajendran, L. and W. Annaert (2012). "Membrane trafficking pathways in Alzheimer's disease." Traffic **13**(6): 759-770.
Ramelot, T. A., L. N. Gentile and L. K. Nicholson (2000). "Transient structure of the amyloid precursor protein cytoplasmic tail indicates preordering of structure for binding to cytosolic factors." Biochemistry **39**(10): 2714-2725.
Robinson, M. S. and J. S. Bonifacino (2001). "Adaptor-related proteins." Curr Opin Cell Biol **13**(4): 444-453.
Robinson, M. S. and T. E. Kreis (1992). "Recruitment of coat proteins onto Golgi membranes in intact and permeabilized cells: effects of brefeldin A and G protein activators." Cell **69**(1): 129-138.
Rothman, J. E. and L. Orci (1992). "Molecular dissection of the secretory pathway." Nature **355**(6359): 409-415.
Rothman, J. E. and F. T. Wieland (1996). "Protein sorting by transport vesicles." Science **272**(5259): 227-234.
Sabo, S. L., L. M. Lanier, A. F. Ikin, O. Khorkova, S. Sahasrabudhe, P. Greengard and J. D. Buxbaum (1999). "Regulation of beta-amyloid secretion by FE65, an amyloid protein precursor-binding protein." J Biol Chem **274**(12): 7952-7957.
Saito, Y., M. Akiyama, Y. Araki, A. Sumioka, M. Shiono, H. Taru, T. Nakaya, T. Yamamoto and T. Suzuki (2011). "Intracellular trafficking of the amyloid beta-protein precursor (APP) regulated by novel function of X11-like." PLoS One **6**(7): e22108.
Seaman, M. N. (2004). "Cargo-selective endosomal sorting for retrieval to the Golgi requires retromer." J Cell Biol **165**(1): 111-122.
Selkoe, D. J. (1994). "Cell biology of the amyloid beta-protein precursor and the mechanism of Alzheimer's disease." Annu Rev Cell Biol **10**: 373-403.
Selkoe, D. J. (1998). "The cell biology of beta-amyloid precursor protein and presenilin in Alzheimer's disease." Trends Cell Biol **8**(11): 447-453.
Selkoe, D. J., T. Yamazaki, M. Citron, M. B. Podlisny, E. H. Koo, D. B. Teplow and C. Haass (1996). "The role of APP processing and trafficking pathways in the formation of amyloid beta-protein." Ann N Y Acad Sci **777**: 57-64.
Shrivastava-Ranjan, P., V. Faundez, G. Fang, H. Rees, J. J. Lah, A. I. Levey and R. A. Kahn (2008). "Mint3/X11{gamma} Is an ADP-Ribosylation Factor-dependent Adaptor that Regulates the Traffic of the Alzheimer's Precursor Protein from the Trans-Golgi Network." Mol Biol Cell **19**(1): 51-64.
Siman, R. and J. Velji (2003). "Localization of presenilin-nicastrin complexes and gamma-secretase activity to the trans-Golgi network." J Neurochem **84**(5): 1143-1153.
Sisodia, S. S. (1992). "Beta-amyloid precursor protein cleavage by a membrane-bound protease." Proc Natl Acad Sci U S A **89**(13): 6075-6079.
Strous, G. J., E. G. Berger, P. van Kerkhof, H. Bosshart, B. Berger and H. J. Geuze (1991). "Brefeldin A induces a microtubule-dependent fusion of galactosyltransferase-containing vesicles with the rough endoplasmic reticulum." Biol Cell **71**(1-2): 25-31.
Szul, T., R. Garcia-Mata, E. Brandon, S. Shestopal, C. Alvarez and E. Sztul (2005). "Dissection of membrane dynamics of the ARF-guanine nucleotide exchange factor GBF1." Traffic **6**(5): 374-385.
Thinakaran, G. and E. H. Koo (2008). "Amyloid precursor protein trafficking, processing, and function." J Biol Chem **283**(44): 29615-29619.
Valnes, K. and P. Brandtzaeg (1985). "Retardation of immunofluorescence fading during microscopy." J Histochem Cytochem **33**(8): 755-761.
Xu, H., D. Sweeney, R. Wang, G. Thinakaran, A. C. Lo, S. S. Sisodia, P. Greengard and S. Gandy (1997). "Generation of Alzheimer beta-amyloid protein in the trans-Golgi network in the apparent absence of vesicle formation." Proc Natl Acad Sci U S A **94**(8): 3748-3752.

CHAPTER 5

CONCLUSIONS, DISCUSSION, AND IMPLICATIONS

5.1. Overview

Membrane traffic is critical to establishing and maintaining specialized subcellular membranous domains, and is particularly important for polarized cells like neurons. Establishing and maintaining membrane identity is necessary for basic cellular function, is critical to life, and is established and maintained through the specific sorting of cargo proteins for delivery and removal at specific structures, such as the Golgi, endosomes, or the PM. In addition, there is another level of complexity to be added as proteins that are not integral to the establishment of membrane identity also traffic through these organelles, and must be sorted appropriately. The objective of my dissertation research was to test the hypothesis that cargo proteins serve as a signaling initiator for the recruitment of ARF-dependent adaptors at the Golgi. My work has focused on elucidating the requirements for cargo-dependent trafficking events at the Golgi and specifically aimed at understanding how cargo that traffic through the Golgi are sorted to their destinations using a limited number of adaptors. To this end, I established protocols for the mild over-expression of cargo proteins of interest in conjunction with experimental manipulations to (i) collect cargo at the Golgi using cold temperature incubations, or (ii) strip endomembranes of activated ARFs using BFA. I then monitored the subsequent recruitment of adaptors, and the post-Golgi destinations of cargo proteins to test my central hypothesis:

Cargo proteins serve as the initiators of specific ARF-dependent adaptor recruitment at the Golgi.

Based on data presented in Ch. 2, 3, and 4, I conclude that:

1) ARF activation is a localized event that does not result in the presence of freely diffusing ARF.

2) Adaptors are recruited to specific membranes in a regulated fashion and in response to the presence of cargo at that site.

3) Sorting motifs affect the traffic of cargo through the Golgi, and to subsequent destinations.

In the following sections I will expand on these conclusions and place them in the broader context of previously published work.

5.2. ARF activation is a localized event that does not result in the presence of freely diffusing ARF

Since the initial identification of ARFs (Kahn and Gilman 1984; Kahn and Gilman 1986), the prevailing model of ARF action has remained largely unchanged (Fig. 6.1), (Serafini, Orci et al. 1991; Donaldson and Jackson 2011) and includes ARF activation, resulting in ARF insertion into membranes (Helms, Palmer et al. 1993).

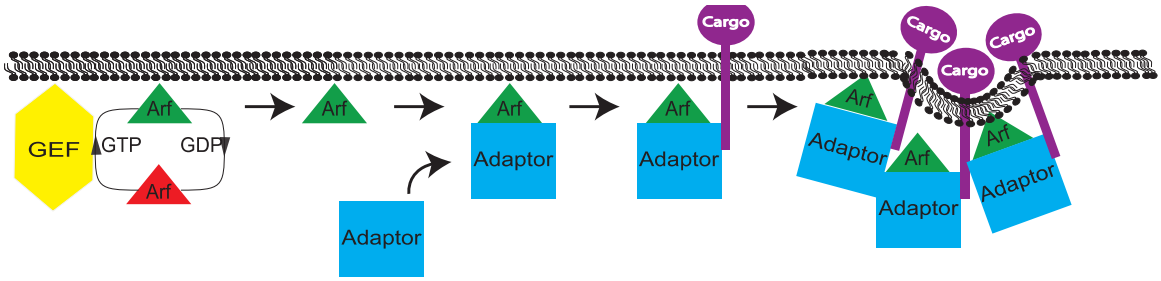

Figure. 5.1 *Prevailing model of ARF-dependent adaptor recruitment.* GEFs exchange ARF•GDP for ARF•GTP, resulting in ARF exposure of the myristate and insertion into the membrane where it remains loosely associated. Activated ARF available to interact with adaptors, which are also associated with cargo.

Inherent in this model is that idea that there is freely diffusible ARF available on membranes (Schimmoller, Simon et al. 1998; Peyroche, Antonny et al. 1999). However, data presented in Ch.3 and 4 shows that cargos, but not dominant active ARF1, can influence the specific recruitment of GEFs. In addition, all the large ARF GEFs are ultimately BFA sensitive, though to varying degrees (Jones, Moss et al. 2005; Niu, Pfeifer et al. 2005), consistent with ARF

itself being necessary for their recruitment. Using the model systems described in Ch. 2, 3, and 4, I found that over-expression of dominant active forms of ARF1 do not enhance the recruitment of any of the adaptors tested (Fig. A.2.) and the recruitment of ARF effectors (i.e. adaptors) occur in response to the presence of cargo (Ch.3, 4). These data are inconsistent with a model that includes ARF activation as the first step in carrier formation. As an alternative, I propose a model that includes the presence of cargo at a donor membrane as one of the initiating steps in ARF-activation and subsequent adaptor recruitment (Fig. 6.2)

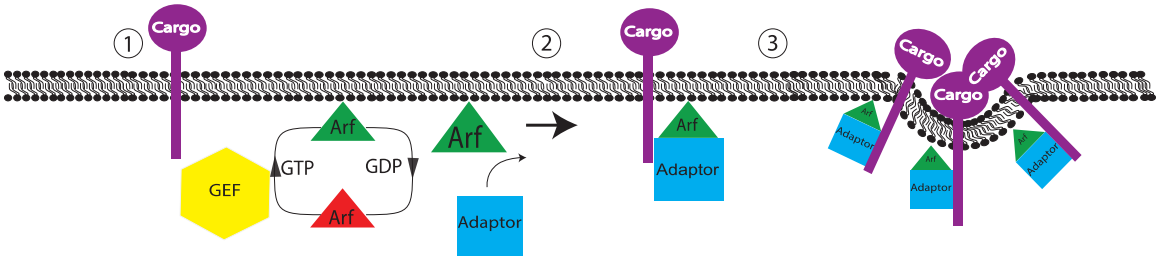

Figure 5.2. *Proposed model of ARF-dependent adaptor recruitment*. The presence of a cargo serves as an initiating signal that results in localized GEF activation of ARFs that is stabilized on a membrane by the cargo-dependent recruitment of adaptors.

The initial model of ARF activation (Helms, Palmer et al. 1993) was based on Arf interacting with heterotrimeric G-proteins in the assay in which it was originally identified ((Kahn and Gilman 1986; Helms, Palmer et al. 1993). In heterotrimeric G-protein signaling, the biological objective is to typically (i) transduce a signal across a membrane, and (ii) amplify that signal (e.g. rhodopsin signaling). Since the formation of that original model, our understanding of ARF activation has expanded with experimentation, and allows us to reconsider the validity of G-coupled proteins as templates for ARF function. Specifically, we now know that ARF-signaling for the purposes of membrane traffic is a very localized phenomenon and results in almost stoichiometric interactions with ARF effectors (Zhu, Boman et al. 2000). Given the very different

biological objectives of these two GTPases, we must modify our conceptual model of ARF activation to reflect its distinct function.

5.3. Adaptors are recruited to specific membranes in a regulated fashion and in response to the presence of cargo at that site

Findings presented in Ch. 3 and 4 indicate that ARF activation is instead a tightly regulated phenomenon that is initiated by the presence of specific cargo, and at specific membranes. The work presented in chapters three and four indicate that enhancing the expression of a cargo results in the recruitment of an adaptor at specific sites, or alternatively when a cargo is enhanced at a specific organelle by imposition of a temperature block there is also an increase in specific adaptors (as in the case of APP and Mint3, or furin and AP-1), consistent with the cargo serving as the initiator of signaling. In addition, if an adaptor functions elsewhere in the trafficking of a given protein, the adaptor will not be recruited until the cargo arrives at the appropriate site (as is the case with M6PR and GGAs and illustrated in Ch. 3). Given that adaptors are present in the cytosol in vast excess of the cargo, this suggests that the cargo serves as the initiating step (Fig. 6.2) in ARF activation.

My work highlights the fact that static views of membrane traffic can be misleading and instead emerging models of membrane traffic should take into account its very dynamic nature. For example, though the interaction between M6PR and AP-1 and GGAs is well established, the location of recruitment is not as straightforward as previously assumed (Caster, Sztul et al. 2013). Data in Ch. 3, obtained using a system of minimal over-expression of CD8-M6PR and temperature block, indicates that GGA1 and AP-1 are not initially recruited to the Golgi though the cargo is present there. Instead, the adaptors are recruited at recycling endosomes, and only once the cargo has arrived there (Caster, Sztul et al. 2013).

5.4. Sorting motifs affect the traffic of cargo through the Golgi.

Work presented here suggests that the traffic of cargo proteins through the Golgi is mediated by sorting signals within their cytoplasmic tails. Two pieces of evidence support this conclusion: (i) when the CD8-M6PR cargo was blocked by 20°C incubation for four hours, the cargo was collected in the Golgi with a bias towards the TGN (Ch. 3, (Caster, Sztul et al. 2013)). However, when the CD8-M6PRΔC cargo (that lacks the GGA1 binding motif) was treated identically, the 20°C incubation resulted in the cargo collecting in the Golgi evenly across compartments, without preference for the late Golgi (Caster, Sztul et al. 2013), suggesting that sorting information contained within the truncated region is responsible for the distribution of the cargo through the Golgi. (ii) Similar results were obtained using CD8-APP mutants: temperature block resulted in the collection of CD8-APP at the TGN, while mutation of Y1A resulted in the cargo arriving at the TGN after release from the blockade, consistent with it being present at earlier Golgi cisternae during the block (Fig. A.1.). In both cases, it is clear that sorting motifs have an effect on the overall distribution of the cargo within the Golgi, and suggest that sorting motifs play a larger part in traffic through the Golgi, or sorting motifs are required to retain a cargo at a specific compartment. Ultimately, determining how sorting motifs regulate traffic, and where within the cell those motifs are relevant, will be critical to understanding the traffic of specific proteins throughout the cell.

Work presented here addresses significant questions in the field of membrane traffic, and proposes a refined model of ARF-activation at the Golgi. In addition, this work provides data in support of a number of hypotheses that stem from the conclusions described herein, and that would potentially warrant further investigation. Some of these hypotheses are described below.

Hypothesis #1 (Ch. 3): Fusion of GGA1/AP-1 mediated M6PR carriers originating at RE for retrieval to the Golgi is the slowest/rate-limiting step.

Hypothesis #2 (Ch. 3/4): Sorting motifs mediate traffic of cargo through the Golgi or function collect cargo at distinct compartments.

Hypothesis #3 (Ch. 4): LAMP1+ endosomes involved in the traffic of APP are non-degradative sorting stations

5.5. Hypothesis #1 (Ch. 3): Fusion of GGA1/AP-1 mediated M6PR carriers originating at RE for retrieval to the Golgi is the slowest/rate-limiting step. Work presented in Ch. 3 indicates that GGA1 and AP-1 are first recruited to recycling endosomes in response to the presence of CD8-M6PR at that site. These data were unexpected, as it is well documented that cells expressing CD8-M6PR enhance GGA1 and AP-1 recruitment to the Golgi (Doray, Bruns et al. 2002; Doray, Ghosh et al. 2002; Ghosh and Kornfeld 2004), and are present together on purified carriers (Pearse and Robinson 1984; Harasaki, Lubben et al. 2005). However, the previously published work focused exclusively on steady state distributions of the cargo, and could not distinguish between fusion and fission events. My work, using minimal cargo over-expression in conjunction with temperature block and BFA treatment, allowed me to focus on a single, well-defined step in the sorting of CD8-M6PR: export from the Golgi. My data indicate that GGA1 and AP-1 are not recruited to the Golgi immediately following temperature block, but are later recruited after the cargo arrives at recycling endosomes (Ch. 3,). These data are supported by similar experiments using BFA treatment where the CD8-M6PR dependent GGA1 and AP-1 recruitment at the Golgi at steady state was lost following treatment with drug, and took longer times to re-recruit (~15 min.) after washout, and occurred on recycling endosomes (Caster, Sztul et al. 2013). These data are consistent with GGA1 and AP-1 (i) functioning in the post-Golgi sorting of CD8-M6PR, and (ii) serving to retrieve CD8-M6PR back to the Golgi. Traditional views of ARF-mediated adaptor formation have proposed that the formation of a carrier (i.e. the recruitment of the adaptor to a given site) is the slowest, rate-limiting step in the process (Kozlovsky and Kozlov 2003). The fact that GGA1- and AP-1 staining are enhanced at

the Golgi at steady state in response to CD8-M6PR expression (Doray, Bruns et al. 2002; Doray, Ghosh et al. 2002; Ghosh and Kornfeld 2004), yet are first recruited to recycling endosomes (Caster, Sztul et al. 2013), suggest that the fusion of these carriers with the Golgi is actually what is being detected in these studies, and results in enhanced staining at that site.

This hypothesis (Fig. 6.3) requires further testing in order to determine how such carriers fuse with the Golgi, but would be potentially very informative to the field of cell biology as a whole, as these adaptors have served as the archetypal models of adaptor function for years (Robinson and Bonifacino 2001).

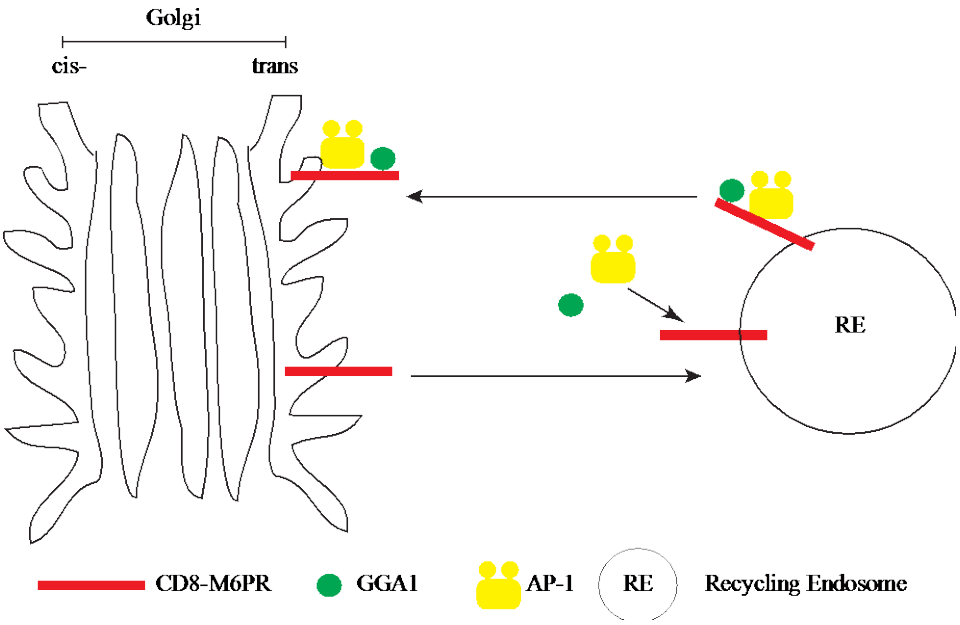

Figure 5.3. *Schematic representation of Hypothesis #1: GGA1/AP-1 mediate CD8-M6PR retrieval to the Golgi.* CD8-M6PR exits the Golgi and traffics to recycling endosomes, where GGA1 and AP-1 are recruited. The cargo/adaptor complex travels back to the Golgi, where the carrier fuses. The fusion is hypothesized to be the step that results in enhanced GGA1 and AP-1 staining seen at the Golgi at steady state.

To test this hypothesis, I believe that the single most important experiment would be to show that GGA1/AP-1 and CD8-M6PR traffic to the Golgi and fuse there. I would express fluorescently tagged forms of GGA1 or AP-1 and CD8-M6PR, and subject the cells to a temperature block and release protocol. I would then image the live cells beginning ~15 min. after release of the block, looking for the accumulation of both cargo and adaptor in the perinuclaer area with a concomitant decrease in fluorescence signal in the cell periphery.

5.6. Hypothesis #2 (Ch. 3/4): Sorting motifs mediate traffic of cargo through the Golgi or function collect cargo at distinct compartments.

Work presented in Ch.3 and 4 indicates that sorting motifs and consequently adaptors play an important part in collecting cargo at a specific compartment within the Golgi. Using the CD8-M6PR or CD8-M6PRΔC constructs I evaluated the cargo's distribution throughout the Golgi before and after temperature block (Ch. 3). At steady state, though a relatively small fraction of the cargo was found to be within the Golgi, the CD8-M6PR cargo showed a preference in localization at the TGN. The CD8-M6PRΔC cargo had the same relative amount of cargo within the Golgi, but showed no preference for any one compartment and was instead distributed evenly across the early, middle and late Golgi (Caster, Sztul et al. 2013). These data are schematically represented in Fig. 6.3 and suggest that sorting information contained within the cytoplasmic tail of CD8-M6PR (that is absent in the CD8-M6PRΔC construct) (i) facilitates it's traffic through the Golgi resulting in a bias towards the TGN, or (ii) interactions that take place in the cytoplasmic tail result in the retention of the cargo at the TGN.

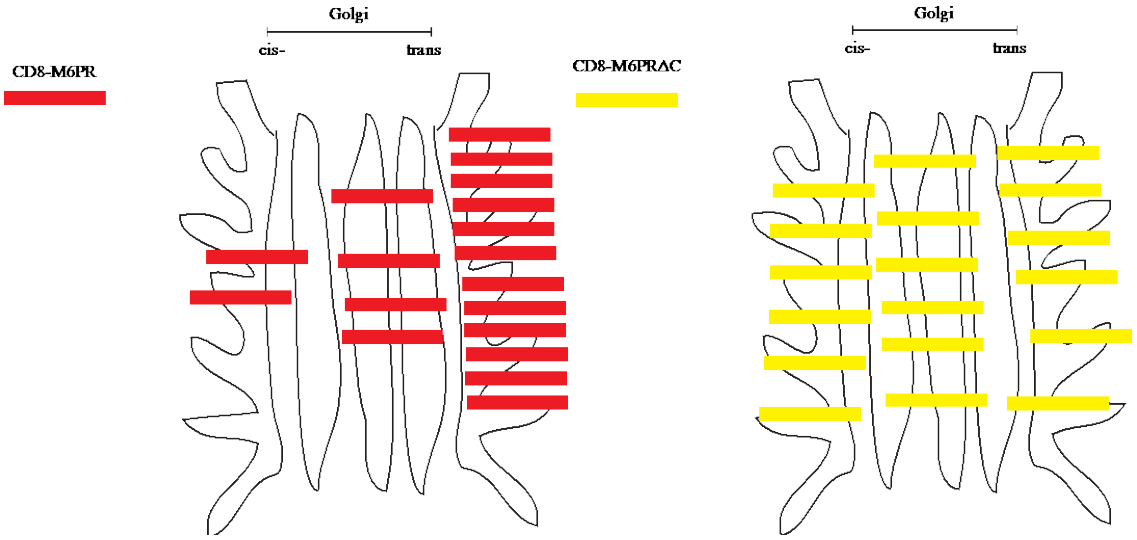

Figure 5.4. *Schematic representation of CD8-M6PR and CD8-M6PRΔC distribution within the Golgi following 20°C block***.** After 4 hr incubation at 20 ℃, CD8-M6PR is collected in the Golgi with a preference for the trans- face of the Golgi, while CD8-M6PRΔC is evenly distributed across the cis-, medial- and trans- Golgi. Note that cargos are not drawn to scale, most of each is lumenal and not cytoplasmic and span a single membrane bilayer.

These possibilities were supported by data presented in Ch. 4 using CD8-APP constructs with mutations in the first tyrosine in the YENPTY (termed Y2) motif. This hypothesis is interesting because it suggests that adaptors play more complicated roles than just mediating export, but can also serve in regulating the physical distribution of a cargo with the Golgi. Published work on the role of Mint3 in furin localization is consistent with this hypothesis in that depletion of Mint3 results in furin escaping the Golgi, in line with the adaptor working to retain furin at that site (Han, Wang et al. 2008).

In addition to the data mentioned above, describing the differences in the way CD8-M6PR and CD8-M6PRΔC are blocked in the Golgi in response to temperature block, it is of note that both cargos leave the Golgi in a similar fashion and arrive at subsequent recycling endosomes with the same amount of time after release. This suggests that though one cargo is

enhanced at the late Golgi compared to the other both are capable of leaving immediately after release of the blockade. It also suggests that sorting motifs in the more membrane-proximal portion of their cytoplasmic tails mediate export from the Golgi, but using adaptors other than GGA1 or AP-1.

Testing the hypothesis that adaptors mediate the retention of cargo at the Golgi is a little more difficult that it might first appear. The obvious experiment is to deplete cells for a specific adaptor, then monitor how it affects the overall distribution of a cargo. However a number of issues immediately arise: (i) depletion typically takes a number of days and during that time period cells can compensate for a deficiency in one pathway very quickly by enhancing the use of another, making the detection of a shift in the cargo's distribution problematic. (ii) Though an adaptor may be thought to function at one location, it is possible it also functions at another to influence later/different steps in sorting. Teasing out two different functions, at different locations can prove difficult. Ideally, in order to look at the role of adaptor proteins and their effect on the distribution of cargo throughout the Golgi, a fluorescently labeled cargo would be expressed in cells then subjected to temperature block. Purified recombinant forms of the adaptor under question that lack the ability to bind to cargo would be microinjected and the real time effect of their competition with endogenous adaptors would be monitored. If adaptors affect the forward movement of the cargo (based on the recovery of fluorescence after photo bleaching) I would conclude that the adaptor mediates traffic through the Golgi. If the cargo can successfully traffic forward through the Golgi, but fails to stay at one compartment, I would conclude that the adaptor is playing a role in retention of the cargo at that site. Because these kinds of experiments are currently beyond the expertise in our laboratory, if might serve to simply express different mutant forms of the a cargo, subject them to temperature block, and quantify the relative fluorescence of the cargo that overlaps with early, middle, and late Golgi markers. This would at least indicate which motifs are important to a cargo's localization within the Golgi, and can be pursued in more detail after the technical experience is acquired.

5.7. Hypothesis #3 (Ch. 4): LAMP1+ endosomes involved in the traffic of APP are non-degradative sorting stations. Work presented in Ch. 4 identifies LAMP1+ endosomes as an early stop in the post-Golgi sorting of APP. Using mild protein over expression and temperature block protocols, I show with confocal and SIM immunofluorescence that APP and CD8-APP constructs exit the Golgi and travel to LAMP1+ structures. This localization is transient, produces discernible populations of structures (some that have APP localizing to the inside of LAMP1, others have discrete lobes of APP and LAMP1), and does not result in an overall reduction in the amount of APP fluorescence consistent with APP trafficking through the organelle rather than being degraded there. In addition, using this same experimental approach, I was unable to detect any APP overlap with LAMP2, another traditional marker of lysosomes thought to by functionally interchangeable with LAMP1. Taken together, these data suggest that LAMP1+ endosomes serve as a sorting station for APP and are distinct from LAMP2. Based on these data, I propose that LAMP1 positive endosomes are functional sorting stations for APP, but raises a number of questions. Are these structures stable within the cell, or are they induced by the presence of cargo? Are they sub-domains of functional lysosomes, or discrete non-degradative endosomes? Given that LAMP1 has its own traffic pattern from the Golgi, do these structures simply mark another waypoint in LAMP1 traffic that happens to overlap with that of APP? Do other markers of lysosomes share similar overlap patterns with APP at this time point after release from temperature block? Answering these questions about the biogenesis of the novel compartments identified during my dissertation work will provide insight into basic cell biology and offer potential sites of clinically relevant interventions.

To test the hypothesis that LAMP1+ endosomes are sorting stations I would need to determine that (i) the LAMP1+ endosomes I see in my experiments are lysosomes, (ii) cargo move into and out of them, and (iii) the cargo is not being degraded. To test this, I would use fluorescently tagged cargo and I would first determine if LAMP1+ endosomes are lysosomes by double labeling for LAMP1 and lysotracker, CD63, and cathepsin D. I would then use live cell

imaging of fluorescently labeled APP in cells stained with lysosotracker to show that the cargo fuses with the lysosome, and then leave.

5.8. Concluding Remarks

I have presented data that suggest a refined model of ARF-dependent adaptor recruitment that includes cargo initiation of ARF signaling, a cascade that is kicked off by the presence of cargo at a specific membrane, that results in the increased function of specific GEFs that activate specific ARFs, that are then in turn recruited to the membrane and stabilize adaptors at that site to ultimately produce a carrier. We have yet to determine how the cargo enhances GEF activity. Why are combinations of ARFs required for adaptor recruitment? Do ARFs mediate GEF recruitment? How do cargo signal that they are in the appropriate location to mediate adaptor recruitment? These questions will all need to be answered for specific cargos, and at clearly defined organelles.

It is clear that ARF-dependent adaptors play complex roles in cargo sorting, ultimately contributing to the overall fate of the cell itself. While functionally analogous mechanisms are beginning to emerge amongst the different adaptors, we still lack many important details that will contribute significantly to our overall understanding of cell biology.

Caster, A. H., E. Sztul, et al. (2013). "A Role for Cargo in Arf-dependent Adaptor Recruitment." J Biol Chem **288**(21): 14788-14804.
Donaldson, J. G. and C. L. Jackson (2011). "ARF family G proteins and their regulators: roles in membrane transport, development and disease." Nat Rev Mol Cell Biol **12**(6): 362-375.
Doray, B., K. Bruns, et al. (2002). "Interaction of the Cation-dependent Mannose 6-Phosphate Receptor with GGA Proteins." J. Biol. Chem. **277**(21): 18477-18482.
Doray, B., P. Ghosh, et al. (2002). "Cooperation of GGAs and AP-1 in packaging MPRs at the trans-Golgi network." Science **297**(5587): 1700-1703.
Ghosh, P. and S. Kornfeld (2004). "The GGA proteins: key players in protein sorting at the trans-Golgi network." Eur J Cell Biol **83**(6): 257-262.
Han, J., Y. Wang, et al. (2008). "Interaction of Mint3 with Furin regulates the localization of Furin in the trans-Golgi network." J Cell Sci **121**(Pt 13): 2217-2223.
Harasaki, K., N. B. Lubben, et al. (2005). "Sorting of major cargo glycoproteins into clathrin-coated vesicles." Traffic **6**(11): 1014-1026.
Helms, J. B., D. J. Palmer, et al. (1993). "Two distinct populations of ARF bound to Golgi membranes." J Cell Biol **121**(4): 751-760.
Jones, H. D., J. Moss, et al. (2005). "BIG1 and BIG2, brefeldin A-inhibited guanine nucleotide-exchange factors for ADP-ribosylation factors." Methods Enzymol **404**: 174-184.
Kahn, R. A. and A. G. Gilman (1984). "Purification of a protein cofactor required for ADP-ribosylation of the stimulatory regulatory component of adenylate cyclase by cholera toxin." J Biol Chem **259**(10): 6228-6234.
Kahn, R. A. and A. G. Gilman (1986). "The protein cofactor necessary for ADP-ribosylation of Gs by cholera toxin is itself a GTP binding protein." J Biol Chem **261**(17): 7906-7911.
Kozlovsky, Y. and M. M. Kozlov (2003). "Membrane fission: model for intermediate structures." Biophys J **85**(1): 85-96.
Niu, T. K., A. C. Pfeifer, et al. (2005). "Dynamics of GBF1, a Brefeldin A-sensitive Arf1 exchange factor at the Golgi." Mol Biol Cell **16**(3): 1213-1222.
Pearse, B. M. and M. S. Robinson (1984). "Purification and properties of 100-kd proteins from coated vesicles and their reconstitution with clathrin." Embo J **3**(9): 1951-1957.
Peyroche, A., B. Antonny, et al. (1999). "Brefeldin A acts to stabilize an abortive ARF-GDP-Sec7 domain protein complex: involvement of specific residues of the Sec7 domain." Mol Cell **3**(3): 275-285.
Robinson, M. S. and J. S. Bonifacino (2001). "Adaptor-related proteins." Curr Opin Cell Biol **13**(4): 444-453.
Schimmoller, F., I. Simon, et al. (1998). "Rab GTPases, directors of vesicle docking." J Biol Chem **273**(35): 22161-22164.
Serafini, T., L. Orci, et al. (1991). "ADP-ribosylation factor is a subunit of the coat of Golgi-derived COP- coated vesicles: a novel role for a GTP-binding protein." Cell **67**(2): 239-253.
Zhu, X., A. L. Boman, et al. (2000). "Effectors increase the affinity of ADP-ribosylation factor for GTP to increase binding." J Biol Chem **275**(18): 13465-13475.